Etablierung eines neuen integrativen multimodalen Imaging-Ansatzes für das Monitoring von kardial transplantierten induzierten pluripotenten Stammzellen im präklinischen Großtiermodell

Von der Naturwissenschaftlichen Fakultät
der Gottfried Wilhelm Leibniz Universität Hannover

zur Erlangung des Grades

Doktor der Naturwissenschaften
Dr. rer. nat.

genehmigte Dissertation
von

Priv.-Doz. Dr. med. Christian Templin
geboren am 19. Mai 1975 in Bremen

2013

Referenten: Prof. Dr. rer. nat. Ulrich Martin

Leibniz Laboratorien für Biotechnologie und artifizielle Organe (LEBAO) und REBIRTH – „Center for Regenerative Medicine", Klinik für Herz-, Thorax-, Transplantations- und Gefäßchirurgie, Medizinische Hochschule Hannover

Korreferent: Prof. Dr. rer. nat. Thomas Scheper

Institut für Technische Chemie,

Leibniz Universität Hannover

Tag der Promotion: 10.01.2013

Vorwort

Die Untersuchungen der vorliegenden kumulativen Dissertationsschrift wurden an den Leibniz Laboratorien für Biotechnologie und artifizielle Organe (LEBAO) und REBIRTH – „Center for Regenerative Medicine" (Direktor: Prof. Dr. rer. nat. Ulrich Martin) der Klinik für Herz-, Thorax-, Transplantations- und Gefäßchirurgie, Medizinische Hochschule Hannover sowie der Klinik für Kardiologie des UniversitätsSpitals Zürich (Direktor: Prof. Dr. med. T. F. Lüscher) durchgeführt. Die Dissertationsschrift umfasst eine Auswahl von drei Originalarbeiten, die sich unter dem gemeinsamen Thema: „Etablierung eines neunen integrativen multimodalen Imaging-Ansatzes für das Monitoring von kardial transplantierten induzierten pluripotenten Stammzellen im präklinischen Großtiermodell" zusammenfassen lässt. Folgende Arbeiten sind im Anhang aufgeführt:

1. Schwanke K, Merkert S, **Templin C**, Jara-Avaca M, Müller S, Haverich A, Martin U, Zweigerdt R.
    Fast and Efficient Multi-transgenic Modification of Human Pluripotent Stem Cells.
    Human Gene Therapy, in revision.

2. **Templin C**, Zweigerdt R, Schwanke K, Olmer R, Ghadri JR, Emmert M, Müller E, Küest SM, Cohrs S, Schibli R, Kronen P, Hilbe M, Strunk D, Haverich A, Hoerstrup SP, Lüscher TF, Kaufmann PA, Landmesser U, Martin U.
    Transplantation and Tracking of Human Induced Pluripotent Stem Cells in a Pig Model of Myocardial Infarction: Assessment of Cell Survival, Engraftment and Distribution by Hybrid Single Photon Emission Computed Tomography/Computed Tomography of Sodium Iodide Symporter Trangene Expression.
    Circulation 2012 Jul 24;126(4):430-9.
    (Impact factor: 14.739)

3. Fiechter M, Ghadri JR, Sidler M, Martin U, Landmesser U, Kaufmann PA, Lüscher TF, **Templin C**.
    Cardiac Quadruple-Fusion Imaging: A Brief Report on a Novel Integrated Multimodality Approach for *in vivo* Visualization of Transplanted Stem Cells.
    Int J Cardiol. 2012 Jul 18. [Epub ahead of print].
    (Impact factor: 7.078)

gewidmet in Liebe und Dankbarkeit

meinen Eltern Lieselotte und Dieter Templin

Inhaltsverzeichnis

Abbildungsverzeichnis

# 1.	Zusammenfassung

Die regenerative Medizin hat das Potential mit neuartigen Therapiekonzepten der Stammzelltherapie erstmals Behandlungsoptionen für degenerative Erkrankungen und ausgedehnte Gewebeschäden zu bieten. Insbesondere die 2006 erstmals beschriebenen induzierten pluripotenten Stammzellen (iPSCs) stellen hierbei aufgrund ihrer pluripotenten Eigenschaften und fehlenden ethischen Bedenken eine attraktive Zellquelle dar. Bevor iPSCs jedoch klinisch eingesetzt werden können, müssen neben einem funktionellen Nutzen auch Sicherheitsaspekte der Zelltherapie analysiert werden. Um einen longitudinalen Nachweis der transplantierten Zellen *in vivo* zu gewährleisten sind spezielle Imaging-Verfahren notwendig.

Die Arbeiten der vorliegenden kumulativen Dissertationsschrift beschreiben systematisch den Einsatz Natrium-Iodid-Symporter transgener humaner iPSCs (NIS$^+$-iPSCs) in einem *ex vivo* und *in vivo* präklinischen Großtiermodell mit der Etablierung von nicht-invasiven Hybrid-SPECT-CT Imaging-Verfahren. So konnte zunächst gezeigt werden, dass transplantierte NIS$^+$-iPSCs in einem *ex vivo* Schweineherzen detektiert werden können. In einer weiteren Arbeit konnte dann in einem präklinischen porcinen Myokardinfarktmodell ein Imaging-Verfahren etabliert werden, welches zum einen die induzierte myokardiale Ischämie und zum anderen intramyokardial transplantierten iPSCs bis zu 15 Wochen nach der Applikation visualisiert. Interessanterweise zeigten die undifferenziert transplantierten iPSCs eine vaskuläre Differenzierung und ein besseres Überleben bzw. „Engraftment" nach Co-Transplantation von mesenchymalen Stammzellen. In der letzten Arbeit wurde dann ein 4-fach Multimodalitäten-Imaging etabliert, welches die myokardiale Ischämie (SPECT), die Injektionspunkte der iPSCs (NOGA) und die resultierende Radiotracer-Aufnahme der Zellen (SPECT) zusammen mit der kardialen Anatomie (CT) in *einem* dreidimensionalen Bild darstellt.

Zusammenfassend beschreiben die Arbeiten der vorliegenden kumulativen Dissertation die Anwendung von NIS$^+$-iPSCs von einem *ex vivo* Modell bis hin zum präklinischen Großtier. Die etablierten nicht-invasiven Imaging-Verfahren ermöglichen eine longitudinale *in vivo* Detektion der transplantierten iPSCs und können sowohl wichtige Hinweise zum Überleben bzw. „Engraftment" der Zellen als auch über mögliche Teratomentstehungen geben. Die Befunde dieser Dissertation können in Zukunft wichtige Beiträge für die Optimierung der Therapie mit iPSCs liefern.

Schlagwörter: Induzierte pluripotente Stammzellen, Myokardinfarkt, Natrium-Iodid-Symporter

1. Summary

Today for the first time ever, regenerative medicine's modern stem cell therapy concepts hold the potential to treat degenerative diseases and extensive tissue damage. Especially induced pluripotent stem cells (iPSCs), first described in 2006, represent an attractive source of cells - mainly because of their pluripotent characteristics and lack of associated ethical concerns. However, before iPSCs can be applied in the clinical setting, it is mandatory to analyze the advantages as well as the security aspects of stem cell therapy. To assure the longitudinal detection of transplanted cells *in vivo*, special imaging methods are necessary.

The publications comprised within this cumulative thesis systematically describe the use of sodium iodide symporter transgenic human iPSCs (NIS$^+$-iPSCs) in an *ex vivo* and *in vivo* large animal model by implementing non-invasive Hybrid-SPECT-CT imaging methods. It shows that transplanted NIS$^+$-iPSCs can be detected in an *ex vivo* porcine heart. As described in a second report, an imaging method could be established to visualize induced myocardial ischemia as well as intramyocardially transplanted iPSCs up to 15 weeks after their application. Interestingly, transplanted undifferentiated iPSCs showed a differentiation towards cells of a vascular phenotype and presented a prolonged life-span and engraftment after the co-transplantation of mesenchymal stem cells. The last paper within this thesis establishes a 4-fold multimodality imaging approach that visualizes myocardial ischemia (SPECT), the injection sites of the iPSCs (NOGA), the resulting radiotracer-uptake of the cells (SPECT) as well as the cardiac anatomy (CT) in only *one* three-dimensional image.

In summary, the papers of this cumulative thesis demonstrate the application of NIS$^+$-iPSCs beginning with an *ex vivo* model up to a pre-clinical large animal model. The described non-invasive imaging methods facilitate the longitudinal *in vivo* detection of transplanted iPSCs and can be used to monitor the cell's life-span and its engraftment, and hint to possible occurrences of teratomas. The findings of this thesis may contribute to an optimized therapeutic application of iPSCs in the future.

Key Wors: Induced pluripotent stem cells, myocardial infarction, sodium iodide symporter

2. Einleitung

2.1 Aktueller Stand der kardialen Stammzelltherapie

Herz-Kreislauferkrankungen stellen die Haupttodesursache in den industrialisierten Ländern dar.[1, 2] So verlieren Patienten mit einem großen Myokardinfarkt ca. 30% ihrer kontraktilen Myokardmasse. Trotz moderner pharmakologischer und interventioneller Therapieverfahren ist die Morbidität und Mortalität dieser Patienten mit schwer eingeschränkter linksventrikulärer Funktion nach Infarkt hoch.[1, 2] Die regenerative Medizin bietet hier erstmals die Möglichkeit eine Restauration bzw. Regeneration untergegangenes Myokardgewebe zu erreichen.[3-5] Stamm- und Progenitorzell-basierte Therapienansätze werden daher gegenwärtig intensiv als potentielle innovative neue Strategien für die Verbesserung der kardialen Funktion untersucht. In klinischen Studien werden am häufigsten Knochenmark-Progenitorzellen eingesetzt. Eine aktuelle Metaanalyse von 29 randomisierten Studien von intrakoronar infundierten oder G-CSF-mobilisierten Knochenmark-Progenitorzellen bei 1830 Patienten mit akutem Myokardinfarkt zeigte im Vergleich zu Kontrollpatienten eine Verbesserung der Ejektionsfraktion von 2,7% im Kurzzeit- und 3,31% im Langzeitverlauf.[6] Ein Benefit der G-CSF Therapie konnte nicht dokumentiert werden.[6] Obwohl erste Studien über eine kardiale Differenzierung adulter Stammzellen berichteten,[7, 8] ist man sich heute einig darüber, dass diese Zelltypen nicht oder wenn überhaupt nur mit sehr geringer Effizienz in Herzmuskelzellen differenzieren und somit auch nicht zu einer signifikanten kardialen Funktionverbesserung beitragen können.[9-11] Im Gegensatz hierzu zeigen embryonale Stammzellen ein robustes kardiales Differenzierungspotential und könnten daher prinzipiell als Quelle für Kardiomyozyten genutzt werden.[12-14] Aufgrund des embryonalen Ursprungs der Zellen stehen jedoch keine Patienten-eigenen Zellen zur Verfügung und eine allogene Transplantation würde für die Patienten eine lebenslange immunsuppressive Therapie bedeuten. Die erst kürzlich mit dem Nobelpreis für Medizin bedachte Reprogrammierung humaner somatischer Zellen in induzierte pluripotente Stammzellen (iPSCs) stellt hier eine extrem vielversprechende neue Option dar.[15-17] Da die iPSCs den embryonalen Stammzellen stark ähneln, jedoch aufgrund des autologen Ursprungs keinerlei ethische Bedenken bestehen, werden iPSCs generell als ein favorisierter Zelltyp für den Ersatz von Gewebeschäden oder degenerativen Erkrankungen angesehen.

2.2 Induzierte pluripotente Stammzellen als neue Zellquelle für die regenerative Medizin

Pluripotente humane embryonale Stammzellen (hESCs) gelten durch ihr potentiell unbegrenztes Expansions- und Differenzierungspotential seit einigen Jahren als aussichtsreiche Zellquelle für die regenerative Medizin.[18] Mit den erstmals in 2006 von Takahashi et al.[15] beschriebenen humanen induzierten pluripotenten Stammzellen (hiPSCs) existiert nun erstmals eine ethisch unbedenkliche Alternative zu humanen embryonalen Stammzellen, die darüber hinaus auch autolog verfügbar wäre und somit neue Möglichkeiten für den myokardialen Gewebeersatz bietet.[19-21] IPSCs können durch die Überexpression bestimmter Pluripotenz-assoziierter Transkriptionsfaktoren wie OCT4, SOX2, c-MYC und KLF4[15, 16] oder OCT4, SOX2, LIN28 und NANOG[17, 22] hergestellt werden und zeigen unter geeigneten Kulturbedingungen Charakteristika von ESCs wie unbegrenzte Selbsterneuerung und ein *in vivo* Differenzierungspotential in Zellen aller 3 Keimblätter. Im Hinblick auf eine mögliche therapeutische Anwendung pluripotenter Stammzellderivate konnten in den letzten Jahren deutliche Fortschritte erzielt werden. So konnten bereits durch die Verwendung episomaler oder Transposon-basierter Vektoren[23-25] sowie durch eine direkte Transduktion mit Proteinen[26] iPSCs ohne genomische Integration eines Transgens erzeugt werden. Weiterhin konnten erhebliche Fortschritte hinsichtlich Massenzellproduktion[27, 28] sowie effiziente und spezifische Differenzierungsprotokolle erzielt werden.[29]

2.3 Aktuelle Limitationen pluripotenter Stammzellen für eine klinische Anwendung

Der Einsatz pluripotenter Stammzellen in der regenerativen Medizin ist gegenwärtig noch aufgrund von zellbiologischen Problemen bzw. Risiken limitiert. Diese beinhalten geringe kardiale Differenzierungsraten, Sicherheitsrisiken, insbesondere durch das Potential Teratome und Tumore zu entwickeln, sowie die generelle Frage, ob transplantierte induzierte pluripotente Stammzellen nach einer intramyokardialen Zellapplikation ausreichend funktionstüchtiges Gewebe mit *de novo* Myokard und Gefäßen bilden, die dann zu einem klinischen Benefit führen können.[30] Weiterhin existieren generelle Applikations-bedingte Hürden durch die geringen „Engraftment"- und Retentionsraten applizierter Zellen.[31-33] Obwohl einige dieser Fragen auch in *in vitro* oder Kleintiermodellen adressiert werden können, sind andere nur in entsprechenden Großtiermodellen und der

damit verbundenen Nähe zum Menschen adäquat zu beantworten.[34] So sind transplantierte humane Kardiomyozyten aufgrund der unterschiedlichen Herzfrequenz von Mensch und Nager nicht in der Lage voll funktionstüchtig in Nagetiermyokard zu integrieren.[35] Daher kann eine aussagekräftige Beurteilung über die Regenerationsfähigkeit humaner Zellen nur in Großtieren wie Hund, Schwein oder Affe erfolgen.[34]

2.4   Methoden des Stammzell-Imagings

Moderne Bildgebungsverfahren haben einen wichtigen Stellenwert für die Entwicklung neuartiger regenerativer Therapiekonzepte. Imaging-Technologien, welche für die longitudinale Detektion von Zelltransplantaten eingesetzt werden, sollen idealerweise das Überleben der transplantierten Zellen, die Zellproliferation, sowie die Verteilung der Zellen oder sogar mögliche Differenzierungsprozesse visualisieren.[36] Gegenwärtig sind Transgen-basierte Imaging-Ansätze, die diesen Vorgaben entsprechen, beschränkt auf Biolumineszenzverfahren mit der Expression von Luciferase. Durch die eingeschränkte Gewebepenetration ist die Biolumineszenztechnologie jedoch auf die Anwendung im Kleintiermodell beschränkt.[37]

Bei Großtiermodellen hingegen kommt hauptsächlich die Magnetresonanztomographie für die Detektion Nanopartikel-markierter Zellen zum Einsatz (Abbildung 1).[38, 39] Der Hauptnachteil dieses Zellnachweises ist jedoch das Unvermögen vitale Zellen von Nanopartikel-markierten toten Zellen bzw. Empfängerzellen wie Makrophagen, welche Zelldebris aufgenommen haben, zu unterscheiden.[38, 39] In anderen Großtierstudien wurden direkte Radionuklid-Imaging-Ansätze verwendet (*direktes Zell-Labeling*). Hierbei wurden die Zellen vor der Transplantation mit „18F-2-Fluor-2-deoxy-D-glucose" (^{18}F-FDG), Indium-111 (In^{111}), „64Cu-pyruvaldehyde-bis(N4-methylthiosemicarbazone)" (^{64}Cu-PTSM) oder „Technetium-99-Hexamethylprophylene amine oxine" (^{99m}Tc) inkubiert und anschließend mittels Positronenemissionstomographie (PET) oder Single-Photon-Emissions-Computertomographie (SPECT) nachgewiesen (Abbildung 1).[38, 39] Ein szintigraphischer Tracer besteht aus zwei Komponenten: Ein Molekül, welches spezifisch an ein molekulares Target bindet (z.B. Rezeptor) und daher über die Verteilung des Tracers entscheidet sowie aus einem radioaktiven Isotop, das die Detektion des Moleküls in der SPECT oder PET ermöglicht. Die Sensitivität der Zelldetektion ist mittels PET (femtomolar) höher als bei der SPECT (nanomolar). SPECT-basierte Imaging-Ansätze haben jedoch den Vorteil, dass simultane Signale unterschiedicher Energien (80-250 keV)

durch die Variation der Detektionsfenster aufgezeichnet werden können.[40] Limitationen dieser direkten Imaging-Verfahren sind die eingeschränkten Halbwertzeiten sowie die natürliche Elimination des Radiotracers aus den Zellen, welches zu einem entsprechendem Signalverlust führt. Daher eignen sich direkte Imaging-Verfahren nicht für einen longitudinalen Zellnachweis.[38, 39] Zusätzlich wurden für magnetische Nanopartikel und Radionuklide wie In[111] zelltoxische Eigenschaften beschrieben.[38, 39]

Eine andere Strategie verfolgt das *indirekte Zell-Labeling*, welches einen Transgen-basierten Zellnachweis darstellt (Abbildung 1). In einer ersten Pilotstudie wurde eine Herpes-Simplex-Thymidin-Kinase (HSVtk)-vermittelte Phosphorylierung von „9-[4-[18F]fluoro-3-(hydroxymethyl)butyl]guanine" ([18F]FHBG) als Transgen-basierter Imaging-Ansatz in Großtiermodellen evaluiert.[41, 42] Die Detektion applizierter Zellen wurde jedoch nur für einige Stunden nach Transplantation beschrieben.[41, 42] Ein anderer vielversprechender Ansatz, welcher die Detektion vitaler transplantierter Zellen durch nuklearmedizinische Verfahren wie PET oder SPECT nach Iod (^{123}I) oder ^{99m}Tc Radiotracerapplikation erlaubt, wurde kürzlich entwickelt. Diese Technologie basiert auf der transgenen Expression des Natrium-Iodid-Symporters (NIS) in transplantierten Zellen.[43] Die physiologische NIS-Expression im adulten Organismus ist auf die Schilddrüse, Magenschleimhaut und Speicheldrüse beschränkt und ist nicht detektierbar in Extremitäten, dem Gehirn oder anderen inneren Organen wie dem Herzen.[43] Die NIS-vermittelte Anreicherung von Iodid in der Schilddrüse ist ein aktiver Transportprozeß, welcher an der basolateralen Plasmamembran der Schilddrüsenfollikelzellen gegen den elektrochemischen Iodidgradienten, stimuliert durch das Thyroid-stimulierende Hormon (TSH), stattfindet und spezifisch durch Perchlorat inhibiert werden kann. Klinisch stellt die NIS-Expression die Basis für die Schilddrüsenkarzinomdiagnostik und effektive Behandlung von Metastasen durch radioaktive Iodid-Isotop Applikation dar.[43] Das Imaging des NIS-Transgens bietet entscheidende Vorteile im Hinblick auf eine klinische Applikation für die longitudinale Detektion von transplantierten Stammzellen. Diese beinhalten das Fehlen der Immunogenität des humanen NIS-Transgens und die Tatsache, dass der nuklearmedizinische Nachweis von Radiotracern wie ^{99m}Tc and ^{123}I eine relativ kostengünstige und weitverbreitete Technologie ist. Weiterhin zeigen Fortschritte in der Quantifizierung von Tracersignalen mittels klinisch eingesetzter SPECT-Geräte das Potential dieses Ansatzes für den Nachweis zellulärer Transplantate in präklinischen Großtiermodellen und Patienten.[44]
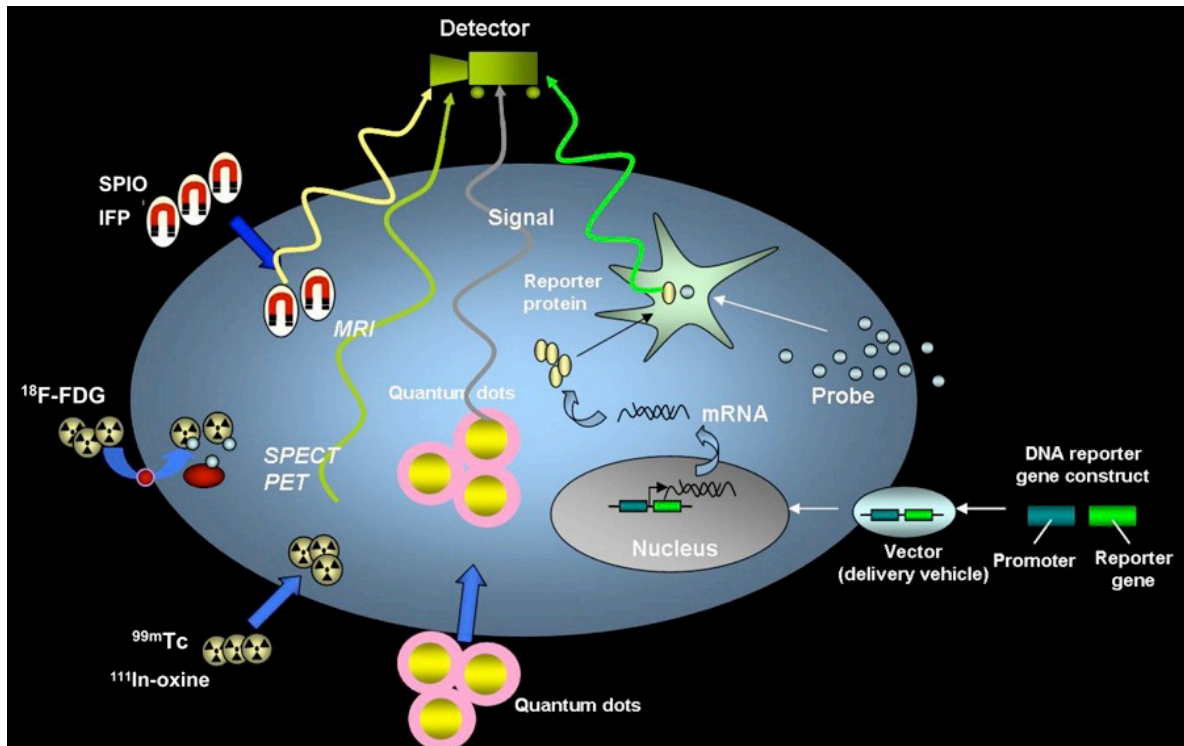
Abbildung 1: Methoden des Stammzell-Imagings (Abbildung aus Wu, JC et al. JNM, 2010)[38]
Direkte Nachweismethoden beinhalten die Markierung der Zellen mit magnetischen Nanopartikeln
(„superparamagnetic iron oxide" = SPIO; „iron fluorescent particles" = IFP) und die Detektion
mittels Magnetresonanztomographie oder das Inkubieren der Zellen mit Radiotracern wie ^{99m}TC,
In^{111} oder ^{18}F-FDG und die Detektion mittels nuklearmedizinischer Techniken wie SPECT oder
PET. Beim indirekten Zellnachweis wird vor der Zelltransplantation ein Reportergen in die Zellen
eingeschleust, welches sich in das Genom der Zellen integriert und *in vivo* durch die Applikation
eines Substrates mittels SPECT oder PET visualisiert werden kann.

2.5   Die kumulative Dissertationsschrift im Kontext der Forschung

Die Anwendung pluripotenter Stammzellen für die Therapie des akuten Myokardinfarktes
und der chronisch ischämischen Kardiomyopathie stellt ein neues hochinnovatives
Therapiekonzept dar, welches erstmals darauf abzielt, eine wirkliche Regeneration des
infarzierten Myokards zu erreichen und somit die Perspektive eröffnet, die eingeschränkte
Funktion wieder herzustellen. Vor einer klinischen Anwendung einer solchen Zelltherapie
sind jedoch noch eine Reihe offener Fragen, insbesondere Aspekte zur Sicherheit und
Effektivität zu adressieren. Grundvoraussetzung für weiterführende Untersuchungen an
pluripotenten Stammzellen ist die Etablierung präklinischer Großtiermodelle mit
entsprechenden Imaging-Modalitäten für den longitudinalen Nachweis von vitalen
transplantierten Stammzellen.

Im Rahmen der vorliegenden Dissertationsschrift werden drei aufeinander folgende experimentelle Arbeiten über die Etablierung eines solchen neuen integrativen multimodalen Imaging-Ansatzes für die Visualisierung von kardial transplantierten humanen induzierten pluripotenten Stammzellen beschrieben und diskutiert.

3 Ergebnisse und Diskussion

3.1 Publikation 1: „Fast and Efficient Multi-transgenic Modification of Human Pluripotent Stem Cells"

Schwanke K, Merkert S, Templin C, Jara-Avaca M, Müller S, Haverich A, Martin U, Zweigerdt R.

Human Gene Therapy, in revision.

In der Untersuchung *„Fast and Efficient Multi-transgenic Modification of Human Pluripotent Stem Cells"* wurde ein unkomplizierter Ansatz für das schnelle und hocheffiziente parallele Integrieren mehrerer Plasmide in humane pluripotente Stammzellen (hPSCs) beschrieben. Hierbei wurden multi-transgene Klone durch eine einzige Medikamentenresistenz auf einem Plasmid etabliert. Der Vorteil dieser Methode ist die direkte Anwendung auf konventionelle „Feeder"-basierte Zellkulturen ohne die Adaptation der hPSCs auf die Einzelzellkultur vor der genetischen Manipulation. Diese etablierten multi-trangenen hPSCs exprimieren unter anderem den NIS, der eine nicht-invasive Detektion transplantierter Stammzellen mittels SPECT-Computertomographie (CT) Imaging ermöglicht.[45]

HPSCs, wie ESCs und iPSCs sind aufgrund ihres extensiven Expansionspotentials und der Differenzierungsfähigkeit in alle somatischen Zelllinien eine bevorzugte Zellquelle für die regenerative Medizin. Die Integration bestimmter Transgene in hPSCs stellt eine wichtige Grundvoraussetzung für die präklinische Anwendung wie Zellaufreinigung bestimmter Zelllinien während der Differenzierung[46-48] und das *in vivo* Monitoring[49] in relevanten Großtiermodellen dar.

In den letzten Jahren wurden eine Reihe genetischer Methoden zur Manipulation hPSCs wie die virale Transduktion,[50, 51] chemische Transfektion[52] und Elektroporation[53, 54] etabliert. Obwohl mit lentiviralen Vektoren eine hohe Transduktionseffizienz von >90% und eine hohe initiale Transgenexpression erzielt werden kann,[55, 56] ist eine substantielle Suppression der Langzeitexpression des Transgens für HIV-abgeleitete Vektoren beschrieben.[57, 58] Weiterhin kann die Integration viraler Vektoren zur Insertionsmutagenese mit der Aktivierung oder Inaktivierung von Tumorsuppressorgenen und malignen Transformation von Zellen führen.[59] Letztendlich stellt die Produktion viraler Vektoren eine zeitintensive Methode dar und bedarf Einrichtungen mit erhöhter Sicherheitsstufe. Die Technik der Plasmidtransfektion beinhaltet sowohl die

Elektroporation als auch Methoden der chemische Transfektion. Die Generation stabiler Klone ist bei der chemischen Transfektion gewöhnlich niedriger[52] und stark Zelllinien-abhängig.[60] Bei der Elektroporation wird die Plasmamembran transient durch elektrische Pulse permeabilisiert und erlaubt die Aufnahme exogener Nukleinsäuremoleküle, welche nur in relativ geringem Maße durch die Vektorgröße limitiert ist.[61] Die Anwendung der Elektroporation setzt bisher jedoch die Generierung von Einzelzellsuspensionen voraus,[62] welches bei hPSCs jedoch zu einer deutlichen Abnahme der Zellviabilität nach der Elektroporation führt.

Im Rahmen dieser Arbeit wurde erstmals die schnelle und hocheffiziente Generierung multi-transgener hPSC beschrieben, welche die direkte Anwendung auf „Feeder"-basierten Zellkulturen erlaubt. Der eigene Beitrag zu dieser Publikation war die funktionelle Testung der generierten transgenen NIS$^+$-hiPSCs in *ex vivo* Schweineherzen und die anschließende Etablierung des Zellnachweises mittels SPECT-CT Imaging.

Die hiPSCs trugen zwei Plasmide, welche 4 funktionelle Transgene exprimierten. Diese waren das Plasmit αMHCneoPGKhygro, welches eine klonale Selektion und eine Kardiomyozytenanreicherung nach Differenzierungsinduktion erlaubte. Der co-transfizierte bizistronische Vektor pCAG_rNIS_IRES2_Venus_nucmem kodiert für den transmembranen Ratten NIS. Die endogene Expression des NIS befindet sich exklusiv in der Schilddrüse, Speicheldrüse und Magenschleimhaut und führt zu einer aktiven Aufnahme von Iodid-Isotopen in diesen Zellen, so dass mittels nuklearmedizinischen Bildgebungstechniken wie SPECT oder PET eine Radiotraceraufnahme visualisiert werden kann. Die generierten transgenen Klone exprimierten zudem das nukleäre Venus, welches für die Identifizierung der injizierten Zellen in situ verwendet wurde. Zur Testung der funktionellen Aktivität wurden NIS$^+$-hIPSCs mit ^{123}I inkubiert und intramyokardial mit einem klinisch einsetzbaren Injektionskatheter (MyoStar) in *ex vivo* Schweineherzen appliziert. Um eine spätere *in vivo* Situation zu simulieren wurde zur Absorptionsschwächung eine Schweine-Thoraxwand über die Herzen gelegt. Die Detektion applizierter NIS$^+$-hiPSCs erfolgte anschließend mit einem klinischen Hybrid-SPECT-CT-Scanner (Abbildung 2).
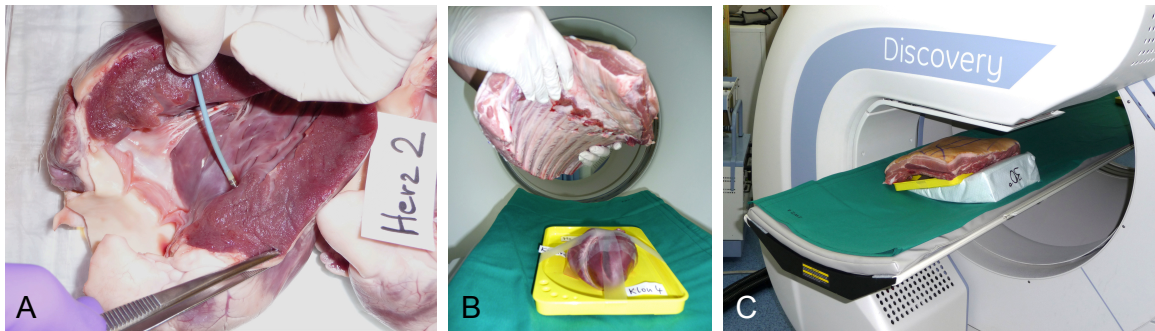
Abbildung 2: *Ex vivo* Stammzellapplikation und Nachweis mittels Hybrid-SPECT-CT Imaging

A.) *Ex vivo* Applikation ^{123}I markierter NIS+-hiPSCs mittels MyoStar-Injektionskatheter.

B.) Plazierung einer porcinen Thoraxwand über das Schweineherz zur Simulation der Absorptionsschwächung.

C.) Durchführung des Hybrid-SPECT-CT Imagings (Discovery NM 570C, GE Healthcare).

Hybrid-SPECT-CT Aufnahmen zeigten deutlich die Radiotraceraktivität in den Bereichen der injizierten NIS+-hiPSCs (Abbildung 3). Diese Etablierungsarbeiten stellten die Grundlage für die weiteren Arbeiten zur *in vivo* Transplantation und Detektion NIS+-hiPSCs dar.
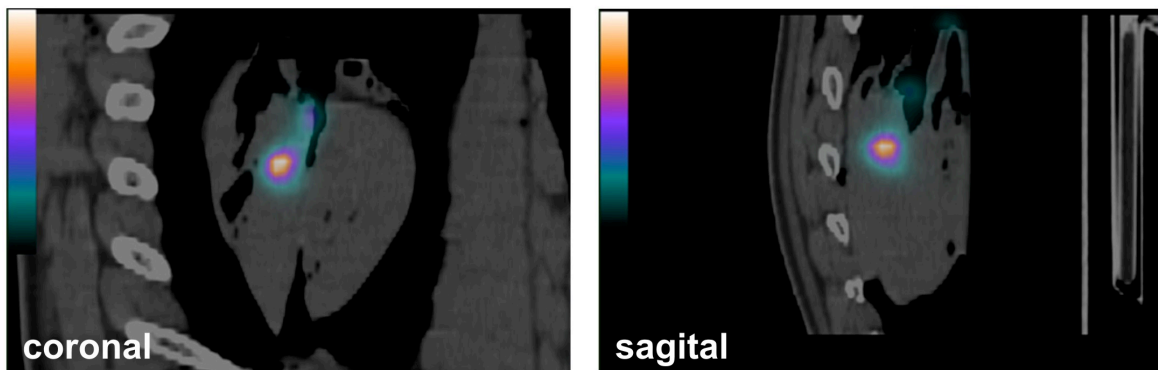
Abbildung 3: *Ex vivo* SPECT-CT Imaging ^{123}I markierter NIS+-hiPSCs

SPECT Signal nach Applikation von 5×10^6 ^{123}I markierter NIS+-hiPSCs in der coronalen und sagitalen Sicht.

3.2 Publikation 2: „Transplantation and Tracking of Human Induced Pluripotent Stem Cells in a Pig Model of Myocardial Infarction: Assessment of Cell Survival, Engraftment and Distribution by Hybrid Single Photon Emission Computed Tomography/Computed Tomography of Sodium Iodide Symporter Trangene Expression"

Templin C, Zweigerdt R, Schwanke K, Olmer R, Ghadri JR, Emmert M, Müller E, Küest SM, Cohrs S, Schibli R, Kronen P, Hilbe M, Strunk D, Haverich A, Hoerstrup SP, Lüscher TF, Kaufmann PA, Landmesser U, Martin U.
Circulation 2012 Jul 24;126(4):430-9.

In der Arbeit *„Transplantation and Tracking of Human Induced Pluripotent Stem Cells in a Pig Model of Myocardial Infarction: Assessment of Cell Survival, Engraftment and Distribution by Hybrid Single Photon Emission Computed Tomography/Computed Tomography of Sodium Iodide Symporter Trangene Expression"* wurde eine Transgen-basierte Nuklear-Hybrid Imaging-Methode etabliert, um hiPSCs in einem präklinischen Myokardinfarkt-Großtiermodell nach intramyokardialer Transplantation zu detektieren. Die Verfügbarkeit einer Transgen-basierten Imaging-Technologie, welche auch für Großtiere angewandt werden kann und zudem nicht-toxisch, nicht-invasive und in longitudinalen Untersuchungen vitale Zelltransplantate visualisieren kann, stellt für die Weiterentwicklung der präklinischen und klinischen kardialen Zelltherapie eine Grundvoraussetzung dar.

Zunächst wurden hiPSCs (Klon hCBiPSC2)[20] mit dem bizistronischen Vektor pCAG_rNIS_IRES2_Venus_nucmem (NIS = Natrium-Iodid-Symporter, Venus = Fluorenzenzprotein) und dem Plasmid αMHCneoPGKhygro,[48] welcher eine Selektion Hygromycin-resistenter Klone erlaubt, co-transfiziert. Anschließend wurden transgene- und Kontrollzellen für die NIS-spezifische Iodid-Aufnahme durch *in vitro* Inkubation mit ^{125}I, einem Isotop mit einer Halbwertzeit von 59 Tagen, analysiert. Die intrazelluläre Labeling-Effizienz ist abhängig von der entsprechenden Halbwertzeit des Isotops und der Kinetik der Isotopanreicherung bzw. -abgabe. Die ^{125}I Aufnahme in NIS$^+$-hiPSCs erreichte ein Plateau nach ~ 90 Minuten. Insgesamt zeigte sich in NIS$^+$-hiPSCs eine ~ 100-fach höhere ^{125}I Anreicherung als für nicht-transgene hiPSC Kontrollzellen. Zudem konnte die komplette Iodid Aufnahme durch den spezifischen NIS-Blocker Perchlorat unterdrückt werden. Das Maximun der ^{125}I Akkumulation wurde innerhalb von 2 Stunden wieder in das Medium freigegeben (Abbildung 4). Hervorzuheben ist, dass weder die NIS-Expression noch das Radio-Labeling die Zellviabilität beeinflußt hat.
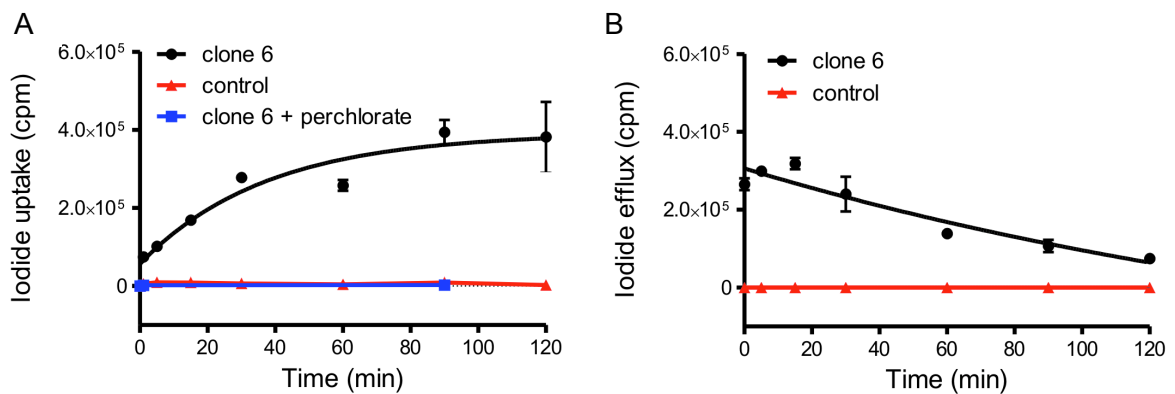
Abbildung 4: Kinetik der ^{125}Iodid-Aufnahme und -Abgabe NIS^{+}-hiPSCs

A.) Die ^{125}Iodid-Akkumulation in NIS^{+}-hiPSCs zeigte eine maximale Aufnahme von ~ 100 über der Hintergrundaktivität und erreichte einen Staedy-State nach 90 Minuten. Kontroll-transduzierte und mit Perchlorat (100 μmol/L) geblockte NIS^{+}-hiPSCs zeigten keine ^{125}Iodid-Aufnahme.

B.) ^{125}Iodid-Abgabe aus NIS^{+}-hiPSCs.

In *ex vivo* Schweineherzen wurde das Detektionslimit von ^{123}I prä-markierten NIS^{+}-hiPSCs nach intramyokardialer Injektion mittels SPECT-CT analysiert. Hierzu wurden gleiche Volumen einer Verdünnungsreihe der markierten Zellen appliziert. Um die Gewebeabsorption *in vivo* zu simulieren, wurde eine explantierte Schweine-Thoraxwand über die Herzen gelegt. Die Detektionsgrenze der NIS^{+}-hiPSCs in *ex vivo* Schweineherzen lag bei 1×10^{5} Zellen (Abbildung 5).
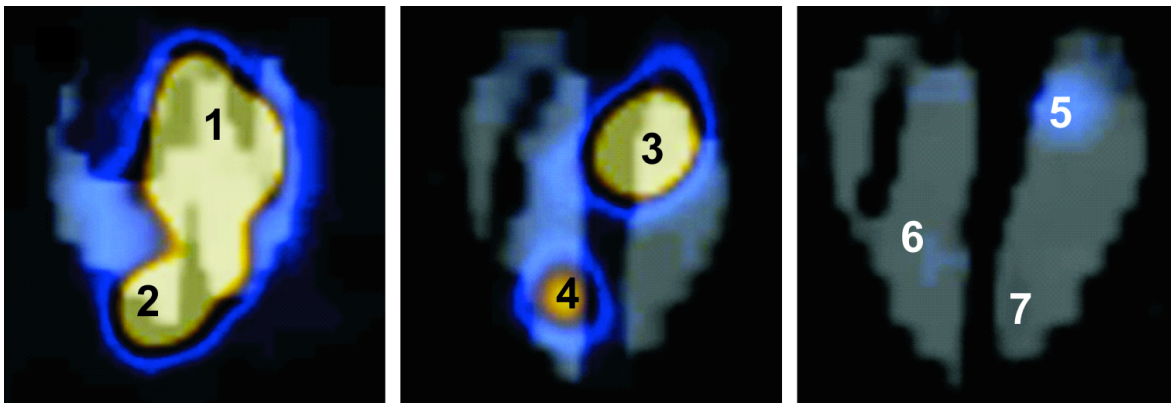
Abbildung 5: *Ex vivo* SPECT-CT Imaging einer Verdünnungsreiche NIS^{+}-hiPSCs nach intramyokardialer Applikation
Verdünnungsreihe: 1 = $1{,}2 \times 10^{7}$; 2 = 6×10^{6}; 3 = 3×10^{6}; 4 = 1×10^{6}; 5 = 5×10^{5}; 6 = 1×10^{5}; 7 = 1×10^{4}. Injizierte NIS^{+}-hiPSCs zeigten eine Detektionsgrenze bis zu 1×10^{5} Zellen.

Aufbauend auf diesen Ergebnissen wurden für weitere *in vivo* Experimente basierend auf einer hypothetischen Detektionsschwelle von ~ 2 % persistierender Zellen 5×10^{7} prä-markierte NIS^{+}-hiPSCs appliziert. Die dokumentierte Zell-Detektionsgrenze entspricht in

etwa den bisher publizierten Daten in Rattenherzen von Terrovitis et al., die $1,5 \times 10^5$ Zellen als minimale Grenze nachweisen konnten.[63] Erwähnenswert ist jedoch, dass diese beiden Versuchsansätze aufgrund folgender Unterschiede nicht direkt vergleichbar sind: 1.) unterschiedliche Vektorsysteme und Markierungsansätze (NIS-SPECT versus HSVtk-PET), 2.) andere Zelltypen (hiPSCs versus kardiale Stammzellen), 3.) unterschiedliche Signalabschwächung durch umliegendes Gewebe (Schweinethorax versus Rattenthorax). Weitere Vorteile des NIS-SPECT Imagings gegenüber des HSVtk-PET Imagings ist die weitverbreitete Verfügbarkeit des SPECT und die Verwendung herkömmlicher Radiotracer ohne die Notwendigkeit spezieller Tracer-Syntheseeinrichtungen sowie die fehlende Immunogenität des NIS, welche insbesondere für die Langzeitdetektion von Zellen wichtig sein kann.

Für die *in vivo* Versuche wurde zunächst bei 13 Schweinen durch eine 180 minütige Ballonokklusion im mittleren Drittel des Ramus interventricularis anterior (RIVA) ein experimenteller Myokardinfarkt induziert. Während dieser Zeit zeigten sich die typischen ischämischen EKG-Veränderungen (ST-Streckenhebungen in den Ableitungen I, aVL, V1 bis V5) eines anterioren Myokardinfarktes (Abbildung 6).
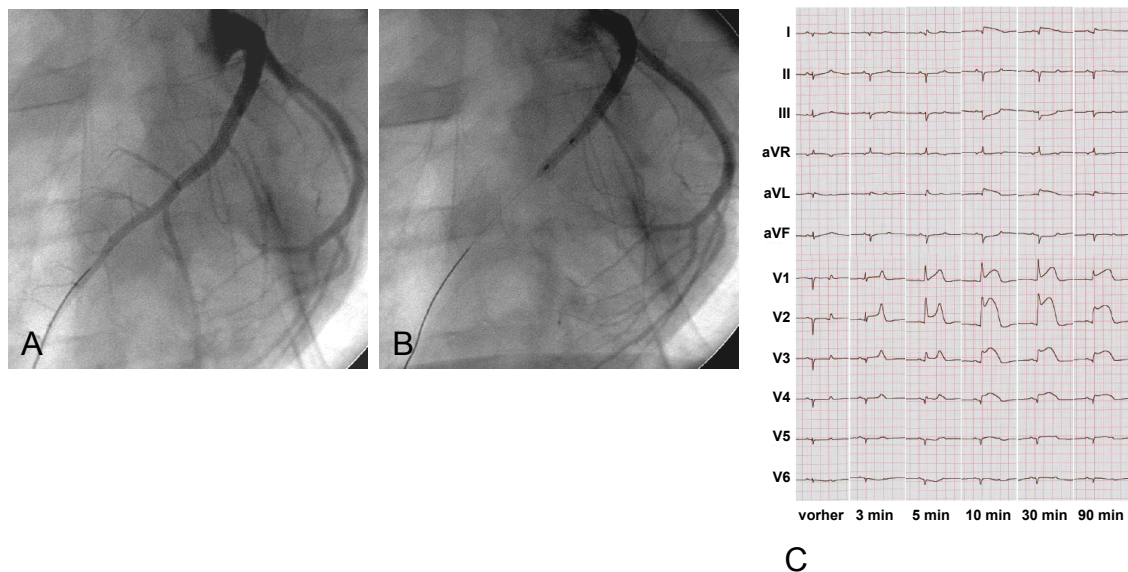
Abbildung 6: Infarktinduktion durch intrakoronare Ballonokklusion
Koronarangiographie eines Versuchsschweins mit A.) Drahtpassage des Ramus interventricularis anterior (RIVA) und B.) Ballonokklusion im mittleren Drittel des RIVA. Während der Zeit der Ballonokklusion konnten typische elektrokardiographische Ischämiezeichen (ST-Streckenhebungen in den Ableitungen I, aVL, V1 bis V5) eines anterioren Myokardinfarktes dokumentiert werden (C).

Aufgrund von peri- und postinterventionellen Ausfällen konnten 10 Tiere in die Studie eingeschlossen werden (Abbildung 7).

13 pigs underwent MI

2 pigs died during MI induction

1 pig died at the first postoperative day

10 pigs enrolled

10 mg/kg CsA and 2.5 mg/kg prednisolon daily

2 pigs received PBS	8 pigs received iPSCs

SPECT-CT after PBS / iPSC injection (day 0)

2 iPSC pigs completed **1 day follow-up:** -SPECT-CT -(Immuno-)histology	3 iPSC pigs completed **5 day follow-up:** -SPECT-CT -(Immuno-)histology	3 iPSC pigs completed **12-15 week follow-up:** -SPECT-CT -(Immuno-)histology

Abbildung 7: Studiendesign der *in vivo* Versuche

Zehn Tage nach Infarktinduktion wurde eine SPECT-CT zur Dokumentation des myokardialen Perfusionsdefektes durchgeführt. Die Infarktausdehnung wurde anschließend auch mittels dreidimensionalem (3D) NOGA-Mapping bestätigt. Dieses Mapping diente auch als Vorbereitung für die anschließende Zelltransplantation, da im Randgebiet des Infarktes die Applikationsareale definiert wurden. Die Zellapplikation selbst erfolgte über den MyoStar Applikationskatheter, welcher über die Arteria carotis retrograd über die Aortenkalppe in den linken Ventrikel eingeführt wurde, so dass die ^{123}I prä-markierten NIS$^+$-hiPSCs (5×10^7 hiPSCs oder 5×10^7 hiPSCs co-appliziert mit 5×10^7 humanen mesenchymalen Stammzellen, MSCs) bzw. ^{123}I prä-markierten NIS$^-$-Kontrollzellen von endokardial in zuvor definierte Areale im Randgebiet des Infarktes appliziert werden konnten (Abbildung 8).
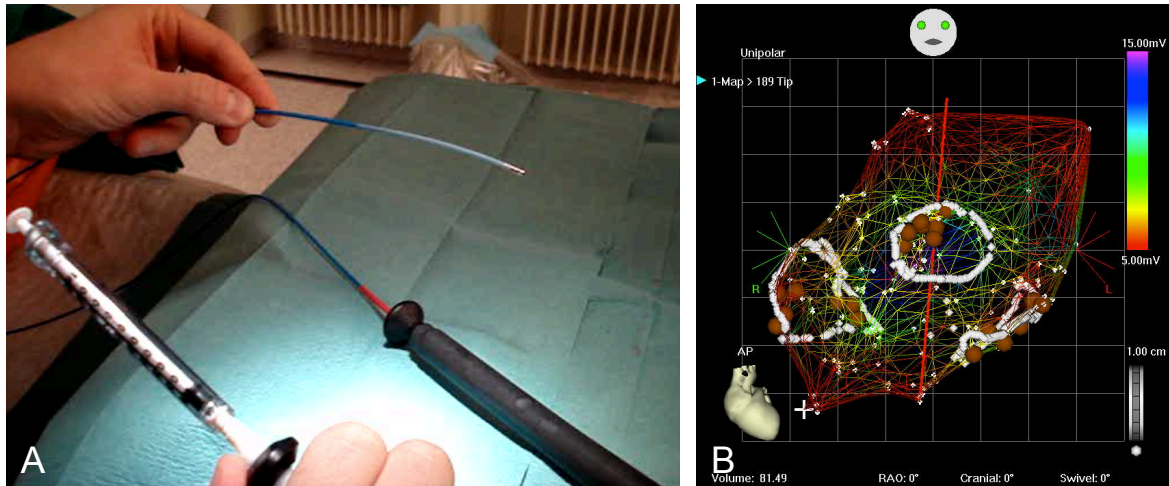
Abbildung 8: MyoStar-Injektionskatheter und NOGA-Mapping

A.) MyoStar-Injektionskatheter mit aufgesetzter Spritze am proximalen Ende und beweglicher Nadel am distalen Ende.

B.) NOGA-Mapping des linken Ventrikels mit eingezeichneten Applikationsarealen (weiße Kreise) und erfolgten Stammzellinjektionen (braune Punkte).

Die ersten postinterventionellen SPECT-CTs erfolgten 1-3 Stunden nach der Zelltransplantation. Hier zeigten sich entsprechend den NIS$^+$-hiPSCs Applikationsarealen intensive ^{123}I Signale im Septum und in der Lateralwand des linken Ventrikels. Wie erwartet konnten im Bereich der applizierten NIS$^-$-Kontrollzellen (anteriore Wand) keine ^{123}I Signale detektiert werden (Abbildung 9). Interessanterweise konnten jeweils intensivere SPECT-Signale in den Bereichen dokumentiert werden, in denen MSCs co-transplantiert wurden. Dies könnte auf eine verbesserte Retentionsrate der hiPSCs im Myokard hindeuten. Die höchste Signalintensität wurde in den ersten Stunden nach der Zelltransplantation nachgewiesen und zeigte dann eine kontinuierliche Abnahme, so dass nach 24 Stunden kein Signal mehr dokumentiert werden konnte (Abbildung 10). Wie erwartet zeigten SPECT-CT Aufnahmen von Kontrolltieren die mit PBS behandelt wurden keine Traceraufnahme. Immunhistologische Analysen zeigten deutlich die Stichkanäle im Myokard. Zudem konnten in den Bereichen, in denen NIS$^+$-hiPSCs transplantiert wurden, rundliche Zellen mit einer Fraktion von Venus$^+$ und OCT4$^+$ Zellen dokumentiert werden (Abbildung 9).

SPECT/CT imaging of myocardial perfusion (7 days after myocardial infarction)

NOGA-mapping of myocardial infarction and sites of cell injection (7 days after myocardial infarction)

SPECT/CT imaging of ^{123}I for detection of hiPSC grafts (3 hours after pre-labeled NIS$^+$ hiPSC injection)

Anti-VENUS

Anti-OCT4

100 µm

100 µm
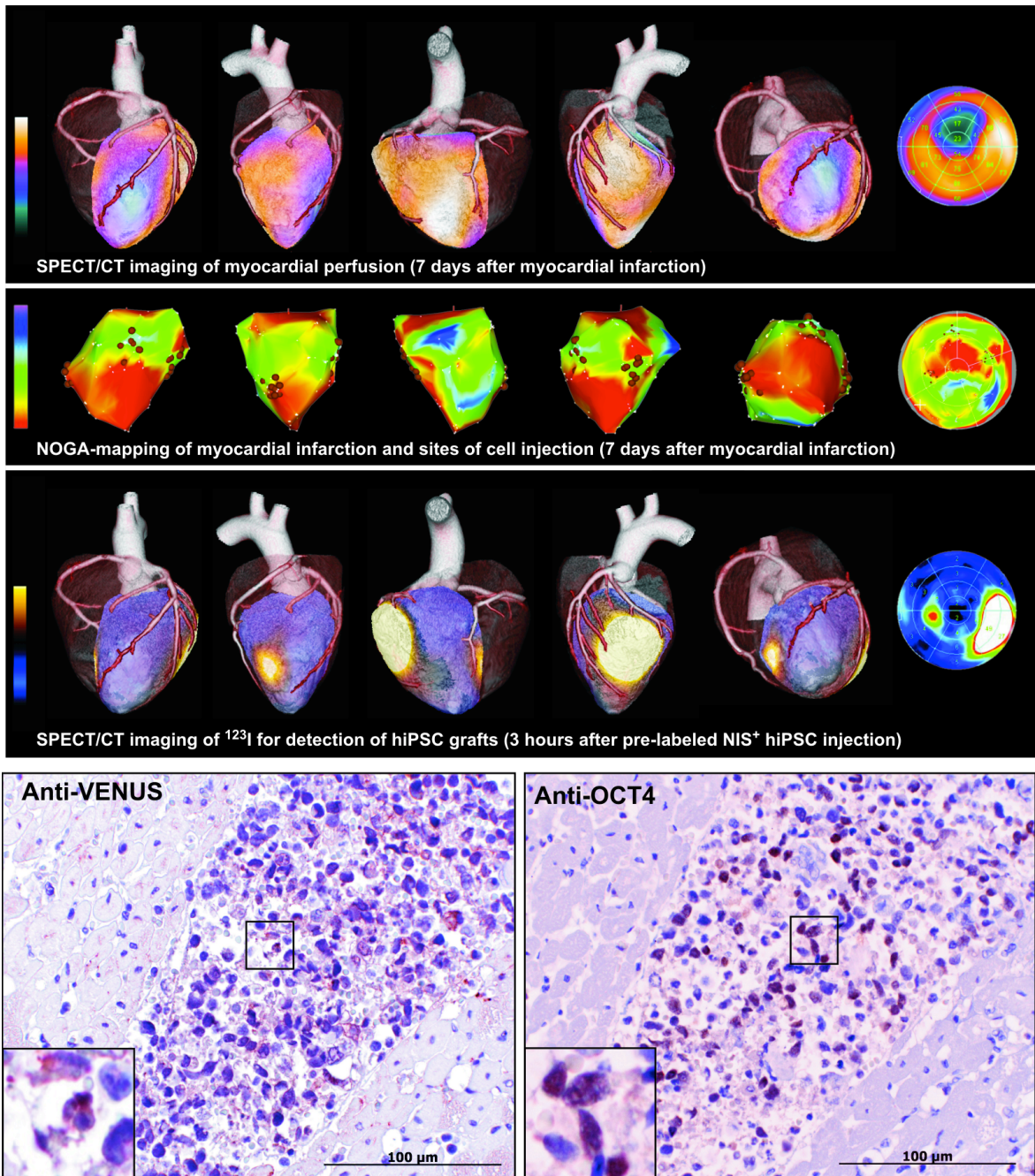
Abbildung 9: *In vivo* **Hybrid-SPECT-CT Imaging zur Detektion des myokardialen Perfusionsdefektes und der transplatierten NIS$^+$-hiPSCs**

1. Zeile: *In vivo* SPECT-CT des linken Ventrikels zur Darstellung des myokardialen Perfusionsdefektes (blaue Areale) nach experimentellem Infarkt. Die gelben/orangen Areale stellen normal perfundiertes Myokard dar.

2. Zeile: 3D-NOGA-Mapping des linken Ventrikels zur Darstellung des Infarktgebietes (rote Areale). Vitale Bereiche imponieren als grün-blaue Areale. Stammzellinjektionspunkte sind als braune Punkte im Randgebiet des Infarktes zu erkennen.

3. Zeile: SPECT-CT Aufnahmen des linken Ventrikels eine Stunde nach Stammzellinjektion zeigen intensive ^{123}I Signale (gelbe Areale) in der lateralen und septalen Wand und korrespondierten exakt mit den Stammzellinjektionspunkten aus dem NOGA-Mapping. Kontrollzellen (anteriore Wand) zeigen keine ^{123}I Traceraufnahme. Die Co-Applikation humaner MSCs steigert deutlich die

Signalintensität (laterale Wand).

Immunhistochemie: Immunhistologische Färbungen der lateralen Wand zeigen einen Injektionskanal 6 Stunden nach Zellapplikation mit co-transplantierten humanen MSCs und Venus$^+$-NIS$^+$-hiPSCs (gefärbt mit einem kreuz-reagierenden anti-GFP-Antikörper und anti-OCT4-Antikörper).
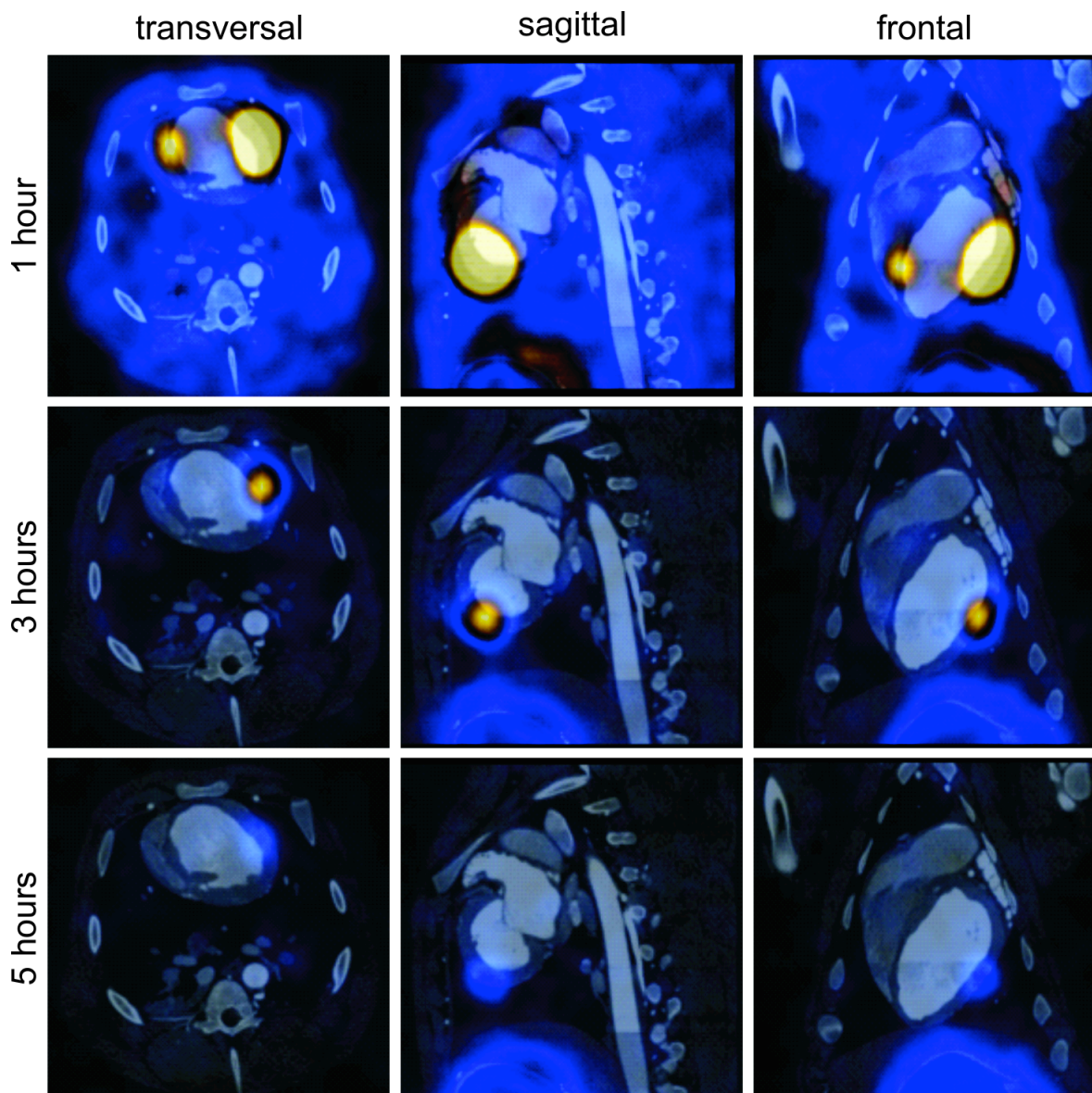
Abbildung 10: *In vivo* **Hybrid-SPECT-CT Imaging transplantierter** ^{123}**I-markierter NIS$^+$-hiPSCs zeigt einen deutlichen Signalverlust innerhalb der ersten 5 Stunden nach Zellapplikation**
In vivo SPECT-CT Aufnahmen (transversal, sagittal und frontal) eines Schweineherzens 1, 3 und 5 Stunden nach Zellapplikation. In der transversalen und frontalen Sicht sind zwei ^{123}I Signale zu erkennen. Der hellere Bereich entspricht dem Areal, in dem ^{123}I prä-markierte hiPSCs mit humanen MSCs co-transplantiert wurden; der weniger stark leuchtende Bereich entspricht einem Areal, in dem ^{123}I prä-markierte hiPSCs alleine transplantiert wurden. 5 Stunden nach Zellapplikation ist kaum noch ein Signal detektierbar.

Eine semiquantitative Analyse der ^{123}I SPECT Signale der beiden Schweine, welche nach einem Tag geopfert wurden, zeigte, dass in den Bereichen, in denen hiPSCs und MSCs gemeinsam transplantiert wurden, ein 6,8-fach bzw. 1,7-fach stärkeres Signal dokumentiert werden konnte, als in den Bereichen, in denen hiPSCs alleine appliziert wurden.

Für die Detektion transplantierter NIS[+]-hiPSC Derivative 5 Tage und 12-15 Wochen nach intramyokardialer Zellinjektion wurde den Schweinen der Radiotracer ^{123}I intrakoronar über den RIVA, den Ramus circumflexus und der rechten Koronararterie infundiert. Eine Stunde nach der Tracerinjektion erfolgten die SPECT-CT Aufnahmen zur Detektion des resultierenden [123]I Signals. Eine Übersicht über die angewandten Imaging-Protokolle stellt Abbildung 11 dar.
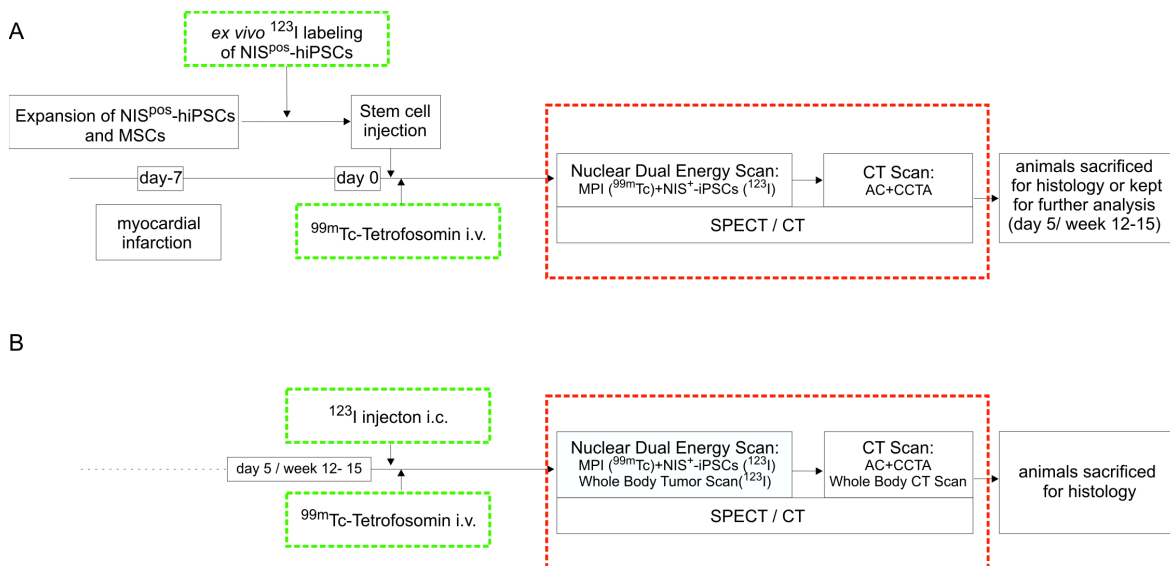
Abbildung11: Schematische Übersicht über die angewandten Imaging-Protokolle
A.) Imaging von *ex vivo* markierten iPSCs kombiniert mit einem myokardialen Perfusions-Imaging gefolgt von einer Computertomographie.
B.) Follow up Imaging mit identischem Protokoll nach intrakoronarer Injektion von [123]I für die *in vivo* iPSC Markierung. Anschließend wurde ein Ganzkörper SPECT-CT Scan zur möglichen Tumordetektion ergänzt.
Abkürzungen: AC = „attenuation correction" (=Schwächungskorrektur), CCTA = „coronary computed tomography angiography" (=koronare Computertomographie Angiographie), MPI = „myocardial perfusion imaging" (myokardiale Perfusionsbildgebung).

Wie erwartet konnte eine hohe Traceraufnahme in der Schilddrüse und eine etwas schwächere Traceraufnahme in der Magenschleimhaut verzeichnet werden. Interessanterweise konnte in den Herzen nur in den Bereichen ein [123]I Signal detektiert werden, in denen neben den NIS[+]-hiPSCs auch die MSCs co-transplantiert wurden. Im

Gegensatz dazu zeigte sich kein [123]I Signal in den Bereichen, in denen ausschließlich NIS[+]-hiPSCs oder Kontrollzellen transplantiert wurden (Abbildung 12).
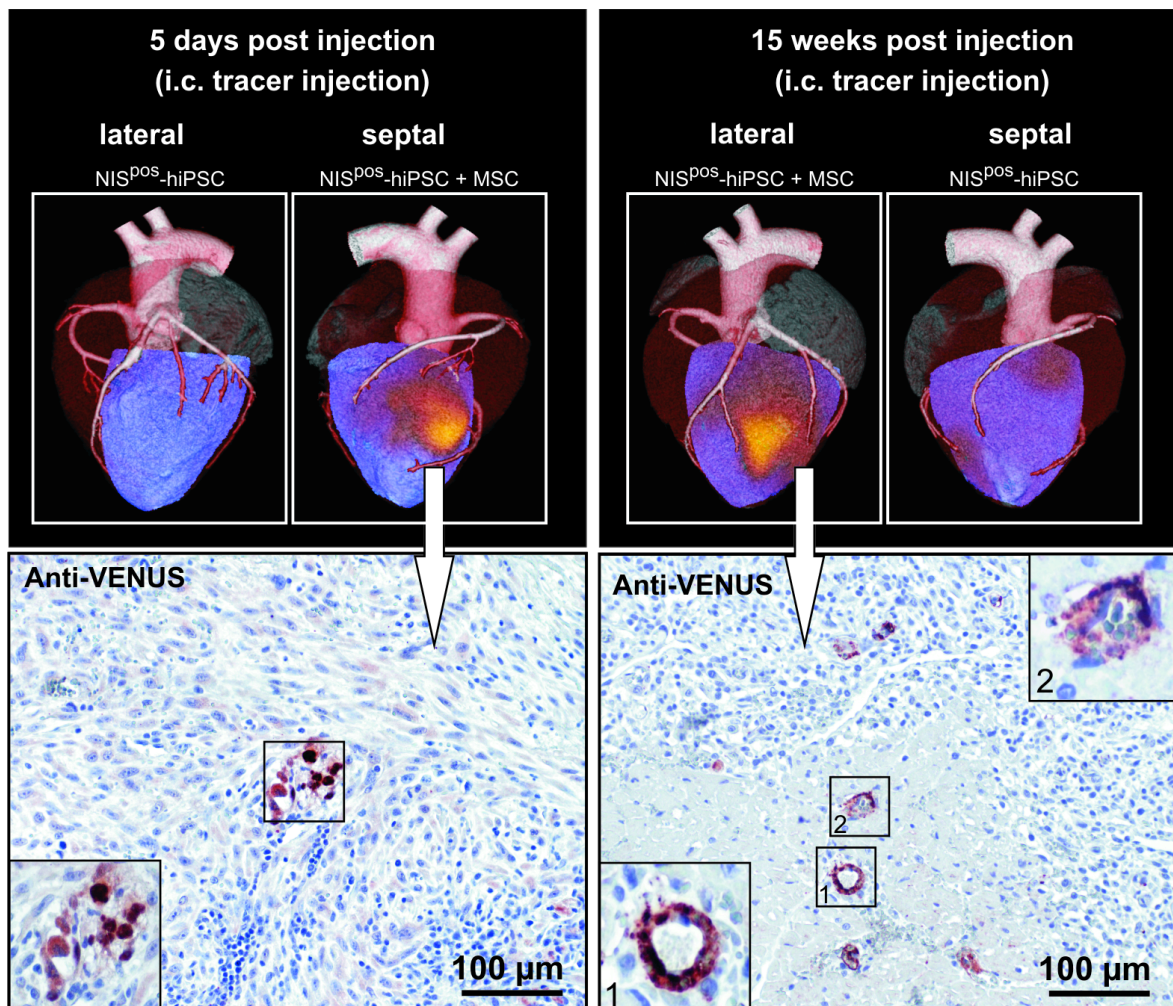
Abbildung 12: *In vivo* **Hybrid-SPECT-CT Imaging zur Detektion des Langzeitüberlebens NIS[+]-hiPSC**

Nicht prä-markierte NIS[+]-hiPSCs konnten 5 Tage und 15 Wochen nach Transplantation eine Stunde nach intrakoronarer [123]I Injektion im Herzen detektiert werden. Immunhistochemische Färbungen korrespondierender Bereiche des linken Ventrikels zeigten Venus[+]-NIS[+]-hiPSC Derivate (gefärbt mit kreuz-reagierenden anti-GFP-Antikörpern). Ein Großteil der Venus[+]-hiPSC Derivate zeigte 15 Wochen nach der Transplantation einen endothelialen Phänotyp. OCT4^{+} Zellen konnten nicht detektiert werden.

Die Beobachtung der geringen Retentions- und Überlebensraten transplantierter Zellen stellt ein bekanntes Problem der kardialen Zelltherapie dar.[13, 64, 65] Typischerweise wird ein Großteil der intramyokardial transplantierten Zellen direkt nach der Zellapplikation durch den Injektionskanal wieder aus dem Herzen gespült[65, 66] oder überlebt die initiale Phase nach der Transplantation nicht.[64] Laflamme et al. haben kürzlich einen neuen Überlebens-Cocktail, der in athymischen Ratten das Einwandern transplantierter humaner ESC

differenzierter Kardiomyozyten dramatisch steigert, beschrieben.[13] Um einen möglichen anti-apoptotischen Effekt der MSCs auf die hiPSCs in unserem Versuchsansatz zu untersuchen, wurden *in vitro* Co-Kulturversuche unter hypoxischen Bedingungen durchgeführt. Interessanterweise haben die MSCs die Apoptoserate der NIS[+]-hiPSCs signifikant reduziert. Dieser Effekt beruhte sowohl auf Zell-Zell-Kontakte, als auch auf parakrine Faktoren. Es ist jedoch fraglich, ob die anti-apoptotischen Effekte alleine für die gesteigerte Traceraufnahme und damit vermehrte Zellretention verantwortlich sind. Wahrscheinlich spielen jedoch auch MSC-abhängige Effekte, welche die Zellaggregation fördern und damit das Auswaschen der Zellen verringern, eine wesentliche Rolle. Da jedoch nach 5 Tagen und 12-15 Wochen NIS[+]-hiPSCs ausschließlich nur in den Bereichen detektiert werden konnten, in denen MSCs co-transplantiert wurden, scheint es zudem einen Langzeiteffekt der MSCs auf die NIS[+]-iPSCs zu geben.

Für eine erleichterte spätere *ex vivo* Detektion durch histologische Analysen wurden dem Injektionsmedium der NIS[+]-iPSCs rote Fluorospheren beigemengt, die während der Organpräparation unter ultraviolettem Licht makroskopisch sichtbar waren (Abbildung 13).
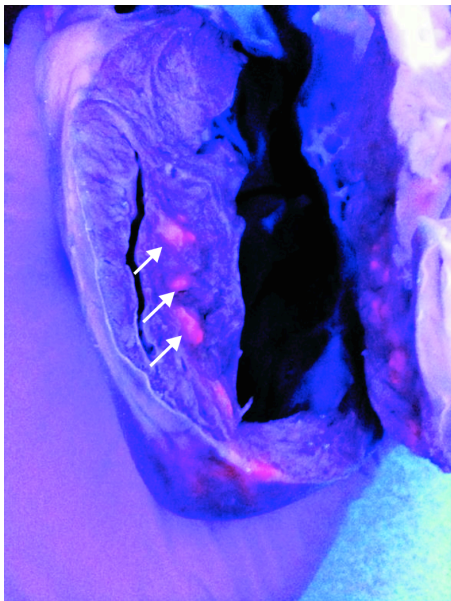
Abbildung 13: Makroskopische Detektion der Stammzellinjektionsstellen
Fluorosphere-basierte intramyokardiale Fluoreszenz ermöglichte die Lokalisation der Injektionsstellen (weiße Pfeile) unter ultraviolettem Licht.

In der histologischen Untersuchung zeigten sich typische Zeichen eines Myokardinfarktes mit Aufhebung der Kardiomyozytenstruktur sowie Fibrosebildung und moderater Einwanderung inflammatorischer Zellen wie Granulozyten und Lymphozyten. Weiterhin konnte ein persistierendes Einwandern einiger NIS[+]-iPSCs durch die Detektion Venus[+]-hiPSC Derivate 5 und 12-15 Wochen nach der Zelltransplantation nachgewiesen werden. Interessanterweise zeigten die hiPSC Derivate nach 12-15 Wochen einen endothelialen Phänotyp, welcher durch eine Färbung mit einem von Willebrand Faktor Antikörper

bestätigt wurde. Semiquantitative Analysen zur Kapillardichte in transplantierten Herzregionen zeigten eine gesteigerte Kapillarisierung in den Bereichen, in denen NIS[+]-iPSCs zusammen mit MSCs co-transplantiert wurden. Im Vergleich zu den frühen histologischen Analysen (5 Stunden nach Zellapplikation) konnten zu den beiden späteren Zeitpunkten (5 Tage und 12-15 Wochen) keine OCT4^{+} iPSC Derivate mehr nachgewiesen werden, welches auf eine *in vivo* Differenzierung der Zellen hindeutet. Diese Beobachtung wirft die Frage auf, ob die hohe Inzidenz dokumentierter Teratome nach Transplantation PSCs in immuninkompetenten Mäusen für eine klinische Applikation relevant ist oder eher durch Speziesinkompatibilitäten und der damit verbundenen fehlenden natürlichen Kontrolle der Zellproliferation bedingt ist. Das Fehlen undifferenzierter iPSCs und die gleichzeitige Existenz differenzierter vaskulärer NIS[+]-iPSC Derivate könnte durch das angewandte Immunsuppressionsprotokoll mit relativ hohen Cyclosporin A (CsA) und Prednisolon Dosierungen erklärt sein. Allgemein zeigt jedoch die Langzeitpersistenz hiPSC Derivate mit einem endothelialen Phänotyp die Effektivität des angewandten Immunsuppressionsprotokolls, zumindest in Bezug auf die T-Zell Reaktivität hinsichtlich differenzierter iPSC Derivate. Es gibt jedoch auch Hinweise darauf, dass CsA nicht effektiv gegen natürliche Killerzellen (NK) wirkt,[67] welches dann zu einer selektiven NK vermittelten Eliminierung undifferenzierter PSCs geführt hätte.[68]

Die hier beschriebene Methode zum *in vivo* Stammzell-Imaging hat natürlich auch ihre Limitationen. Wie bei jeder anderen Methode gibt es ein Detektionslimit für transplantierte Zellen. Daher kann eine Verteilung einzelner undifferenzierter oder differenzierter hiPSC Derivate in andere Organe nicht sicher ausgeschlossen werden. Die hier etablierte Nachweismethode erbrachte jedoch keine [123]I Traceranreicherung außerhalb des Herzens mit Ausnahme anderer NIS-exprimierender Gewebe wie Schilddrüse, Speicheldrüse und Magenschleimhaut. Ebenso konnten keine Teratome oder anderen Tumore in den autopsierten Tieren diagnostiziert werden. Die Tatsache, dass es auch eine endogene NIS-Expression in einigen Organen gibt, welche schwächere Tracersignale aus transplantierten Zellen überstrahlen kann, stellt natürlich auch eine Limitation der Methode dar. In präklinischen Großtiermodellen ist jedoch das starke Schilddrüsensignal aufgrund der räumlichen Distanz für kardial transplantierte Zellen nicht als Beeinträchtigung anzusehen.

Für zukünftige Anwendungen dieses Nachweisverfahrens gibt es einige Möglichkeiten der Weiterentwicklung. Die NIS[+]-Expressionslevel könnten durch optimierte Vektorsysteme und selektierte stabile Zellklone gesteigert werden, welches dann zu einer weiteren Steigerung der [123]I Akkumulation führen könnte. Weiterhin ist nicht bekannt, ob potentielle „Silencing"-Effekte während der *in vivo* Differenzierung der transplantierten NIS[+]-hiPSCs

die NIS-Expression reduzierten und ob Expressionssysteme mit reduziertem „Silencing" eine Steigerung des [123]I Signals zur Folge hätten. Um *in vivo* Differenzierungsvorgänge nicht invasiv zu monitoren, könnte der NIS hinter einem Zelltyp-spezifischen Promotor, z.B. dem Kardiomyozyten-spezifischen αMHC-Promotor kloniert werden,[69] so dass ein Tracersignal erst nach erfolgter Kardiomyozytendifferenzierung zu detektieren wäre. In Bezug auf eine klinische Anwendung sollte die benötigte Strahlendosis reduziert werden. Obwohl die applizierte [123]I Dosis ähnlich hoch ist, wie sie im Rahmen von klinischen Protokollen zur Tumortherapie eingesetzt wird, ist sie deutlich höher als für eine Routine Schilddrüsendiagnostik.

Insgesamt zeigt diese Studie erstmals den Nutzen der transgenen NIS-Expression für die longitudinale *in vivo* Detektion des Zellüberlebens, des Zell-„Engraftments" und der Verteilung zellulärer humaner iPSC Derivate durch die Anwendung der klinisch verfügbaren SPECT-CT Technologie. Weiterhin konnte erstmals das Langzeitüberleben und die Differenzierung humaner iPSCs in einem präklinischen Myokardinfarkt-Großtiermodell dokumentiert werden. Die angewandten dreidimesionalen Hybrid-Imaging-Protokolle ermöglichen die kombinierte Beurteilung der kardialen Anatomie und myokardialen Perfusion sowie das Monitoring der transplantierten Stammzellen mit einer Hybrid-Bildgebungsmodalität. Der entwickelte Imaging-Ansatz kann zu einer Optimierung Zell-basierter Therapiestrategien beitragen und ist ebenfalls geeignet potentielle Nebeneffekte einer Therapie mit pluripotenten Stammzellen, wie die Tumor- und Teratomentwicklung zu monitorisieren.

3.3 Publikation 3: „Cardiac Quadruple-Fusion Imaging: A Brief Report on a Novel Integrated Multimodality Approach for *in vivo* Visualization of Transplanted Stem Cells"

Fiechter M, Ghadri JR, Sidler M, Martin U, Landmesser U, Kaufmann PA, Lüscher TF, <u>Templin C</u>.

Int J Cardiol. 2012 Jul 18. [Epub ahead of print].

Im Rahmen der Publikation *„Cardiac Quadruple-Fusion Imaging: A Brief Report on a Novel Integrated Multimodality Approach for in vivo Visualization of Transplanted Stem Cells"* wurde aufbauend auf den vorangegangenen Publikationen ein neuer integrativer vierfach Multimodalitäten Imaging-Ansatz zur Detektion kardial transplantierter NIS[+]-hiPSCs beschrieben, bei dem unterschliedliche Bildgebungstechnologien zum Einsatz kamen und in einer gemeinsamen Fusion Informationen über den Injektionsort transplantierter Zellen, die daraus resultierende myokardiale Iodanreicherung, den Perfusionsdefekt des Myokardinfarktes und die kardiale Anatomie inklusive Koronargefäßbaum lieferte.

Eine Grundvoraussetzung für eine erfolgreiche kardiale Stammzelltherapie ist die sichere myokardiale Applikation vitaler Zellen in Randgebiete des Myokardinfarktes. Im Gegensatz zur intrakoronaren Stammzelltherapie, bei dem die Zellen über einen Ballonkatheter in das zuvor wiedereröffnete Koronargefäß infundiert werden, ist insbesondere bei der direkten endokardialen Stammzelltransplantation ein genaues Verständnis von anatomischen Strukturen inklusive funktioneller Parameter wie Areale eingeschränkter Perfusion oder Wandbewegung essentiell, um die Zellen möglichst genau in die Zielregionen zu applizieren.

Der am häufigsten experimentell und klinisch eingesetzte Katheter für direkte endokardiale Zellapplikationen ist der MyoStar[TM]-Injektionskatheter, welcher zusammen mit dem NOGA[®] XP Navigationssystem (Biologics Delivery System Group, Cordis Corporation, Diamond Bar, CA, USA) verwendet wird. Das NOGA[®] XP Navigationssystem ist eine Technologie, die ultraniedrige Magnetfelder (5×10^{-5} bis 5×10^{-6} Tesla) und Sensor-reiche Katheterelektroden kombiniert, um den Katheter innerhalb des linken Ventrikels mit einer Genauigkeit von 1 mm zu navigieren. Die elektrophysiologischen und mechanischen endokardialen Mapping-Informationen werden in Echtzeit zu einem dreidimensionalen, farbkodierten endoventrikulären Datensatz rekonstruiert. Die elektrischen Spannungsamplituden („Voltage Mapping") und mechanischen Kontraktilitäts-informationen (ausgedrückt als „linear local shortening ratio", LLS) werden kombiniert um

regionale Gebiete eingeschränkter Myokardfunktion, Perfusion und Vitalität zu identifizieren. Dies ermöglicht die Unterscheidung in nicht-vitale Narbengebiete, Infarktrandgebiete und vitales nicht-infarziertes Myokard. Anhand dieser Informationen können dann die Zielgebiete für die Transplantation der NIS$^+$-hiPSCs definiert werden.

Die kardiale SPECT Untersuchung ist ein nuklearmedizinisches Verfahren und basiert auf dem Gammakameraprinzip, das mithilfe von Kollimatoren und Radiotracern Ansichten unterschiedlicher Aktivitätsverteilung im Herzen aus verschiedenen Sichtwinkeln akquiriert und je nach Durchführung Informationen über die Durchblutungsverhältnisse, Vitalität und Funktion des Myokards liefert. Zudem kann die SPECT auch die spezifische Iodanreicherung der transplantierten NIS$^+$-hiPSCs darstellen. Die Bilder werden durch den Einsatz von Rekonstruktionstechniken zu einer dreidimensionalen Verteilung der Aktivität verrechnet. Ein Nachteil der SPECT ist jedoch der fehlende anatomische Bezug zu anderen kardialen Strukturen.

Die Computertomographie des Herzens ist eine spezielle CT-Angiographie der Koronargefäße (CCTA = kardiale Computertomographie Angiographie), bei der mit einer Kontrastmittelapplikation der gesamte Koronarbaum des Herzens in sehr hoher Auflösung dargestellt werden kann. Kombiniert man die SPECT mit der CT (Hybrid-SPECT-CT), ist eine exakte Zuordnung einzelner Koronargefäße zu dem dazugehörigen myokardialen Perfusionsdefekt möglich.

Jede einzelne Imaging-Modalität ist alleine nicht in der Lage alle benötigten Informationen für eine erfolgreiche myokardiale Stammzellapplikation und die anschließende longitudinale Detektion der transplantierten Zellen bereitzustellen. So ermöglicht die SPECT zwar die exakte Lokalisation verstärkter Radiotraceraufnahme, welches mit der Detektion transplantierter Stammzellen einhergeht, es fehlen jedoch die dazugehörigen genauen anatomischen Markierungspunkte. Die CCTA ermöglicht zwar die Darstellung genauer anamtomischer Strukturen, kann jedoch transplantierte Stammzellen nicht detektieren. Die NOGA-Technologie wurde primär für die Elektrophysiologie entwickelt und ist in der Lage vitales von nicht-vitalem Myokard zu differenzieren. Darüber hinaus können die Stammzellinjektionspunkte genau erfasst werden. Die Limitation hierbei besteht jedoch in der geringen räumlichen Auflösung.

Daher war das Ziel dieser Arbeit einen neuen integrativen Imaging-Ansatz zu etablieren, um in einer finalen Aufnahme funktionelle und anatomische Informationen gemeinsam zu erhalten. Hierzu wurde der gleiche Versuchsansatz wie in der zuvor beschriebenen Arbeit angewandt. Zunächst wurde bei Schweinen ein experimenteller Myokardinfarkt durch eine 180-minütige intrakoronare Ballonokklusion des RIVA induziert. Anschießend wurde mittels NOGA-Mapping der myokardiale Perfusionsdefekt lokalisiert und Gebiete im

Randgebiet des Infarktes für die Injektion der NIS[+]-hiPSCs und Kontrollzellen definiert. Nach erfolgter Stammzellapplikation wurde ein ^{99m}Tc-Tetrofosmin SPECT zur Verifizierung des Perfusionsdefektes und ein ^{123}I SPECT zur Detektion der transplantierten Zellen durchgeführt. Abschließend kam eine Kontrastmittel-angereicherte CT zur Darstellung der kardialen und koronaren Anatomie zur Anwendung. Die erhobenen SPECT und CT Daten wurden dann durch die Software CardIQ Fusion (GE Healthcare) zu Hybrid-SPECT-CT Bildern umgewandelt. Die dreidimensionalen Aufnahmen lieferten Informationen über die kardiale Anatomie und Perfusion des linksventrikulären Myokards (Abbildung 14 A) sowie der Lokalisation der transplantierten NIS[+]-hiPSCs (Abbildung 14 B). Eine Fusion dieser Aufnahmen führte zu der simultanen Detektion der zuvor markierten und transplantierten Stammzellen zusammen mit dem myokardialen Perfusionsdefekt und der kardialen Anatomie (Abbildung 14 C). Weiterhin wurden die Stammzellinjektionspunkte (braune Punkte) in den NOGA-Aufnahmen des unipolaren „Voltage Mappings" und „LLS" des linken Ventrikels als Polarplots (Abbildung 14 D) und als dreidimensional rekonstruierte NOGA-LLS-Aufnahmen dargestellt (Abbildung 14 E). Eine Überlagerung der NOGA-Injektionspunkte mit der zuvor generierten dreifach Fusions-Hybrid-Aufnahme (Abbildung 14 C) zeigte die eindeutige Übereinkunft der Injektionspunkte (Lateralwand und Septum) mit den Iod-Signalen der transplantierten NIS[+]-hiPSCs im linksventrikulären Myokard (Abbildung 14 F). Die Transplantation von Kontrollzellen (anteriore Wand) führte zu keiner Iodanreicherung.
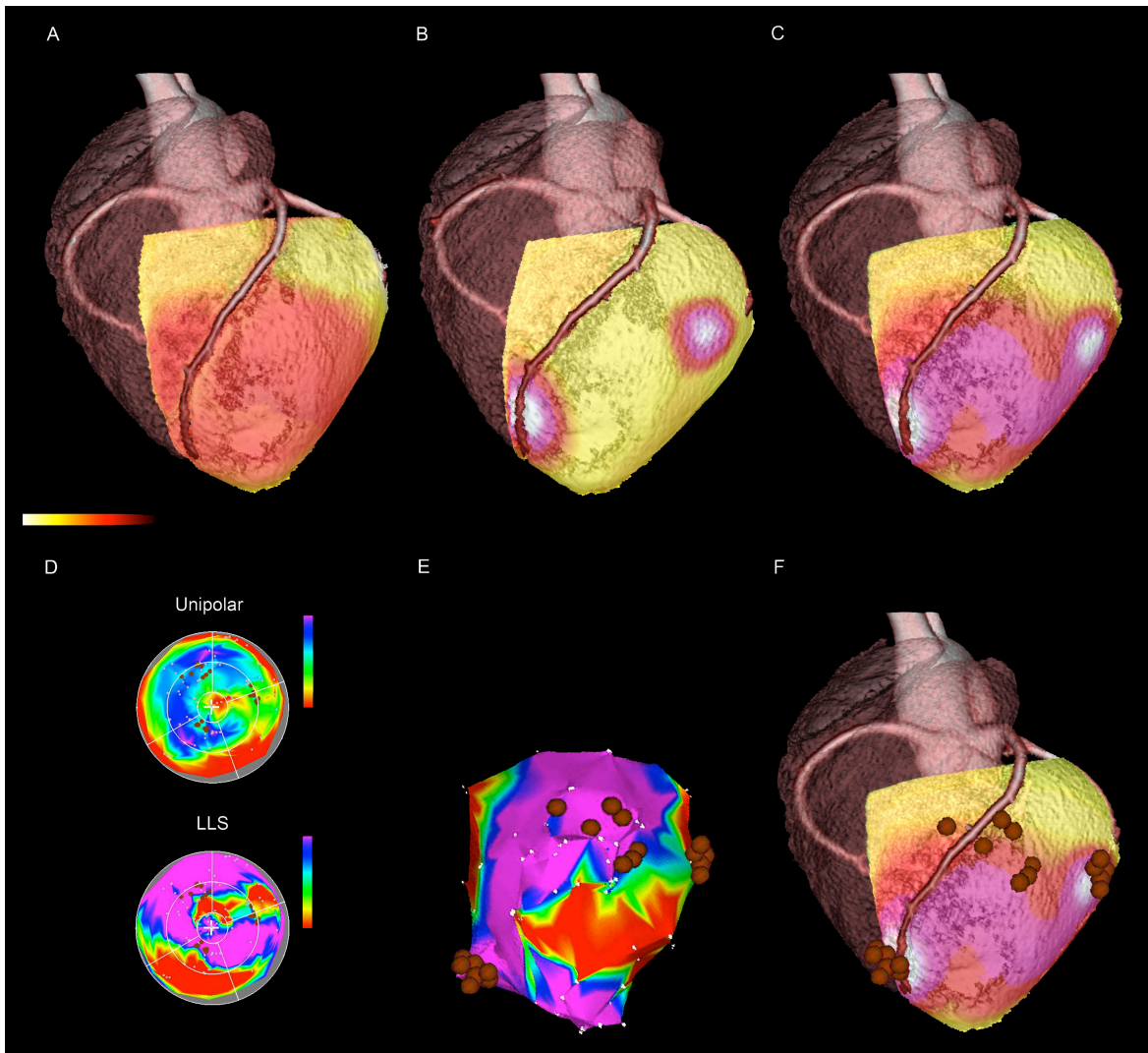
Abbildung 14: Integratives multimodales vierfach Imaging kardial transplantierter NIS⁺-iPSCs in einem präklinischen Infarktmodell

A.) 3D-Fusion einer kardialen CCTA mit einer ^{99m}Tc-Tetrofosmin SPECT zur Detektion des myokardialen Perfusionsdefektes (rote Areale; normal perfundiertes Myokard erscheint in gelb) nach Ballonokklusion des RIVA. Anatomische Strukturen wie Aortenbogen und Koronarbaum sind erkennbar, rechter Vorhof und Ventrikel sind ebenfalls als durchsichtige Strukturen sichtbar.

B.) Kardiale 3D-Fusion der CCTA und ^{123}I SPECT zur Detektion der transplantierten NIS⁺-hiPSCs (weiß/rote Punkte) im linken Ventrikel.

C.) Kardiale 3D-dreifach-Fusion von CCTA, ^{99m}Tc-Tetrofosmin SPECT und ^{123}I SPECT zeigt den myokardialen Perfusionsdefekt (rot/pink) zusammen mit Signalen der transplantierten NIS⁺-hiPSCs (weiße Punkte) im Randgebiet des Myokardinfarktes.

D.) Polarplots des NOGA „unipolar voltage" und „linear local shortening" = LLS Mappings zusammen mit den Stammzellinjektionspunkten (braue Punkte).

E.) 3D-Rekonstruktion des LLS Mappings mit den Stammzellinjektionspunkten (braue Punkte). Rote Areale = eingeschränkte Wandbewegung (Infarktgebiet), blaue/lila Areale = vitales Myokard, gelbe/grüne Areale = Randgebiet des Infarktes.

F.) Überlagerung der NOGA-Stammzell-Injektionspunkte mit dem kardialen 3D-dreifach-Hybrid-Imaging, woraus dann eine 3D-vierfach-Fusion resultiert und die exakte Lokalisation

der ^{123}I Aufnahme (Signale der transplantierten NIS^{+}-hiPSCs in der Lateralwand und im Septum) mit den Bereichen der Stammzellinjektionspunkte zeigt. Transplantierte Kontroll-Stammzellen (anteriore Wand) zeigen keine ^{123}I Aufnahme. Weiterhin sind die Infarktausdehnung im Versorgungsgebiet des RIVA und weitere kardiale Strukturen zu erkennen.

Diese Studie zeigt erstmals die Etablierung einer neuen kardialen multimodalen vierfach-Fusion bestehend aus dreidimensionaler-dreifach Fusion (myokardialer Perfusionsdefekt, Stammzelldetektion durch resultierendes Iod-Signal transplantierter NIS^{+}-hiPSCs und kardialer Anatomie) kombiniert mit einer vierten Dimension des NOGA-Mappings (Stammzellinjektionspunkte).

Der longitudinale Nachweis transplantierter Stammzellen hat einen großen Stellenwert in der regenerativen Medizin um essentielle Fragestellungen hinsichtlich Zelltyp, Zelldosis, Applikationseffizienz, Zellverteilung, „Engraftment" und Mechanismus beantworten zu können. Die Anwendung dieses etablierten Imaging-Ansatzes kann in Zukunft zu einer Optimierung Zell-basierter Therapiestrategien im präklinischen Großtiermodell beitragen.

4.   Ausblick

Mit den 2006 von Takahashi et al.[15] beschriebenen iPSCs existiert nun erstmals ein ethisch unbedenklicher Zelltyp, der ein potentiell unbegrenztes Expansions- und Differenzierungspotential aufweist. Diese Entwicklung wurde auf dem Gebiet der regenerativen Medizin als bahnbrechende neue Errungenschaft angesehen und deshalb auch gerade mit dem Nobelpreis für Medizin gewürdigt. Im Hinblick auf eine mögliche therapeutische Anwendung von iPSCs konnten in den letzten Jahren deutliche Fortschritte erzielt werden. So konnten bereits iPSCs ohne die genomische Integration eines Transgens erzeugt werden.[23-26] Weiterhin wurden Protokolle für die Massenzellproduktion[27, 28] sowie effiziente und spezifische Differenzierungsprotokolle etabliert.[29]

Vor einer klinischen Anwendung ist jedoch der Transfer vom Kleintiermodell in ein präklinisches Großtiermodell notwendig, damit zunächst insbesondere Sicherheitsrisiken dieser pluripotenten Zelltherapie untersucht werden können. Hierfür spielen klinisch relevante Bildgebungsstudien eine große Rolle, um neben dem exakten Injektionsort auch den kurzzeitigen und langzeitigen Verbleib der Stammzellen zu visualisieren und mögliche Nebenwirkungen wie Teratom- oder Tumorentstehungen zu erfassen.

Mit dem im Rahmen dieser Dissertation etablierten neuen multimodalen Imaging-Ansatzes ist es nun erstmals gelungen iPSCs in einem klinisch relevanten Großtiermodell über einen Zeitraum von 15 Wochen zu monitorisieren. Durch die Kombination mehrerer Bildgebungsmodalitäten ist es zudem möglich, sowohl funktionelle als auch anatomische Informationen in einer einzigen Darstellung zu erhalten.

Mit Hilfe dieser Entwicklung sollen nun weiterführende Analysen im Hinblick auf eine klinische Anwendung der iPSCs erfolgen. So ist beabsichtigt, zu Kardiomyozyten und Endothelzellen differenzierte iPSC-Derivate sowie kardiogene Mikroaggregate (Kombination kardialer Zelltypen wie Kardiomyozyten, Endothelzellen und Fibroblasten) im Schweine-Infarktmodell hinsichtlich der regenerativen Kapazität und Sicherheit zu testen. Die kardiale Funktionsdisgnostik soll hierbei um die kardiale Magnetresonanztomographie erweitert werden, um neben der Infarktausbreitung („late enhancement") auch funktionelle Parameter wie linksventrikuläre Ejektionsfraktion, endsystolisches - und enddiastolisches Volumen zu erhalten. Neben dem „Engraftment" der Zellen sollen weiterhin auch Nebenwirkungen der Zelltherapie mittels Ganzkörper SPECT-CT Untersuchungen erfolgen. Hierfür bietet das etablierte Transgen-basierte (NIS) Imaging-Protokoll die notwendigen Voraussetzungen. Zudem sollen die Tiere mit einem implantierbaren Event-Recorder („Reveal insertable loop recorder") ausgestattet

werden, um die Inzidenz potentieller maligner Herzrhythmusstörungen zu dokumentieren. Weiterhin sollen mit Hilfe der im Rahmen dieser Dissertation beschriebenen Imaging-Technologie unterschiedliche Stammzell-Trägermedien wie Hydrogele hinsichtlich dem „Engraftment" von Zellen analysiert werden.

5.   Literaturverzeichnis

1. Weir RA, McMurray JJ. Epidemiology of heart failure and left ventricular dysfunction after acute myocardial infarction. *Curr Heart Fail Rep*. 2006;3:175-180
2. Weir RA, McMurray JJ, Velazquez EJ. Epidemiology of heart failure and left ventricular systolic dysfunction after acute myocardial infarction: Prevalence, clinical characteristics, and prognostic importance. *Am J Cardiol*. 2006;97:13F-25F
3. Templin C, Krankel N, Luscher TF, Landmesser U. Stem cells in cardiovascular regeneration: From preservation of endogenous repair to future cardiovascular therapies. *Curr Pharm Des*. 2011;17:3280-3294
4. Templin C, Luscher TF, Landmesser U. Cell-based cardiovascular repair and regeneration in acute myocardial infarction and chronic ischemic cardiomyopathy-current status and future developments. *Int J Dev Biol*. 2011;55:407-417
5. Templin C, Luscher TF, Landmesser U. [stem and progenitor cell-based therapy approaches: Current developments on treatment of acute myocardial infarction and chronic ischemic cardiomyopathy]. *Herz*. 2010;35:445-456
6. Zimmet H, Porapakkham P, Sata Y, Haas SJ, Itescu S, Forbes A, Krum H. Short- and long-term outcomes of intracoronary and endogenously mobilized bone marrow stem cells in the treatment of st-segment elevation myocardial infarction: A meta-analysis of randomized control trials. *Eur J Heart Fail*. 2012;14:91-105
7. Orlic D, Kajstura J, Chimenti S, Limana F, Jakoniuk I, Quaini F, Nadal-Ginard B, Bodine DM, Leri A, Anversa P. Mobilized bone marrow cells repair the infarcted heart, improving function and survival. *Proc Natl Acad Sci U S A*. 2001;98:10344-10349
8. Orlic D, Kajstura J, Chimenti S, Jakoniuk I, Anderson SM, Li B, Pickel J, McKay R, Nadal-Ginard B, Bodine DM, Leri A, Anversa P. Bone marrow cells regenerate infarcted myocardium. *Nature*. 2001;410:701-705
9. Murry CE, Soonpaa MH, Reinecke H, Nakajima H, Nakajima HO, Rubart M, Pasumarthi KB, Virag JI, Bartelmez SH, Poppa V, Bradford G, Dowell JD, Williams DA, Field LJ. Haematopoietic stem cells do not transdifferentiate into cardiac myocytes in myocardial infarcts. *Nature*. 2004;428:664-668
10. Balsam LB, Wagers AJ, Christensen JL, Kofidis T, Weissman IL, Robbins RC. Haematopoietic stem cells adopt mature haematopoietic fates in ischaemic myocardium. *Nature*. 2004;428:668-673
11. Nygren JM, Jovinge S, Breitbach M, Sawen P, Roll W, Hescheler J, Taneera J, Fleischmann BK, Jacobsen SE. Bone marrow-derived hematopoietic cells generate cardiomyocytes at a low frequency through cell fusion, but not transdifferentiation. *Nat Med*. 2004;10:494-501
12. Klug MG, Soonpaa MH, Koh GY, Field LJ. Genetically selected cardiomyocytes from differentiating embronic stem cells form stable intracardiac grafts. *J Clin Invest*. 1996;98:216-224
13. Laflamme MA, Chen KY, Naumova AV, Muskheli V, Fugate JA, Dupras SK, Reinecke H, Xu C, Hassanipour M, Police S, O'Sullivan C, Collins L, Chen Y, Minami E, Gill EA, Ueno S, Yuan C, Gold J, Murry CE. Cardiomyocytes derived from human embryonic stem cells in pro-survival factors enhance function of infarcted rat hearts. *Nat Biotechnol*. 2007;25:1015-1024
14. Schwanke K, Wunderlich S, Reppel M, Winkler ME, Matzkies M, Groos S, Itskovitz-Eldor J, Simon AR, Hescheler J, Haverich A, Martin U. Generation and characterization of functional cardiomyocytes from rhesus monkey embryonic stem cells. *Stem Cells*. 2006;24:1423-1432
15. Takahashi K, Yamanaka S. Induction of pluripotent stem cells from mouse embryonic and adult fibroblast cultures by defined factors. *Cell*. 2006;126:663-676

16. Takahashi K, Tanabe K, Ohnuki M, Narita M, Ichisaka T, Tomoda K, Yamanaka S. Induction of pluripotent stem cells from adult human fibroblasts by defined factors. *Cell*. 2007;131:861-872

17. Yu J, Vodyanik MA, Smuga-Otto K, Antosiewicz-Bourget J, Frane JL, Tian S, Nie J, Jonsdottir GA, Ruotti V, Stewart R, Slukvin, II, Thomson JA. Induced pluripotent stem cell lines derived from human somatic cells. *Science*. 2007;318:1917-1920

18. Wong SS, Bernstein HS. Cardiac regeneration using human embryonic stem cells: Producing cells for future therapy. *Regen Med*. 2010;5:763-775

19. Mauritz C, Schwanke K, Reppel M, Neef S, Katsirntaki K, Maier LS, Nguemo F, Menke S, Haustein M, Hescheler J, Hasenfuss G, Martin U. Generation of functional murine cardiac myocytes from induced pluripotent stem cells. *Circulation*. 2008;118:507-517

20. Haase A, Olmer R, Schwanke K, Wunderlich S, Merkert S, Hess C, Zweigerdt R, Gruh I, Meyer J, Wagner S, Maier LS, Han DW, Glage S, Miller K, Fischer P, Scholer HR, Martin U. Generation of induced pluripotent stem cells from human cord blood. *Cell Stem Cell*. 2009;5:434-441

21. Mauritz C, Martens A, Rojas SV, Schnick T, Rathert C, Schecker N, Menke S, Glage S, Zweigerdt R, Haverich A, Martin U, Kutschka I. Induced pluripotent stem cell (ipsc)-derived flk-1 progenitor cells engraft, differentiate, and improve heart function in a mouse model of acute myocardial infarction. *Eur Heart J*. 2011;32:2634-2641

22. Nakagawa M, Koyanagi M, Tanabe K, Takahashi K, Ichisaka T, Aoi T, Okita K, Mochiduki Y, Takizawa N, Yamanaka S. Generation of induced pluripotent stem cells without myc from mouse and human fibroblasts. *Nat Biotechnol*. 2008;26:101-106

23. Kaji K, Norrby K, Paca A, Mileikovsky M, Mohseni P, Woltjen K. Virus-free induction of pluripotency and subsequent excision of reprogramming factors. *Nature*. 2009;458:771-775

24. Woltjen K, Michael IP, Mohseni P, Desai R, Mileikovsky M, Hamalainen R, Cowling R, Wang W, Liu P, Gertsenstein M, Kaji K, Sung HK, Nagy A. Piggybac transposition reprograms fibroblasts to induced pluripotent stem cells. *Nature*. 2009;458:766-770

25. Yu J, Hu K, Smuga-Otto K, Tian S, Stewart R, Slukvin, II, Thomson JA. Human induced pluripotent stem cells free of vector and transgene sequences. *Science*. 2009;324:797-801

26. Kim D, Kim CH, Moon JI, Chung YG, Chang MY, Han BS, Ko S, Yang E, Cha KY, Lanza R, Kim KS. Generation of human induced pluripotent stem cells by direct delivery of reprogramming proteins. *Cell Stem Cell*. 2009;4:472-476

27. Olmer R, Haase A, Merkert S, Cui W, Palecek J, Ran C, Kirschning A, Scheper T, Glage S, Miller K, Curnow EC, Hayes ES, Martin U. Long term expansion of undifferentiated human ips and es cells in suspension culture using a defined medium. *Stem Cell Res*. 2010;5:51-64

28. Zweigerdt R, Olmer R, Singh H, Haverich A, Martin U. Scalable expansion of human pluripotent stem cells in suspension culture. *Nat Protoc*. 2011;6:689-700

29. Murry CE, Keller G. Differentiation of embryonic stem cells to clinically relevant populations: Lessons from embryonic development. *Cell*. 2008;132:661-680

30. Yoshida Y, Yamanaka S. Ips cells: A source of cardiac regeneration. *J Mol Cell Cardiol*. 2011;50:327-332

31. Muller-Ehmsen J, Krausgrill B, Burst V, Schenk K, Neisen UC, Fries JW, Fleischmann BK, Hescheler J, Schwinger RH. Effective engraftment but poor mid-term persistence of mononuclear and mesenchymal bone marrow cells in acute and chronic rat myocardial infarction. *J Mol Cell Cardiol*. 2006;41:876-884

32. Templin C, Kotlarz D, Marquart F, Faulhaber J, Brendecke V, Schaefer A, Tsikas D, Bonda T, Hilfiker-Kleiner D, Ohl L, Naim HY, Foerster R, Drexler H, Limbourg FP. Transcoronary delivery of bone marrow cells to the infarcted murine myocardium: Feasibility, cellular kinetics, and improvement in cardiac function. *Basic Res Cardiol*. 2006;101:301-310

33. Templin C, Kotlarz D, Faulhaber J, Schnabel S, Grote K, Salguero G, Luchtefeld M, Hiller KH, Jakob P, Naim HY, Schieffer B, Hilfiker-Kleiner D, Landmesser U, Limbourg FP, Drexler H. Ex vivo expanded hematopoietic progenitor cells improve cardiac function after myocardial infarction: Role of beta-catenin transduction and cell dose. *J Mol Cell Cardiol*. 2008;45:394-403

34. Gandolfi F, Vanelli A, Pennarossa G, Rahaman M, Acocella F, Brevini TA. Large animal models for cardiac stem cell therapies. *Theriogenology*. 2011;75:1416-1425

35. van Laake LW, Passier R, Doevendans PA, Mummery CL. Human embryonic stem cell-derived cardiomyocytes and cardiac repair in rodents. *Circ Res*. 2008;102:1008-1010

36. Bengel FM, Schachinger V, Dimmeler S. Cell-based therapies and imaging in cardiology. *Eur J Nucl Med Mol Imaging*. 2005;32 Suppl 2:S404-416

37. de Almeida PE, van Rappard JR, Wu JC. In vivo bioluminescence for tracking cell fate and function. *Am J Physiol Heart Circ Physiol*. 2011;301:H663-671

38. Wu JC, Abraham MR, Kraitchman DL. Current perspectives on imaging cardiac stem cell therapy. *J Nucl Med*. 2010;51 Suppl 1:128S-136S

39. Ruggiero A, Thorek DL, Guenoun J, Krestin GP, Bernsen MR. Cell tracking in cardiac repair: What to image and how to image. *Eur Radiol*. 2012;22:189-204

40. Psaltis PJ, Simari RD, Rodriguez-Porcel M. Emerging roles for integrated imaging modalities in cardiovascular cell-based therapeutics: A clinical perspective. *Eur J Nucl Med Mol Imaging*. 2012;39:165-181

41. Willmann JK, Paulmurugan R, Rodriguez-Porcel M, Stein W, Brinton TJ, Connolly AJ, Nielsen CH, Lutz AM, Lyons J, Ikeno F, Suzuki Y, Rosenberg J, Chen IY, Wu JC, Yeung AC, Yock P, Robbins RC, Gambhir SS. Imaging gene expression in human mesenchymal stem cells: From small to large animals. *Radiology*. 2009;252:117-127

42. Lee AS, Xu D, Plews JR, Nguyen PK, Nag D, Lyons JK, Han L, Hu S, Lan F, Liu J, Huang M, Narsinh KH, Long CT, de Almeida PE, Levi B, Kooreman N, Bangs C, Pacharinsak C, Ikeno F, Yeung AC, Gambhir SS, Robbins RC, Longaker MT, Wu JC. Preclinical derivation and imaging of autologously transplanted canine induced pluripotent stem cells. *J Biol Chem*. 2011;286:32697-32704

43. Dohan O, De la Vieja A, Paroder V, Riedel C, Artani M, Reed M, Ginter CS, Carrasco N. The sodium/iodide symporter (nis): Characterization, regulation, and medical significance. *Endocr Rev*. 2003;24:48-77

44. Stodilka RZ, Blackwood KJ, Kong H, Prato FS. A method for quantitative cell tracking using spect for the evaluation of myocardial stem cell therapy. *Nucl Med Commun*. 2006;27:807-813

45. Acton PD, Kung HF. Small animal imaging with high resolution single photon emission tomography. *Nucl Med Biol*. 2003;30:889-895

46. Huber I, Itzhaki I, Caspi O, Arbel G, Tzukerman M, Gepstein A, Habib M, Yankelson L, Kehat I, Gepstein L. Identification and selection of cardiomyocytes during human embryonic stem cell differentiation. *FASEB J*. 2007;21:2551-2563

47. Kita-Matsuo H, Barcova M, Prigozhina N, Salomonis N, Wei K, Jacot JG, Nelson B, Spiering S, Haverslag R, Kim C, Talantova M, Bajpai R, Calzolari D, Terskikh A, McCulloch AD, Price JH, Conklin BR, Chen HS, Mercola M. Lentiviral vectors and protocols for creation of stable hesc lines for fluorescent tracking and drug resistance selection of cardiomyocytes. *PLoS One*. 2009;4:e5046

48. Xu XQ, Zweigerdt R, Soo SY, Ngoh ZX, Tham SC, Wang ST, Graichen R, Davidson B, Colman A, Sun W. Highly enriched cardiomyocytes from human embryonic stem cells. *Cytotherapy*. 2008;10:376-389

49. Sun N, Lee A, Wu JC. Long term non-invasive imaging of embryonic stem cells using reporter genes. *Nat Protoc*. 2009;4:1192-1201

50. Jang JE, Shaw K, Yu XJ, Petersen D, Pepper K, Lutzko C, Kohn DB. Specific and stable gene transfer to human embryonic stem cells using pseudotyped lentiviral vectors. *Stem Cells Dev*. 2006;15:109-117

51. Wurm M, Gross B, Sgodda M, Standker L, Muller T, Forssmann WG, Horn PA, Blasczyk R, Cantz T. Improved lentiviral gene transfer into human embryonic stem cells grown in co-culture with murine feeder and stroma cells. *Biol Chem*. 2011;392:887-895

52. Liu J, Jones KL, Sumer H, Verma PJ. Stable transgene expression in human embryonic stem cells after simple chemical transfection. *Mol Reprod Dev*. 2009;76:580-586

53. Costa M, Dottori M, Ng E, Hawes SM, Sourris K, Jamshidi P, Pera MF, Elefanty AG, Stanley EG. The hesc line envy expresses high levels of gfp in all differentiated progeny. *Nat Methods*. 2005;2:259-260

54. Zwaka TP, Thomson JA. Homologous recombination in human embryonic stem cells. *Nat Biotechnol*. 2003;21:319-321

55. Ma Y, Ramezani A, Lewis R, Hawley RG, Thomson JA. High-level sustained transgene expression in human embryonic stem cells using lentiviral vectors. *Stem Cells*. 2003;21:111-117

56. Moore JC, van Laake LW, Braam SR, Xue T, Tsang SY, Ward D, Passier R, Tertoolen LL, Li RA, Mummery CL. Human embryonic stem cells: Genetic manipulation on the way to cardiac cell therapies. *Reprod Toxicol*. 2005;20:377-391

57. Cherry SR, Biniszkiewicz D, van Parijs L, Baltimore D, Jaenisch R. Retroviral expression in embryonic stem cells and hematopoietic stem cells. *Mol Cell Biol*. 2000;20:7419-7426

58. Xia X, Zhang Y, Zieth CR, Zhang SC. Transgenes delivered by lentiviral vector are suppressed in human embryonic stem cells in a promoter-dependent manner. *Stem Cells Dev*. 2007;16:167-176

59. Kustikova O, Fehse B, Modlich U, Yang M, Dullmann J, Kamino K, von Neuhoff N, Schlegelberger B, Li Z, Baum C. Clonal dominance of hematopoietic stem cells triggered by retroviral gene marking. *Science*. 2005;308:1171-1174

60. Liew CG, Draper JS, Walsh J, Moore H, Andrews PW. Transient and stable transgene expression in human embryonic stem cells. *Stem Cells*. 2007;25:1521-1528

61. Moore JC, Atze K, Yeung PL, Toro-Ramos AJ, Camarillo C, Thompson K, Ricupero CL, Brenneman MA, Cohen RI, Hart RP. Efficient, high-throughput transfection of human embryonic stem cells. *Stem Cell Res Ther*. 2010;1:23

62. Schinzel RT, Ahfeldt T, Lau FH, Lee YK, Cowley A, Shen T, Peters D, Lum DH, Cowan CA. Efficient culturing and genetic manipulation of human pluripotent stem cells. *PLoS One*. 2011;6:e27495

63. Terrovitis J, Kwok KF, Lautamaki R, Engles JM, Barth AS, Kizana E, Miake J, Leppo MK, Fox J, Seidel J, Pomper M, Wahl RL, Tsui B, Bengel F, Marban E, Abraham MR. Ectopic expression of the sodium-iodide symporter enables imaging of transplanted cardiac stem cells in vivo by single-photon emission computed tomography or positron emission tomography. *J Am Coll Cardiol*. 2008;52:1652-1660

64. Muller-Ehmsen J, Krausgrill B, Burst V, Schenk K, Neisen UC, Fries JW, Fleischmann BK, Hescheler J, Schwinger RH. Effective engraftment but poor mid-term persistence of mononuclear and mesenchymal bone marrow cells in acute and chronic rat myocardial infarction. *Journal of molecular and cellular cardiology*. 2006;41:876-884

65. Teng CJ, Luo J, Chiu RC, Shum-Tim D. Massive mechanical loss of microspheres with direct intramyocardial injection in the beating heart: Implications for cellular cardiomyoplasty. *J Thorac Cardiovasc Surg*. 2006;132:628-632

66. Al Kindi A, Ge Y, Shum-Tim D, Chiu RC. Cellular cardiomyoplasty: Routes of cell delivery and retention. *Front Biosci*. 2008;13:2421-2434

67. Wai LE, Fujiki M, Takeda S, Martinez OM, Krams SM. Rapamycin, but not cyclosporine or fk506, alters natural killer cell function. *Transplantation*. 2008;85:145-149

68. Drukker M, Benvenisty N. The immunogenicity of human embryonic stem-derived cells. *Trends Biotechnol*. 2004;22:136-141

69. Xu XQ, Soo SY, Sun W, Zweigerdt R. Global expression profile of highly enriched cardiomyocytes derived from human embryonic stem cells. *Stem Cells*. 2009;27:2163-2174

6. Danksagung

Die Durchführung und Niederschrift dieser Arbeit wäre nicht möglich gewesen ohne die uneingeschränkte Unterstützung und intensive Förderung der im Folgenden genannten Personen, denen ich deshalb zu besonderem Dank verpflichtet bin:

Professor Dr. rer. nat. Ulrich Martin, Direktor der Leibniz Laboratorien für Biotechnologie und artifiziellen Organe der Klinik für Thorax-, Transplantations-, Herz- und Gefäßchirurgie der Medizinischen Hochschule Hannover für die ausgezeichnete Betreuung während der Dissertation und zahlreichen Diskussionen bei der Verfassung der Manuskripte. Er ist mir in all den Jahren ein enger Wegbegleiter meiner wissenschaftlichen Karriere und Freund gewesen.

Professor Dr. med. Thomas F. Lüscher, Direktor der Klinik für Kardiologie am UniversitätsSpital Zürich für seine großartige Unterstützung in klinischen und wissenschaftlichen Angelegenheiten. Durch seine Hingabe zur klinischen und experimentellen Kardiologie begeisterte er mich als Mentor und Lehrer. Zudem bot er mir die Gelegenheit in seiner Klinik unter hervorragenden Bedingungen einen Teil meiner Dissertation anfertigen zu können.

Dr. rer. nat. Robert Zweigerdt, Dr. rer. nat. Kristin Schwanke und Dr. rer. nat. Ruth Olmer, wissenschaftliche Mitarbeiter/innen der Leibniz Laboratorien für Biotechnologie und artifiziellen Organe der Klinik für Thorax-, Transplantations-, Herz- und Gefäßchirurgie der Medizinischen Hochschule Hannover für die kontinuierliche sehr wertvolle Unterstützung und Diskussionen bei der Durchführung der Experimente. Ohne die exzellenten zell- und molekularbiologischen Vorarbeiten wären zudem die Versuche im Rahmen dieser Dissertation nicht möglich gewesen.

Meinen Eltern, die mir das Studium und damit auch die vorliegenden Arbeiten ermöglicht haben, gilt mein ganz besonderer Dank. Ohne ihre liebevolle Unterstützung wären diese Arbeiten nicht möglich gewesen.

Meiner Freundin Dr. med. Jelena-Rima Ghadri, die mein akademisches Vorankommen stets mit Liebe und Geduld unterstützt hat sowie für ihr Verständnis für die nicht vorhandene Zeit meinerseits.

7.   Curriculum Vitae

ALLGEMEINE INFORMATIONEN UND BILDUNG

PERSONALIEN

Name:	Templin, Christian
Adressen:	Culmannstrasse 37, 8006 Zürich
	Gärtnerstraße 8, 28816 Stuhr
Geburtstag:	19.05.1975
Geburtsort:	Bremen
Nationalität:	deutsch

SCHULBILDUNG

1981 – 1985:	Grundschule, Stuhr-Seckenhausen
1985 – 1987:	Orientierungsstufe, Stuhr-Brinkum
1987 – 1995:	Kooperative Gesamtschule, Stuhr-Brinkum
06/1995:	Allgemeine Hochschulreife

ZIVILDIENST

08/1995 – 09/1996:	Rettungssanitäter
	Lehrrettungswache Malteser Hilfsdienst, Bremen-Huchting

HOCHSCHULBILDUNG

10/1996 – 11/2002:	Medizinische Hochschule Hannover
09/1998:	ärztliche Vorprüfung
09/1999:	1. Staatsexamen
09/2001:	2. Staatsexamen
11/2002:	3. Staatsexamen (Gesamtprädikat: *gut*)
11/2003:	Promotion zum Dr. med., Medizinische Hochschule Hannover
09/2011:	Habilitation, UniversitätsSpital Zürich, Schweiz

FACHARZTTITEL

07/2008:	Erwerb der **Zusatzbezeichnung „Notfallmedizin"** (Ärztekammer Niedersachsen, Deutschland, 2008/001860)
04/2009:	Erwerb des Facharzttitels **„Facharzt für Innere Medizin"** (Ärztekammer Niedersachsen, Deutschland, 2009/000569)
02/2010:	Erwerb des Facharzttitels **„Facharzt für Innere Medizin und Kardiologie"** (Ärztekammer Niedersachsen, Deutschland, 2010/000134)

BERUFUNGEN

08/2012:	2. Platz für die W2-Professur für Kardiologische Epidemiologie in der Klinik für Innere Medizin B (Direktor: Prof. Dr. S. Felix) der Universitätsmedizin Greifswald

KLINISCHE AUSBILDUNG UND TÄTIGKEITEN

AUSBILDUNG UND TÄTIGKEITEN IN INNERE MEDIZIN UND KARDIOLOGIE

01/2003 – 03/2008: **Facharztausbildung in Innere Medizin und Kardiologie**
Medizinische Hochschule Hannover, Deutschland
Zentrum Innere Medizin
Klinik für Kardiologie (Direktor: Prof. Dr. med. H. Drexler)

03/2008 – 02/2010: **Facharztausbildung in Innere Medizin und Kardiologie**
UniversitätsSpital Zürich, Schweiz
Medizinbereich Herz-Gefäss-Thorax
Klinik für Kardiologie (Direktor: Prof. Dr. med. T. F. Lüscher)

02/2010 – 10/2011: **Facharzt**
(Interventionelle Kardiologie und Echokardiographie)
UniversitätsSpital Zürich, Schweiz
Medizinbereich Herz-Gefäss-Thorax
Klinik für Kardiologie (Direktor: Prof. Dr. med. T. F. Lüscher)

seit 10/2011: **Interventional Fellow**
„Andreas Grüntzig Herzkatheterlabore"
UniversitätsSpital Zürich, Schweiz
Medizinbereich Herz-Gefäss-Thorax
Klinik für Kardiologie (Direktor: Prof. Dr. med. T. F. Lüscher)

01/2012 – 04/2012: **Oberarzt i.v.**
UniversitätsSpital Zürich, Schweiz
Medizinbereich Herz-Gefäss-Thorax
Klinik für Kardiologie (Direktor: Prof. Dr. T. F. Lüscher)

seit 05/2012: **Oberarzt**
UniversitätsSpital Zürich, Schweiz
Medizinbereich Herz-Gefäss-Thorax
Klinik für Kardiologie (Direktor: Prof. Dr. T. F. Lüscher)

FORSCHUNGSTÄTIGKEITEN

MEDIZINISCHE PROMOTION

Thema: Untersuchung zur Übertragung porciner endogener Retroviren im Rahmen der Xenotransplantation

03/1999 – 08/2000: Leibniz Forschungslaboratorien für Biotechnologie und künstliche Organe (LEBAO)
Betreuer: Priv.-Doz. Dr. rer. nat. U. Martin
Medizinische Hochschule Hannover
Klinik für Thorax-, Herz- und Gefäßchirurgie
(Direktor: Prof. Dr. med. A. Haverich)

08/2000 – 02/2001: **Doctoral Fellow**
BioTransplant Incorporated und Immerge Biotherapeutics
Boston, Massachusetts, USA
Betreuer: Dr. C. Patience, Ph.D.

(Direktor: Dr. E. Lebowitz, Ph.D.)

Promotionsstipendium, gefördert durch die Herbert-Quandt-Stiftung der VARTA AG
Datum der Promotion: 25.11.2003
Prädikat: *summa cum laude*

NATURWISSENSCHAFTLICHE PROMOTION

Thema:	Etablierung eines neunen integrativen multimodalen Imaging-Ansatzes für das Monitoring von kardial transplantierten induzierten pluripotenten Stammzellen im präklinischen Großtiermodell
04/2009 – 09/2009:	Kenntnisprüfungen in den Fächern Genetik, Zell- und Entwicklungsbiologie sowie Biochemie, Leibniz Universität Hannover
seit 09/2009:	Leibniz Forschungslaboratorien für Biotechnologie und artifizielle Organe (LEBAO) (Direktor: Prof. Dr. rer. nat. U. Martin) Excellence Cluster „*REBIRTH* – From *Re*generative *Bi*ology to *Re*constructive *The*rapy" Medizinische Hochschule Hannover

HABILITATION

Thema:	Experimentelle Stammzelltherapie der myokardialen Ischämie: Grundlagen und präklinische Applikationen
	UniversitätsSpital Zürich, Schweiz Medizinbereich Herz-Gefäss-Thorax Klinik für Kardiologie (Direktor: Prof. Dr. med. T. F. Lüscher)
Datum der Habilitation:	27.09.2011

PREISE UND AUSZEICHNUNGEN

02/2000:	Promotionsstipendium gefördert durch die Herbert-Quandt-Stiftung der VARTA AG
11/2003:	Promotion zum Dr. med. mit *summa cum laude*
04/2005:	Braukmann-Wittenberg Award Braukmann-Wittenberg-Herz-Stiftung, Hannover
09/2005:	EVBA Travel Award – Young Investigator Award 3rd European Meeting on Vascular Biology and Medicine, Hamburg
08/2009:	Moderated Poster Award European Society of Cardiology, Barcelona, Spanien

06/2011:   SGK-Forschungspreis (Schweizerischen Gesellschaft für
                                  Kardiologie) CHF 30.000,-

EINGEWORBENE DRITTMITTEL

1.   Finanzierungsquelle: Hochschulinterne Leistungsförderung (HiLF II)
                                  Medizinische Hochschule Hannover
     Hauptantragsteller: Christian Templin
     Projekt: Innovative Strategien zur Stammzelltherapie nach akutem
                                  Herzinfarkt
     Zeitperiode: 01/2004 – 04/2005
     Betrag: Euro 60.000,-

2.   Finanzierungsquelle: Braukmann-Wittenberg-Herz-Stiftung, Hannover
     Hauptantragsteller: Christian Templin
     Projekt: Therapie der myokardialen Ischämie durch gentechnisch
                                  manipulierte Stammzellen - Grundlagen und klinische
                                  Applikationen -
     Zeitperiode: 04/2005 – 04/2006
     Betrag: Euro 18.700,-

3.   Finanzierungsquelle: Schweizerischer Nationalfonds (SNF)
                                  Spezialprogramm Universitäre Medizin (SPUM)
     Co-Antragsteller: Christian Templin
     Projekt: Inflammation and acute coronary syndrome (ACS) – novel
                                  strategies for prevention and clinical management
     Zeitperiode: 01/2009 – 12/2011
     Betrag: CHF 390.000,-

4.   Finanzierungsquelle: Medtronic
     Hauptantragsteller: Christian Templin
     Projekt: Catheter-based transplantation of human induced pluripotent
                                  stem cell (IPSC) derivates after myocardial infarction: First
                                  study in a pre-clinical large animal model
     Zeitperiode: 03/2011
     Betrag: CHF 37.200,-

5.   Finanzierungsquelle: Swiss Life Jubiläumsstiftung
     Hauptantragsteller: Christian Templin
     Projekt: Catheter-based transplantation of human induced pluripotent
                                  stem cell (iPSC) derivatives after myocardial infarction
     Zeitperiode: 05/2011
     Betrag: CHF 20.000,-

6.   Finanzierungsquelle: Biosensors Europe SA
     Hauptantragsteller: Christian Templin
     Projekt: Differentialdiagnose Takotsubo – ein klassisches akutes
                                  Koronarsyndrom
     Zeitperiode: 10/2011 – 10/2012
     Betrag: CHF 101.400,-

7.   Finanzierungsquelle: Gottfried und Julia Bangerter-Rhyner-Stiftung
     Hauptantragsteller: Christian Templin

Projekt:	Catheter-based transplantation of human induced pluripotent stem cell (iPSC) derivatives after myocardial infarction
Zeitperiode:	03/2012
Betrag:	CHF 90.000,-

8.

Finanzierungsquelle:	Swiss Life Jubiläumsstiftung
Hauptantragsteller:	Christian Templin
Projekt:	Catheter-based transplantation of human induced pluripotent stem cell (iPSC) derivatives after myocardial infarction
Zeitperiode:	05/2012
Betrag:	CHF 20.000,-

9.

Finanzierungsquelle:	Prof. Otto Beisheim-Stiftung
Hauptantragsteller:	Christian Templin
Projekt:	Die Takotsubo Kardiomyopathie – „Das gebrochene Herz als Krankheit"
Zeitperiode:	09/2012 – 09/2013
Betrag:	CHF 10.000,-

MITGLIEDSCHAFTEN

Deutsche Gesellschaft für Kardiologie, Herz- und Kreislaufforschung (DGK)
Schweizerische Gesellschaft für Kardiologie (SGK)
Europäische Gesellschaft für Kardiologie (ESC)
European Association of Percutaneous Cardiovascular Interventions (EAPCI)
Deutsche Gesellschaft für Stammzellforschung (GSZ)

FELLOWSHIPS IN PROFESSIONAL SOCIETIES

European Society of Cardiology (F.E.S.C.)

EDITORIAL BOARD MEMBER

Stem Cell Discovery

REVIEWER FÜR PEER-REVIEWED JOURNALS

Annals of Internal Medicine	(Impact factor: 16.733)
Journal of the American College of Cardiology	(Impact factor: 14.156)
European Heart Journal	(Impact factor: 10.478)
Stem Cells	(Impact factor: 7.781)
JACC Cardiovascular Imaging	(Impact factor: 6.800)
Journal of Cellular and Molecular Medicine	(Impact factor: 5.166)
PLoS One	(Impact factor: 4.092)
Mediators of Inflammation	(Impact factor: 3.263)
Transplantation International	(Impact factor: 2.921)
Current Vascular Pharmacology	(Impact factor: 2.896)

PD Dr. med. Christian Templin   Hannover, im Oktober 2012

8.   Publikationsverzeichnis

PERSÖNLICHER IMPACTFAKTOR

Kumulativer Impactfaktor (gesamt – 2000 - 2012):   293.906
Kumulativer Impactfaktor (Erstautor – 2000 - 2012):   100.558
Kumulativer Impactfaktor (Erst- oder Letztautor – 2000 - 2012):   126.897

Kumulativer Impactfaktor (letzten 5 Jahre - 2008 - 2012):   238.648
Kumulativer Impactfaktor (Erstautor - 2008 - 2012):   81.172
Kumulativer Impactfaktor (Erst- oder Letztautor - 2008 - 2012):   107.511

Zitationen ("Science Citation Index"):   560
H-Index: 9
Anzahl Publikationen (ohne Abstracts):   60
Abstracts: 73

Zusammenfassung Publikationen in „peer-reviewed Journals"

Journal	Impactfaktor	Anzahl Publikationen
Circulation	14.739	3
Journal of the American College of Cardiology	14.156	1
The Journal of Clinical Investigation	13.069	1
European Heart Journal	10.478	8
Proc Natl Acad Sci U S A	9.681	1
Basic Research in Cardiology	7.348	1
International Journal of Cardiology	7.078	7
JACC Cardiovascular Interventions	6.800	1
Journal of Nuclear Medicine	6.381	1
Journal of Virology	5.402	1
Journal of Molecular and Cellular Cardioliology	5.166	1
Heart	4.223	1
Journal of Hypertension	4.021	1
Current Pharmaceutical Design	3.870	1
Experimental Dermatology	3.543	1
Clinical Research in Cardiology	2.950	3
Experimantal Hematology	2.905	1
Int. Journal of Developmental Biology	2.823	1
Rapid Communications in Mass Spectrom	2.790	1
Eur Heart J – Cardiovascular Imaging	2.317	1
International Journal of Cardiovascular Imaging	2.285	1
Annals of Transplantation	2.020	2
Cardiology	1.705	1
Transplantation Procedings	1.005	4
Herz	0.924	1
Acute Cardiac Care	$\varnothing$	2
Cardiovascular Medicine	$\varnothing$	2
Praxis	$\varnothing$	1
Rev Med Suisse	$\varnothing$	1
Tx Med	$\varnothing$	1

ORIGINALARBEITEN

1. Blusch JH, Patience C, Takeuchi Y, **Templin C**, Roos C, von der Helm K, Steinhoff G, Martin U.
    Infection of nonhuman primate cells by pig endogenous retrovirus.
    J Virol. 2000 Aug;74(16):7687-90.
    (Impact factor: 5.402)

2. Simon AR, Schroder C, Martin U, Chikobava M, **Templin C**, Laaf G, Kohl J, Lapin B, Haverich A, Steinhoff G.
    An attempt to induce peripheral tolerance in a pig-to-primate transplantation model by infusion of ultrahigh numbers of donor peripheral blood mononuclear cells: first promising results.
    Transplant Proc. 2000 Aug;32(5):1052-3.
    (Impact factor: 1.005)

3. **Templin C**, Schroder C, Simon AR, Laaf G, Kohl J, Chikobava M, Lapin B, Steinhoff G, Martin U.
    Analysis of potential porcine endogenous retrovirus transmission to baboon in vitro and in vivo.
    Transplant Proc. 2000 Aug;32(5):1163-4.
    (Impact factor: 1.005)

4. **Templin C**, Schroder C, Simon AR, Laaf G, Kohl J, Chikobava M, Lapin B, Winkler ME, Wiebe K, Steinhoff G, Martin U.
    Long-term monitoring of xenotransplanted baboons: no evidence for pig endogenous retrovirus transmission.
    Transplant Proc. 2001 Feb-Mar;33(1-2):692.
    (Impact factor: 1.005)

5. Simon AR, Schroder C, Martin U, Chikobava M, **Templin C**, Laaf G, Wiebe K, Lapin B, Haverich A, Steinhoff G.
    Induction of long-term chimerism in a pig-to-primate model of peripheral tolerance induction.
    Transplant Proc. 2001 Feb-Mar;33(1-2):705.
    (Impact factor: 1.005)

6. Simon AR, Schroder C, Martin U, Tessmann R, **Templin C**, Laaf G, Wiebe K, Steinhoff G, Lapin B, Chikobava M, Haverich A.
    Induction of long-term peripheral microchimerism in non-human primates in a model of xenogeneic peripheral tolerance induction.
    Ann Transplant. 2002;7(3):40-5.
    (Impact factor: 2.020)

7. Ericsson TA, Takeuchi Y, **Templin C**, Quinn G, Farhadian SF, Wood JC, Oldmixon BA, Suling KM, Ishii JK, Kitagawa Y, Miyazawa T, Salomon DR, Weiss RA, Patience C.
    Identification of receptors for pig endogenous retrovirus.
    Proc Natl Acad Sci U S A. 2003 May 27;100(11):6759-64.
    (Impact factor: 9.681)

8. Simon AR, **Templin C**, Schröder C, Laaf G, Tessmann R, Winkler ME, Tacke S, Denner J, Lapin B, Chikobava M, Patience C, Steinhoff G, Agrba VZ, Haverich A, Martin U.

No evidence for productive PERV infection of baboon cells in in vivo infection model.
Ann Transplant. 2003;8(3):24-34.
(Impact factor: 2.020)

9.   **Templin C**, Simon AR, Schröder C, Winkler ME, Laaf G, Chikobava M, Agrba VZ, Lapin B, Haverich A, Martin U.
      Analyse potentieller PERV-Infektionen in einem klinisch relevanten Schwein-auf-Pavian Zelltransplantationsmodell.
      Tx Med. 2002; 14(4):225-230.
      (Ø Impact factor)

10.   Landmesser U, Engberding N, Bahlmann FH, Schaefer A, Wiencke A, Heineke A, Spiekermann S, Hilfiker-Kleiner D, **Templin C**, Kotlarz D, Mueller M, Fuchs M, Hornig B, Haller H, Drexler H.
      Statin-induced improvement of endothelial progenitor cell mobilization, myocardial neovascularization, left ventricular function, and survival after experimental myocardial infarction requires endothelial nitric oxide synthase.
      Circulation. 2004 Oct 5;110(14):1933-9.
      (Impact factor: 14.739)

11.   **Templin C**, Kotlarz D, Marquart F, Faulhaber J, Brendecke V, Schaefer A, Tsikas D, Bonda T, Hilfiker-Kleiner D, Ohl L, Naim HY, Foerster R, Drexler H, Limbourg FP.
      Transcoronary delivery of bone marrow cells to the infarcted murine myocardium: feasibility, cellular kinetics, and improvement in cardiac function.
      Basic Res Cardiol. 2006 Jul;101(4):301-10.
      (Impact factor: 7.348)

12.   Salguero G, Akin E, **Templin C**, Kotlarz D, Doerries C, Landmesser U, Grote K, Schieffer B.
      Renovascular hypertension by two-kidney one-clip enhances endothelial progenitor cell mobilization in a p47^{phox}-dependent manner.
      J Hypertens. 2008 Feb;26(2):257-68.
      (Impact factor: 4.021)

13.   **Templin C**, Kotlarz D, Rathinam C, Rudolph C, Schätzlein S, Ramireddy K, Rudolph KL, Schlegelberger B, Klein C, Drexler H.
      Establishment of immortalised multipotent hematopoetic progenitor cell lines by retroviral-mediated gene transfer of beta-catenin.
      Exp Hematol. 2008 Feb;36(2):204-215.
      (Impact factor: 2.905)

14.   **Templin C**, Kotlarz D, Faulhaber J, Schnabel S, Grote K, Salguero G, Luchtefeld M, Hiller KH, Jakob P, Naim HY, Schieffer B, Hilfiker-Kleiner D, Landmesser U, Limbourg FP, Drexler H.
      Ex vivo expanded hematopoietic progenitor cells improve cardiac function after myocardial infarction: role of beta-catenin-transduction and cell dose.
      J Mol Cell Cardiol. 2008 Sep.;45(3):394-403.
      (Impact factor: 5.166)

15.   **Templin C**, Grote K, Schledzewski K, Ghadri JR, Schnabel S, Napp LC, Schieffer B, Kurzen H, Goerdt S, Landmesser U, Koenen W, Faulhaber J.
      Ex vivo expanded hematopoietic progenitor cells improve dermal wound healing by paracrine mechanisms.
      Exp Dermatol. 2009 May;18(5):445-53.

(Impact factor: 3.543)

16. Gardiwal A, Reissmann LM, Kotlarz D, Oswald H, Korte T, Landmesser U, Klein G, **Templin C**.
Arrhythmia susceptibility in mice after therapy with beta-catenin-transduced hematopoietic progenitor cells after myocardial ischemia/reperfusion.
Cardiology. 2009;114(3):199-207.
(Impact factor: 1.705)

17. Luecke N, **Templin C**, Muetzelburg MV, Neumann D, Just I, Pich A.
Secreted proteome of the murine multipotent hematopoietic progenitor cell line DKmix.
The first two authors contributed equally to this work.
Rapid Commun Mass Spectrom. 2010 Mar 15;24(5):561-570.
(Impact factor: 2.790)

18. **Templin C**, Meyer M, Djonov V, Hlushchuk R, Dimova I, Flueckiger S, Müller MF, Kronen P, Sidler M, Klein K, Nicholls F, Ghadri JR, Weber K, Paunovic D, Corti R, Hoerstrup S, Lüscher TF, Landmesser U.
Coronary optical frequency domain imaging (OFDI) for in vivo evaluation of stent healing: comparison with light and electron microscopy.
Eur Heart J. 2010 Jul;31(14):1792-801.
(Impact factor: 10.478)

19. **Templin C**, Ghadri JR, Rougier JS, Baumer A, Kaplan V, Albesa M, Sticht H, Rauch A, Puleo C, Hu D, Barajas-Martinez H, Antzelevitch C, Lüscher TF, Abriel H, Duru F.
Identification of a novel loss-of-function calcium channel gene mutation in short QT syndrome (SQTS 6).
Eur Heart J. 2011 May;32(9):1077-88.
(Impact factor: 10.478)

20. Ghadri JR, Pazhenkottil AP, Nkoulou RN, Buechel RR, Goetti R, Husmann L, Herzog BA, Wolfrum M, Wyss CA, **Templin C**, Kaufmann PA.
Very high coronary calcium score unmasks obstructive coronary artery disease in patients with normal SPECT MPI.
Heart. 2011 Jun;97(12):998-1003.
(Impact factor: 4.223)

21. Ghadri JR, Goetti R, Fiechter M, Pazhenkottil AP, Küest SM, Nkoulou RN, Windler C, Herzog BA, Gaemperli O, **Templin C**, Kaufmann PA.
Inter-scan variability of coronary artery calcium scoring assessed on 64-multidetector computed tomography vs. dual-source computed tomography: a head-to-head comparison.
Eur Heart J. 2011 Aug;32(15):1865-74.
(Impact factor: 10.478)

22. Besler C, Heinrich K, Rohrer L, Doerries C, Riwanto M, Shih DM, Chroni A, Yonekawa K, Stein S, Schaefer N, Mueller MF, Akhmedov A, Daniil G, Manes C, **Templin C**, Wyss C, Maier W, Tanner FC, Matter CM, Corti R, Furlong C, Lusis AJ, von Eckardstein A, Fogelman AM, Lüscher TF, Landmesser U.
Mechanisms underlying adverse effects of HDL on eNOS-activating pathways in patients with coronary artery disease.
J Clin Invest. 2011 Jul; 121(7):2693-708.
(Impact factor: 13.069)

23. Ghadri JR, Küest SM, Goetti R, Fiechter M, Pazhenkottil AP, Nkoulou RN, Kuhn FP, Pietsch C, von Schulthess P, Gaemperli O, **Templin C**, Kaufmann PA.
Image quality and radiation dose comparison of prospectively triggered low-dose CCTA: 128-slice dual-source high-pitch spiral versus 64-slice single-source sequential acquisition.
Int J Cardiovasc Imaging. 2012 Jun;28(5):1217-25.
(Impact factor: 2.285)

24. Jaguszewski M, Targonski R, Fijalkowski M, Masiewicz E, Dubaniewicz W, **Templin C**, Koprowski A, Ciecwierz D, Nallamothu BK, Rynkiewicz A.
Recanalization of isolated chronic total occlusions in patients with stable angina.
Int J Cardiol. 2012 May 9. [Epub ahead of print].
(Impact factor: 7.078)

25. Ghadri JR, Fiechter M, Verguth K, Gebhard C, Pazhenkottil AP, Fuchs T, **Templin C**, Gaemperli O, Kaufmann PA.
Coronary calcium score as an adjunct to nuclear myocardial perfusion imaging for risk stratification before noncardiac surgery.
J Nucl Med. 2012 Jul;53(7):1081-6.
(Impact factor: 6.381)

26. Ghadri JR, Fiechter M, Fuchs TA, **Templin C**, Lüscher TF, Kaufmann PA.
The value of coronary calcium score in daily clinical routine, a case series of patients with extensive coronary calcifications.
Int J Cardiol. 2012 Jun 15. [Epub ahead of print].
(Impact factor: 7.078)

27. **Templin C**, Zweigerdt R, Schwanke K, Olmer R, Ghadri JR, Emmert M, Müller E, Küest SM, Cohrs S, Schibli R, Kronen P, Hilbe M, Reinisch A, Strunk D, Haverich A, Hoerstrup SP, Lüscher TF, Kaufmann PA, Landmesser U, Martin U.
Transplantation and tracking of human-induced pluripotent stem cells in a pig model of myocardial infarction: assessment of cell survival, engraftment and distribution by hybrid single photon emission computed tomography/computed tomography of sodium iodide symporter trangene expression.
Circulation. 2012 Jul 24;126(4):430-9.
(Impact factor: 14.739)

28. Fiechter M, Ghadri JR, Sidler M, Martin U, Landmesser U, Kaufmann PA, Lüscher TF, **Templin C**.
Cardiac quadruple-fusion imaging: A brief report on a novel integrated multimodality approach for in vivo visualization of transplanted stem cells.
Int J Cardiol. 2012 Jul 18. [Epub ahead of print].
(Impact factor: 7.078)

29. Emmert MY, Weber B, Wolint P, Behr L, Sammut S, Frauenfelder T, Frese L, Scherman J, Brokopp CE, **Templin C**, Grünenfelder J, Zünd G, Falk V, Hoerstrup SP.
Stem cell-based transcatheter aortic valve implantation: first experiences in a pre-clinical model.
JACC Cardiovasc Interv. 2012 Aug;5(8):874-83.
(Impact factor: 6.800)

30. Doerries C, Briand S, Jakob P, Mocharla P, Besler C, Müller MF, Manes C, **Templin C**, Baltes C, Rudin M, Adams H, Wolfrum M, Noll G, Ruschitzka F, Lüscher TF, Landmesser U.
     Loss of pro-AngiomiR 126 and 130a in early endothelial progenitor cells and CD34$^+$ progenitor cells from patients with chronic heart failure: critical role for cardiac and endothelial repair capacity.
     Circulation in press.
     (Impact factor: 14.739)

31. Ghadri JR, Fiechter M, Fuchs T, Gebhard C, Scherrer A, Herzog A, Pazhenkottil AP, Klaeser B, **Templin C**, Gaemperli O, Kaufmann PA.
     Registry for the Evaluation of the PROgnostic value of a novel hybrid imaging approach integrating Single Photon Emission Computed Tomography with coronary calcification imaging (REPROSPECT).
     Eur Heart J – Cardiovascular Imaging in press.
     (Impact factor: 2.317)

32. Schwanke K, Merkert S, **Templin C**, Müller S, Roa-Lara A, Gruh I, Haverich A, Martin U, Zweigerdt R.
     Efficient multi-transgenic modification of human pluripotent stem cells.
     Human Gene Therapy invited major revision.

33. Ghadri JR, Kazakauskaite E, Braunschweig, Fiechter M, Fuchs T, Gebhard C, Stehli J, Gaemperli O, Corti R, **Templin C**, Lüscher TF, Schmied C, Kaufmann PA.
     Incidence of coronary anomalies detected by coronary computed tomography compared to invasive coronary angiography.
     Submitted to *Int J Cardiol.*

34. Fiechter M, Ghadri JR, Jaguszewski M, Siddique A, Vogt S, Haller RB, Halioua R, Handzic A, Kaufmann PA, Corti R, Lüscher TF, **Templin C**.
     Additive impact of humoral and cellular inflammation on major adverse cardiovascular events and left ventricular function in patients with acute coronary syndromes.
     Submitted to *Int J Cardiol.*

35. Ghadri JR, Sarcon A, Srikantharupan S, Pfister P, Jaguszewski M, Siddique A, Kaufmann PA, Wyss C, Gaemperli O, Landmesser U, Altwegg L, Maier W, Corti R, Lüscher TF, **Templin C**.
     Current outcome of acute coronary syndromes: Data from the Zurich-Acute Coronary Syndrome (Z-ACS)-Registry.
     Submitted to *Cardiovascular Medicine.*

36. Jaguszewski M, Ghadri JR, Seifert B, Hiestand T, Herrera P, Wyss C, Altwegg L, Gaemperli O, Landmesser U, Maier W, Windecker S, Corti R, Lüscher TF, **Templin C**.
     Drug-eluting stents vs. bare-metal stents in patients with cardiogenic shock: A head-to-head comparision by propensity score analysis.
     Submitted to *J Am Coll Cardiol.*

37. **Templin C**, Osipova J, Emmert M, Kraenkel N, Ghadri JR, Manes C, Styp-Rekowska B, Briand S, Klingenberg R, Jaguszewski M, Matter C, Djonov V, Hoerstrup SP, Lüscher TF, Thum T, Landmesser U.

Increased proangiogenic capacity of mobilized CD34$^+$ progenitor cells from patients with an acute ST-elevation myocardial infarction: Role of differential microRNA expression
Submitted to *Circulation Research.*

CASE REPORTS

1. **Templin C**, Schaefer A, Stumme B, Drexler H, von Depka M.
Combined aspirin and clopidogrel resistance associated with recurrent coronary stent thrombosis.
Clin Res Cardiol. 2006 Feb;95(2):122-6.
(Impact factor: 2.950)

2. **Templin C**, Pertschy S, Schaefer A.
Cardiac hemochromatosis.
Int J Cardiol. 2007 Apr 4;116(3):e109-10.
(Impact factor: 7.078)

3. **Templin C**, Ghadri JR, Wilkens L, Niehaus M.
Difficult differential diagnosis of a right atrial intracardiac mass.
Int J Cardiol. 2008 Mar 28;125(1):e19-20.
(Impact factor: 7.078)

4. **Templin C**, Westhoff-Bleck M, Ghadri JR.
Hypokalemic paralysis with rhabdomyolysis and arterial hypertention caused by liquorice ingestion.
Clin Res Cardiol. 2009 Feb;98(2):130-2.
(Impact factor: 2.950)

5. **Templin C**, Ghadri JR, Wyss C, Lüscher TF, Kaufmann P, Landmesser U.
Severe left main coronary stenosis and mitral regurgitation in a young female patient without cardiovascular risk factors 14 years after mediastinal radiation therapy.
Clin Res Cardiol. 2010 Mar;99(3):199-201.
(Impact factor: 2.950)

6. Hasun M, Goetti R, **Templin C**.
Life-threatening early saphenous vein interponat stenosis after left main artery replacement.
Eur Heart J. 2011 Apr;32(7):913.
(Impact factor: 10.478)

7. Ghadri JR, Fiechter M, **Templin C**, Lüscher TF, Kaufmann PA, Landmesser U.
Cardiac hybrid imaging in a patient with a single coronary artery originating from the right sinus of Vasalva.
Eur Heart J. 2011 Nov;32(22):2757.
(Impact factor: 10.478)

8. Ghadri JR, Jaguszewski M, Corti R, Lüscher TF, **Templin C**.
Different wall motion patterns of three consecutive episodes of takotsubo cardiomyopathy in the same patient.
Int J Cardiol. 2012 Oct 4;160(2):e25-7.
(Impact factor: 7.078)

9.   Jaguszewski M, Fijalkowski M, Nowak R, Czapiewski P, Ghadri JR, **Templin C**, Rynkiewicz A.
      Ventricular rupture in Takotsubo Cardiomyopathy.
      Eur Heart J. 2012 Apr;33(8):1027.
      (Impact factor: 10.478)

10.   Saguner AM, Haegeli LM, **Templin C**, Wolber T, Landmesser U, Duru F.
      Arrhythmogenic cardiomyopathy suspected by electrocardiogram: confirmed by angiography.
      Eur Heart J. 2012 Jun;33(11):1343.
      (Impact factor: 10.478)

11.   Jaguszewski M, Widmer N, Ghadri JR, Alibegovic J, Gaemperli O, Emmert MY, Corti R, Lüscher TF, Wyss CA, **Templin C**.
      Hemodynamic tracing pattern reveals acute type A aortic dissection.
      Acute Card Care. 2012 Sep;14(3):94-5.
      (Ø Impact factor)

12.   Jaguszewski M, Küest SM, **Templin C**, Landmesser U.
      Optical frequency domain imaging to reveal an angiographically inapparent very late stent thrombosis as the cause of an acute coronary syndrome.
      J Am Coll Cardiol. 2012 Aug 14;60(7):e11.
      (Impact factor: 14.156)

13.   **Templin C**, Ghadri JR, Noll G, Lüscher TF, Ruschitzka F.
      Allograft vasculopathy vs. coronary artery disease: comparison by optical coherence tomography.
      Eur Heart J. 2012 Sep 10. [Epub ahead of print].
      (Impact factor: 10.478)

14.   Ghadri JR, Fuchs TA, **Templin C**, Lüscher TF, Maier W, Kaufmann PA.
      Cardiac hybrid imaging guides revascularization prior to non-cardiac surgery.
      Int J Cardiol. 2012 Sep 25.
      (Impact factor: 7.078)

15.   Ghadri JR, Gstrein C, Lüscher TF, **Templin C**.
      A giant right-sided heart due to idiopathic pulmonary hypertension.
      Acute Card Care in press.
      (Ø Impact factor)

REVIEWS / EDITORIALS

1.   Matter CM, Klingenberg R, **Templin C**, Altwegg L, Räber L, Carballo D, Auer R, Landmesser U, Maier W, Windecker S, Jüni P, Mach F, Keller PF, Rodondi N, Lüscher TF.
      Inflammation and acute coronary syndromes (ACS) – a clinical research network funded by the Swiss National Science Foundation.
      Cardiovascular Medicine. November 15 2009.
      (Ø Impact factor)

2.   Carballo D, Auer R, Carballo S, Windecker S, Matter C, Luscher T, Vogt P, Perneger T, Mach F, Rodondi N, Keller PF, SPUM-ACS.

Collaborators: Raeber L, Windecker S, Jüni P, Klingenberg R, Altweg L, **Templin C**, Landmesser U, Matter C, Maier W, Luscher T, Scherrer F, Golay A, Gache P, Sommer J, Reffet A, Schneider F, Richard-Arlaud A, Hugli O, Waeber G, Cornuz J.
A Swiss multicentric project to improve the prevention of cardiovascular event recurrence after acute coronary sysndromes.
Rev Med Suisse. 2010 Mar 10;6(239):518, 520-2, 524.
 (Ø Impact factor)

3. **Templin C**, Lüscher TF, Landmesser U.
Stem and progenitor cell-based therapy approaches: current developments on treatment of acute myocardial infarction and chronic ischemic cardiomyopathy.
Herz. 2010 Oct;35(7):445-457.
(Impact factor: 0.924)

4. **Templin C**, Lüscher TF, Landmesser U.
Cell-based cardiovascular repair and regeneration in acute myocardial infarction and chronic ischemic cardiomyopathy – Current status and future developments.
Int J Dev Biol. 2011;55(4-5):407-17.
(Impact factor: 2.823)

5. **Templin C**, Kränkel N, Lüscher TF, Landmesser U.
Stem cells in cardiovascular regeneration: from preservation of endogenous repair to future cardiovascular therapies.
Curr Pharm Des. 2011 Oct;17(30):3280-94.
(Impact factor: 3.870)

6. Enseleit F, Sudano I, Ghadri JR, **Templin C**.
Takotsubo Kardiomyopathie: Eine wichtige Differentialdiagnose des Akuten Koronarsyndroms.
Cardiovascular Medicine in press.
 (Ø Impact factor)

7. Emmert MY, **Templin C**.
Kardiale Stamm- und Progenitorzellzelltherapie: Bereit für die Zukunft?
Praxis in press.
(Ø Impact factor)

BUCHBEITRÄGE

1. **Templin C**, Schaefer A, Stumme B, Drexler H, von Depka Prondzinski M.
Recurrent coronary stent thrombosis in a patient with combined aspirin and clopidogrel resistence.
35th Hemophilia Symposium Hamburg 2004. Springer Verlag 2006.

ABSTRACTS VON VORTRÄGEN UND POSTERN

> 70

9.   Anhang

Publikation 1

Titel der Arbeit: „Fast and Efficient Multi-transgenic Modification of Human Pluripotent Stem Cells"

Autoren: Schwanke K, Merkert S, **Templin C**, Jara-Avaca M, Müller S, Haverich A, Martin U, Zweigerdt R.

Publikationsorgan: Human Gene Therapy, in revision.

eigener Beitrag: - funktionelle Testung der generierten transgenen NIS$^+$-hiPSCs in *ex vivo* Schweineherzen
- Etablierung des Zellnachweises mittels SPECT-CT-Imaging
- Schreiben von Teilen des Manuskriptes

Fast and Efficient multi-transgenic modification of human pluripotent stem cells

Fast and Efficient multi-transgenic modification of human pluripotent stem cells

Running title: Schwanke – Non-viral multi-transgenic modification of stem cells

[1,2]Kristin Schwanke, [1,2]Sylvia Merkert,

[1,3]Christian Templin, [1,2]Monica Jara-Avaca, [1,2]Susann Müller, [1,2]Axel Haverich,

[1,2,4]Ulrich Martin & [1,2,4]Robert Zweigerdt

[1]Leibniz Research Laboratories for Biotechnology and Artificial Organs (LEBAO), Department of Cardiac, Thoracic-, Transplantation and Vascular Surgery, [2]REBIRTH-Cluster of Excellence, Hannover Medical School, Carl-Neuberg-Strasse 1, 30625 Hannover, Germany. [3]Cardiovascular Center, Cardiology, University Hospital Zurich, Raemistrasse 100, 8091 Zurich, Switzerland. [4] these authors contributed equally.

Correspondence to

Robert Zweigerdt, Leibniz Research Laboratories for Biotechnology and Artificial Organs (LEBAO), Hannover Medical School, Carl-Neuberg-Str.1, 30625 Hannover, Germany

Fax: +49 511 532 8819 phone: +49 511 532 5023

Email: zweigerdt.robert@mh-hannover.de

Ulrich Martin, Leibniz Research Laboratories for Biotechnology and Artificial Organs (LEBAO), Hannover Medical School, Carl-Neuberg-Str.1, 30625 Hannover, Germany

Fax: +49 511 532 8819 phone: +49 511 532 8820

Email: martin.ulrich@mh-hannover.de

1

Abstract

Human pluripotent stem cells (hPSCs) are a prime cell source for regenerative therapies due to their extensive expansion potential and the ability to differentiate into essentially all somatic lineages *in vitro*. The introduction of transgenes into hPSCs will facilitate their pre-clinical testing and other applications such as purification of desired cell lineages during differentiation and *in vivo* monitoring of transplanted progenies in relevant animal models. To date, several limits regarding the efficient generation of transgenic cell lines exist. This includes low transfection rates via non-viral methods, inefficient recovery of engineered clones and silencing of transgene expression.

Here we describe a fast and highly efficient method for the generation of multi-transgenic hPSC lines by overcoming the need for any pre-adaption of hPSCs to feeder-free conditions before genetic manipulation. Selection for a single antibiotic resistance gene encoded on one plasmid allowed for the stable genomic integration of several independent plasmid constructs thereby generating valuable multi-transgenic cell lines.

Introduction

Human pluripotent stem cells (hPSCs), that is embryonic stem cells (hESCs) and induced pluripotent stem cells (hiPSCs), have become a prime cell source for envisioned regenerative therapies, given their extensive proliferation and multilineage differentiation potential *in vitro*. To date, such cell-based approaches are still under development and numerous issues remain to be addressed before hPSC-derived progenies can enter routine clinical application. Stable transgene expressing hPSC lines could be valuable tools along this path. For example, overexpression of specific transcription or growth factors aiming at direct differentiation into a desired cell type may overcome poor differentiation efficiencies, which exist for several lineages (Odorico *et al.*, 2001). On the other hand, lineage restricted reporter gene expression could be used to enrich specific progenies (Boecker *et al.*, 2004; Huber *et al.*, 2007; Xu, 2008; Kita-Matsuo *et al.*, 2009; Ritner *et al.*, 2011). Another application is a cell type-specific or ubiquitous expression of marker genes to monitor cell engraftment in respective animal models post-transplantation (Dai *et al.*, 2007; Sun *et al.*, 2009; Mauritz *et al.*, 2011).

In the last decade a multitude of methods to genetically manipulate hPSCs was established including viral transduction (Jang *et al.*, 2006; Wurm *et al.*, 2011), chemical transfection (Liu *et al.*, 2009) and electroporation (Zwaka and Thomson, 2003; Costa *et al.*, 2005). Among integrating vector systems that could be used for generation of stable transgenic PSC lines, classical oncoretroviral vectors are well known to become silenced very fast in pluripotent stem cells (Yao *et al.*, 2004). Although using lentiviral vectors, high transduction efficiencies >90% and high levels of initial transgene expression can be achieved (Ma *et al.*, 2003; Moore *et al.*, 2005), murine ESCs and human PSCs were found to substantially suppress long-term expression of transgenes delivered by HIV-derived vectors (Cherry *et al.*, 2000; Xia *et al.*, 2007), also. This effect appears to depend on the applied promoter and the site of integration, and mainly becomes manifested during first days after transduction (Haas *et al.*, 2000; Philippe *et al.*, 2006; Xia *et al.*, 2007; Norrman, 2010 #100). Another objection is the tendency of integrating viral vectors to induce insertional mutagenesis that provokes oncogene activation or inactivation of tumor suppressor genes (Kustikova *et al.*, 2005) thereby increasing the likelihood of malignant transformation. In contrast to plasmid transfection, production of viral vectors is usually time consuming and requires facilities with increased safety levels. Common techniques of plasmid transfection include electroporation and chemical transfection with liposomes or polycationic complexes being the most frequent chemical agents to facilitate cell entry via fusion with the cell membrane or uptake by endocytosis, respectively (Pichon *et al.*, 2010; Ziello *et al.*, 2010). Development of enhanced

3

transfection reagents such as Fugene HD® or Genejammer allowed chemical transfection of hPSCs and generation of stable clones (Braam *et al.*, 2008b; Liu *et al.*, 2009) but efficiencies are usually rather low (Liu *et al.*, 2009) and ESC line-dependent (Liew *et al.*, 2007).

During electroporation the plasma membrane is transiently permeabilized by electrical pulses thereby enabling uptake of exogenous nucleic acid molecules which is in principle not limited by vector size and the nature of the nucleic acid (Moore *et al.*, 2005). However, efficient electroporation necessarily requires generation of a single cell suspension (Schinzel *et al.*, 2011). In contrast to mouse ES and iPS cells, hPSCs are highly sensitive to complete dissociation into single cells resulting in dramatically reduced survival rates after electroporation. Prior approaches have tried to overcome this issue by adapting hPSCs to feeder-free conditions established by trypsine-based cell splitting for several passages before transfection (Moore *et al.*, 2005; Costa, 2007; Braam, 2008). This approach, however, may lead to an inadvertent clonal pre-selection of cells adapted to this treatment and close assessment of pluripotency markers expression and karyotyping is mandatory before setting up experiments (Braam *et al.*, 2008b). Moreover, cell adaption is time consuming thereby extending generation of transgenic lines for several weeks (Costa, 2007; Braam *et al.*, 2008a).

Here we describe a straightforward approach for fast and highly efficient parallel introduction of several plasmids into hPSCs. Stable multi-transgenic clones were established by means of a single drug resistance. The method is applicable directly to conventional feeder-based cultures and does not require any pre-adaption of hPSCs to single cell passaging. Multi-transgenic hPSC lines stably expressing fluorescence emitting reporters, a sodium iodide symporter-(NIS), which allows non-invasive *in vivo* tracking of transplanted cells via SPECT-CT assessment (Acton and Kung, 2003), and enabling transgene-based lineage enrichment, were established. We showed that stable transfected clones maintained their pluripotent character and differentiated into derivatives of all the three germ layers. Reporter gene expression was found to be stable in undifferentiated cells after extensive passaging even if transgenes were encoded on co-introduced plasmids carrying no additional antibiotic resistance marker. Finally, the possibility of NIS-dependent *in situ* imaging after intramyocardial infusion of radionucleotide labelled cells was demonstrated, and antibiotic-based purification of cardiomyocytes (CMs) was performed to demonstrate broad practical applicability of the method for numerous purposes.

Materials and Methods

Feeder-dependent adherent culture

hESCs (hES3 (Hoffman and Carpenter, 2005), I3 (Amit *et al.*, 2003)) and hiPSCs (hCBiPSC clone 2 hFFiPSC clone 4 (Haase, 2009)) lines were cultured under standard conditions. Briefly, cells were grown on irradiated embryonic fibroblasts in 80% knockout-Dulbecco's modified Eagle's medium (ko-DMEM) supplemented with 20% knockout serum replacement, 1 mM L-Glutamine, 0.1 mM β-Mercaptoethanol, 1% non-essential amino acid stock (all from Invitrogen, Karlsruhe, Germany) and either 50 ng/ml (hESC) or 4 ng/ml (hiPSC) bFGF (supplied by the Institute for Technical Chemistry, Leibniz University Hannover, Germany (Knoerzer *et al.*, 1989)). Cells were cultured in six-well plates and passaged once a week using 1mg/ml collagenase type IV (Invitrogen). The medium was changed daily.

Plasmid vectors

The vector αMHCneoPGKhygro is a 10.9kb construct carrying two selection cassettes: 1st the hygromycin resistance gene controlled under the ubiquitously expressed phosphoglycerate kinase (PGK) promoter allowing for the establishment of stable integrants, and 2nd the neomycin resistance gene under the control of the heart-specific alpha myosin heavy chain (αMHC) promoter, allowing the selection of hPSC-derived cardiomyocytes (Klug *et al.*, 1996). Reporter gene constructs are based on pCAGGS2 whereby gene expression is controlled by the chicken β-actin (CBA) promoter combined with the human CMV-IE enhancer (together termed CAG promoter). pCAG_RedStar_nucmem (5.6kb) was constructed by replacing the eGFP with the red fluorescent protein (RedStar) in pCAGGS2 (5.5kb) (Knop *et al.*, 2002) coupled to a nuclear membrane location signal (nucmem) (Okita *et al.*, 2004). The bicistronic vector pCAG_rNIS_IRES2_Venus_nucmem contains the rat sodium iodide symporter (rNIS) (Kelm and Fussenegger, 2010) coupled to the fluorescent reporter Venus_nucmem by an internal ribosomal entry side (IRES2).

Cell transfection and establishment of transgenic clones

All transfections were performed using the Neon™ transfection system (Invitrogen). Several enzyme combinations were tested for cell harvesting. These included treatment with collagenase IV (Invitrogen) for removing the cells from their feeder-layer, followed by an additional incubation step with collagenase B (Roche, Mannheim) or TrypLE™ (Invitrogen) respectively for single cell dissociation according to the manufacturers specifications. In the final protocol the combination of collagenase IV and TrypLE was used. For transfection 1.5 x

5

10^6 of undifferentiated detached hPSCs were washed once with Phosphate Buffered Saline (PBS) w/o Ca^{2+}/Mg^{2+} and pelleted at 1000rpm for 5min, resuspended in 110µl Resuspension buffer R and transferred with the corresponding circular plasmid DNA into sterile microcentrifuge tubes. The cells were electroporated with two pulses at 1200V for 20ms and plated onto matrigel-coated six centimetre dishes in pre-incubated conditioned medium supplemented with 10µM ROCK-Inhibitor Y-27632 (supplied by the Institute for Organic Chemistry, Leibniz University Hannover, Germany) (Palecek *et al.*, 2011). Plasmids were used in their circular form without prior linearization and were applied in equimolar amounts without exceeding 20µg total DNA per electroporation sample. 48-72h after electroporation transfection efficiency was determined and 50µg/ml (hESC) respectively 200µg/ml (hiPS) hygromycin (Invitrogen) was added to the cells to select for stable integrants. Cells were incubated for 4 days in selection medium with a change on the second day. Upcoming colonies were manually picked 14 days after electroporation, transferred onto irradiated feeder cells and expanded clonally. Cell count post-electroporation was performed by means of trypan blue exclusion in a Thoma haemocytometer; the number of vital cells was compared to the initial cell number applied for transfection to express the percentage of vital cells post transfection.

Characterization of multi-transgenic clones

Established clones were analysed for the expression of typical pluripotency-associated markers via immunfluorescence stainings. PCR was applied to test for integrity of the plasmid αMHCneoPGKhygro in the genome (Primer sequences are listed in table S1). Stable expression of fluorescence reporter genes in undifferentiated cells was monitored by flow cytometry up to 23 passages after clone picking and at respective time after initiation of differentiation as indicated in results.

hPSC differentiation and selection of cardiomyocytes

To induce embryoid body (EB) formation, undifferentiated cells were washed in a chemically defined serum-free (SF) medium and subsequently were mechanically harvested. Resulting cell clumps were transferred to ultra-low attachment six well plates (Greiner, Frickenhausen, Germany) and cultured in SF supplemented with SB 203580 (10µM) (supplied by the Institute for Organic Chemistry, Leibniz University Hannover, Germany) (Graichen *et al.*, 2008; Xu *et al.*, 2008a). The medium was replaced every second day. Selection of cardiomyocytes was initiated by the addition of 200µg/ml G418 (Gibco, Karlsruhe, Germany)

2 days after the first beating foci were observed. Antibiotic selection was retained for at least 7 days (Xu *et al.*, 2008b).

Flow Cytometry

72h after transfection cells were washed with PBS w/o Ca^{2+}/Mg^{2+} and dissociated by Trypsin for 3min at 37°C to create a single-cell suspension. Cells were resuspended in PBS w/o Ca^{2+}/Mg^{2+} and analyzed on a FACSCalibur system (BD Biosience, USA) by applying BD CellQuest software (BD Biosience, USA). Non-transgenic hPSCs served as controls.

Immunhistological staining

Cell were fixed with 4% paraformaldehyde, washed with PBS, and treated with 5% donkey serum, 0,25% Triton X-100 diluted in Tris-buffered Saline (TBS) for 20min at room temperature. After rinsing the cells were incubated for at least 1h with respective primary antibodies (1:100 anti-OCT4 mouse IgG Santa Cruz Biotechnology, CA, USA, 1:100 anti-SSEA-3 mouse IgM, Hybridoma Bank, Iowa City, USA, 1:70 anti-SSEA-4 mouse IgG, Hybridoma Bank, Iowa City, USA, 1:100 anti-TRA-1-60 mouse IgM, Abcam, Cambridge, USA, 1:100 anti-GFP (Venus) goat IgG, Acris, Herford, Germany, 1:100 anti-TroponinT, mouse IgG, Thermo Scientific, Karlsruhe, Germany) diluted in PBS / 1% BSA. Further incubation was performed with the respective second antibody (donkey anti-mouse IgG DyLight®549-labeled, 1:200; donkey anti-mouse IgG DyLight®488-labeled,1:200 donkey anti-mouse IgM Cy3-labeled,1:200, and donkey anti-goat IgG Cy2-labeled,1:100, all Jackson Immunoresearch Laboratories) for 30min. Cells were rinsed, counterstained with DAPI (Sigma-Aldrich), and analyzed with an Axio Observer A1 fluorescence microscope (Carl Zeiss MicroImaging, Goettingen, Germany).

Analysis of mRNA expression by qRT-PCR

Total RNA was prepared using the RNeasy Kit (Macherey-Nagel, Düren, Germany) and reverse transcribed with Superscript II (Invitrogen) using oligo dT primers according to manufacturer's instructions. qRT-PCR was performed in triplicate using a Mastercycler® ep *realplex²* (Eppendorf, Hamburg, Germany) and the Absolute™ QPCR SYBR® Green Mix (ABgene, Epsom, Surrey, UK). The size of amplicons and absence of nonspecific products was controlled by melting curves. Sequences of primers are shown in table S2. Relative changes in gene expression were analyzed via $2^{-\Delta\Delta Ct}$ (Livak and Schmittgen, 2001) by comparing transgenic versus control cells using Mastercycler® ep realplex Software Version

7

2.0 (Eppendorf). Expression levels of target genes were normalized to β-actin; mean ± SEM of normalized gene expression levels is presented.

Ex vivo cardiac SPECT-CT imaging

1×10^6 NIS^{pos}-hPSCs were incubated for 90min with 1 MBq ^{123}I, vigorously washed and 5 x 10^6 labelled cells were injected into the anterior wall of the left ventricle of an explanted pig heart. The ^{123}I signal was visualized through a hybrid SPECT-CT camera with semiconductor detector technique (Discovery NM 570C, GE, Healthcare). In order to mimic *in vivo* signal attenuation, imaging of ^{123}I signals was performed through a dissected pig chest wall that was placed above the heart.

Results

Adaptation-free electroporation of plasmid DNA into hPSCs resulted in >60% transient transfection efficiency accompanied by high cell viability

Common feeder-based hPSC cultures were utilized without any pre-adaption in order to establish a straightforward and time saving protocol for the generation of multi-transgenic cell lines in one single-step,. Cells were routinely splitted once per week but harvested already on day four post-passaging for electroporation to ensure log-phase growth. Applying pre-tested electroporation parameters a first step of optimization was implied using different enzyme combinations to detach and dissociate hPSCs. Investigating collagenase IV, collagenase B and TrypLE™, best results regarding cell vitality and transfection efficiency were achieved by combining collagenase IV followed by TrypLE™ treatment (data not shown). Cell survival also critically depended on supplementation of the Rho-associated coiled-coil kinase (ROCK) inhibitor Y-27632 added to the culture medium post-electroporation (data not shown). To assess efficacy and robustness transfection in terms of transient expression, 2 constitutively expressed reporter plasmids (pCAGGS2 and pCAG_RedStar_nucmem, **Figure 1A**) and 4 independent hPSC lines (2 hESC and 2 hiPSC lines) were used. Applying varying DNA amounts ranging from 5-50µg per electroporation sample (corresponding to 1,5 million cells each) revealed that increasing DNA quantity did not inevitably lead to higher expression efficiencies; applying 10-20µg circular plasmid DNA (of the tested vectors with up to ~11kb) resulted in an optimal balance of cell vitality and transgene expression at 48h post-electroporation (data not shown). The resulting optimized protocol was shown efficient for all hPSC lines tested: transient transfection efficiency and cell vitality were well reproducible and similar for all clones tested resulting in 44 ± 4.8 of eGFP[pos] and 63 ± 12.7 of RedStar^{pos} cells (**Figure 1B**). Cell vitality after transfection as measured through cell recovery after 48hours was $100 \pm 20\%$ after RedStar transfection and $89 \pm 21.5\%$ for eGFP transfection compared to the initial number of transfected cells **(Figure 1C)**.

Efficient one-step generation of stable multi-transgenic clones

To test the possibility to generate stable multi-transgenic hPSC clones in a straightforward one step procedure, cells were co-electroporated with different combinations of vectors. All experiments included the selection vector αMHCneoPGKhygro together with one additional expression plasmid (either pCAGGS2, pCAG_RedStar_nucmem or pCAG_rNIS_IRES2_Venus_nucmem) in case of a double-transgenic approach, or two additional plasmids (pCAGGS2 and pCAG_RedStar_nucmem) in case of the triple-transgenic

9

approach (**Figure 1A**). Starting with 1,5 million cells, on average 74 ± 22.8 microscopically-distinguishable, antibiotic resistant colonies were identified within 7-10 days after initiation of hygromycin selection (n = 6 transfection experiments, **Figure 2A**). Interestingly and in contrast to reporter expression after transient transfection, the obtained proportion of GFP expressing colonies among the total number of hygromycin-resistant ones was significantly higher than the number of RedStar^{pos} ($30 \pm 5,3\%$ GFP^{pos} colonies vs. $6 \pm 1,3$ % RedStar^{pos}) colonies (**Figure 2B**). Stable multi-transgenic hPSC clones were established through manual picking of colonies two weeks after electroporation and subsequent selection, and transfer to feeder-based culture (**Figure 3A**). Resulting cell clones were expanded for 4-5 passages before re-analysis of long-term expression of transgenes. Full length integration of the selection vector αMHCneoPGKhygro with both expression cassettes i.e. αMHCneo and PGKhygro was assessed by PCR (**Figure 2D**, exemplified for established RedStar^{pos}/eGFP^{pos} clones). Only clones having integrated both full expression cassettes ($\sim$ 50-60%, **Figure 3B**) were included for further analyses. Loss of transgene expression occurred in ~20% of RedStar^{pos} as well as eGFP^{pos} or RedStar^{pos}/eGFP^{pos} lines during the first three weeks of cultivation. Among the remaining lines, variable intensity of fluorescence reporter expression was observed (**Figure 3C**), with a tendency of low level expressing lines to transgene silencing after additional 3-5 passages. Again, establishing stable long-term eGFP^{pos} cell lines was more efficient compared to RedStar^{pos} lines. The efficiency of stable clone generation for different cell lines and transgenes are summarized in **Table 1**. Notably, establishment of stably long-term expressing double-transgenic lines carrying the selection vector αMHCneoPGKhygro together with the bicistronic plasmid pCAG_rNIS_IRES2_Venus_nucmem was even more difficult than establishment of double-transgenic lines stably expressing RedStar as also outlined in **Table 1.**

In line with this result, in our experiments aiming at the establishment of triple-transgenic clones we found almost no colonies that solely expressed RedStar. In contrast, despite the equimolar transfection with RedStar and eGFP encoding plasmids numerous clonal colonies were found to express eGFP only (24%). At least, 10% of the hygromycin-resistant colonies were triple-transgenic as indicated by co-expression of eGFP and RedStar (**Figure 2B**).

Multi-transgenic cell lines remain undifferentiated and express typical pluripotency markers

Multi-transgenic hPSC lines showed characteristics of their maternal cell lines regarding proliferation (equivalent splitting interval and ratio) and colony morphology, which was

10

apparently independent of the transgene type(s) and their expression level (**Figure 3A**). In the finally selected stable lines, long-term transgene expression was demonstrated via flow cytometry for up to 23 passages after clonal selection; mean fluorescence intensity was extremely stable in respective lines. Cell clones having a mosaic fluorescence marker expression were rarely identified (**Figure 3C**). Transgenic lines expressed the pluripotency associated genes OCT4, TRA-1-60, SSEA3, and SSEA4 at levels equivalent to maternal cells as demonstrated by immunhistology (**Figure 4**).

Partial down-regulation of transgene expression upon differentiation

During EB-induced differentiation, down-regulation of the CAG-promoter-dependent fluorescence reporters was observed to some extend. Whereas the amount of eGFP^{pos} cells was in the same range in all established pluripotent clones in undifferentiated state (98 ± 0,3%), the proportion of transgene expressing cells declined clone-dependent ranging from 53 ± 4,5% (strongest preservation) to 7 ± 1,3% (highest down-regulation) on day 14 of differentiation (**Figure 5 A, B**). This phenomenon was observed for all fluorescence reporters including RedStar^{pos} cells (e.g. 63 ± 12,7%, cells on d14) or Venus^{pos} cells (e.g. ± 14,1%, cells on d14). Comparative analyses of three double-transgenic lines (eGFP^{pos} / αMHCneoPGKhygro) suggested that the issue was rather clone- than transgene-related (**Figure 5**). Of note, in triple-transgenic lines (RedStar^{pos}/eGFP^{pos} / αMHCneoPGKhygro; **Figure 6A**), and in addition to RedStar^{pos}/eGFP^{pos} double-positive cells, populations that were positive for either one or the other fluorescence marker only were observed upon differentiation **(Figure 6 B)**, whereby robust transgene expression was maintained for at least 14 days of spontaneous differentiation in EBs (**Figure 6C**).

Highly efficient transgene-based enrichment of cardiomyocytes from multi-transgenic hiPSCs

As one example for the practical applicability of our straightforward technology, three αMHCneo/eGFP^{pos} double-transgenic lines were tested for possibility to enrich hiPSC-derived cardiomyocytes based on the expression of the introduced αMHC-promoter-dependent neomycin resistance. Cardiac differentiation efficiencies were equivalent between all lines tested and comparable to non-transgenic controls as well (data not shown). Addition of G418 after appearance of beating foci indeed enabled selection of highly enriched cardiomyocytes, which was demonstrated by immunhistological staining specific to cardiac Troponin T (**Figure 7A**). Quantification of enriched populations (counterstained with DAPI

11

to visualize all nuclei) revealed >90% Troponin T positive cells. Similar to non-selected differentiated cells (**Figure 5 A, B**), a mixed pattern of eGFP[highpos], eGFP[lowpos] and GFP^{neg} cells was observed in G418-selected cardiomyocytes (**Figure 7B**).

Non-invasive tracking of multi-transgenic hiPSCs

As second practical applicability of our approach, we assessed the stable expression of the rat sodium iodide symporter (rNIS) as a valuable tool for *in vivo* non-invasive cell tracking in large animal models. To this end, hiPSC clones carrying 2 plasmids encoding for 4 functional transgenes were generated. These included the plasmid αMHCneoPGKhygro enabling, firstly, clonal selection and, secondly, cardiomyogenic enrichment after induction of hPSC differentiation, as described above. The co-introduced bicistronic vector pCAG_rNIS_IRES2_Venus_nucmem encoded for the trans-membrane rat sodium iodide symporter (rNIS); endogenous expression of this gene is almost exclusively restricted to the thyroid gland whose expression results in active uptake of iodide isotopes in transgenic cells, which can then be monitored via single positron emission computed tomography (SPECT) or positron emission tomography (PET) after transplantation. Established clones finally expressed nuclear Venus (**Figure 8A**) serving as a marker to identify injected donor cells *in situ*. In Venus[pos] clones, IRES-dependent expression of rNIS was analysed via quantitative RT-PCR and the relative level of transgene expression was compared to non-transfected hiPSC controls (**Figure 8B**). For functional testing, NIS[pos]-hPSCs were labelled by incubation with ^{123}I followed by catheter-based intramyocardial cell injection (MyoStar injection catheter) into explanted pig hearts, to simulate a clinically applicable route of cell administration. The cells were injected into the anterior wall of the left ventricle and monitored by SPECT-CT, which enables the detection of pre-labelled hPSCs at the site of cell transplantation **(Figure 8C)**. Notably, successful ^{123}I tracer uptake was detected through a dissected pig chest that had been placed above the heart to mimic signal attenuation *in vivo*. For confirmation of the imaging results myocardial tissue biopsies collected at the sites of cell injection were analysed immmunohistologically for the presence of Venus-expressing NIS[pos]-hPSCs. Indeed, Venus[pos] hPSCs could be detected along the presumed injection channel within the troponin T stained myocardial tissue **(Figure 8D)**.

1
2
3
4
5
6
7
8
9
10
11
12
13
14
15
16
17
18
19
20
21
22
23
24
25
26
27
28
29
30
31
32
33
34
35
36
37
38
39
40
41
42
43
44
45
46
47
48
49
50
51
52
53
54
55
56
57
58
59
60

Discussion

The ability to genetically modify human PSCs is essential to fully exploit their potential for *in vitro* assay development, disease modelling, tissue engineering and ultimately in regenerative medicine. For this reason, substantial efforts were invested to establish efficient protocols for transgenic hPSC line generation (Costa *et al.*, 2005; Costa, 2007; Braam, 2008; Braam *et al.*, 2008b; Xu, 2008; Braam *et al.*, 2010). Development of improved electroporation devices has facilitated these efforts.

In our study, we have combined and optimized protocols for single cell dissociation of hPSCs (Watanabe *et al.*, 2007, Olmer *et al.*, 2010) with prominent advantages provided by the Neon™ Transfection System, resulting in a fast and efficient protocol, which is directly applicable to conventional feeder-based cultures and does not require time-consuming pre-adaptation to feeder-free cultures. Another key progress of our work is the straightforward efficient generation of double- and triple-transgenic clones, i.e. stably expressing transgenes encoded on 2 or 3 independent plasmids, based on the genetic selection through one of these vectors, only.

Clearly, a highly efficient transfection protocol composes the basis for our approach. Our typically obtained transient transfection efficiencies are 44 ± 4.8 % for eGFP and 63 ± 12.7 % for RedStar, which is significantly higher than previously reported for electroporation (2 ± 0.4%), nucleofection (16 ± 3.6%), and lentiviral transduction ($25 \pm 4,8$%) (Cao *et al.*, 2010). Using our improved transfection protocol cell viability was highly enhanced, resulting for instance in 74 of stabile integrated transgenic clones after transfection of 1.5×10^6 cells with a combination of pCAGGS2 together with αMHCneoPGKhygro and subsequent antibiotic selection corresponding to an efficiency of stable clone generation of $4,9 \times 10^{-5}$. With ~22 clones approximately 30% of the established colonies were double-transgenic (1.46×10^{-5}) with 10 clones designated as triple-transgenic having integrated three independent plasmids ($0,49 \times 10^{-5}$). Thus, even our data for the integration of 3 independent vectors was marginally lower than the efficiencies generated with only one single vector published by Braam et al. (Braam *et al.*, 2008b) and compared to studies bearing hygromycin resistance gene for selecting stable integrants which was $<1 \times 10^{-6}$ shown by Moore et al. (Moore *et al.*, 2010). In addition, the latter, published approaches critically rely on the adaption of hPSCs to feeder-free conditions with the known disadvantages of increased time requirements and the enrichment of potentially abnormal cell clones that tolerate these culture conditions. Compared to the previously reported techniques, our approach for generation of multi-

13

transgenic clones is considerably faster requiring 14 days for generation of multi-transgenic clones, only.

To our best knowledge this is the first study demonstrating the possibility of achieving stable co-introduction of multiple plasmid vectors with only one of them carrying an antibiotic resistance marker. Despite vector-dependent variations in the efficiency of the generation of stable transgene-expressing clones, this approach works relative efficient in hESCs and hiPSCs. Our data suggest that the observed differences reflect differences between individual transgenes rather than being cell-line or promoter dependent.

Interestingly, the generation of clones with stable RedStar expression was considerable less efficient than in case of eGFP, which was unexpected in view of the ~ 2fold higher transient expression levels of RedStar_nucmem compared to eGFP (44 ± 4.8 of eGFP[pos] vs 63 ± 12.7 of RedStar^{pos} cells). Whether the RedStar protein itself or the coupling to a nuclear membrane location signal (nucmem) might be the underlying reason for the less efficient generation of stable RedStar nucmem expressing cells is not clear at this point, and further side-by-side comparison of different reporters expressed in the same sub-cellular compartments would be mandatory for further clarification of this observation.

In contrast to retroviral and lentiviral vectors, and independent of the used transgenes (Ellis and Yao, 2005) (Pannell and Ellis, 2001), the level of transgene silencing in undifferentiated cells was relatively low reaching ~20% of cells in the stable clones after hygromycin-selection. Notably, our results confirm recent findings (Liew *et al.*, 2007) demonstrating CAG promoter-driven reporter gene expression to be hardly silenced in established lines during long-term passaged as pluripotent cells, with the level of mean fluorescence intensity remaining very stable for up to 20 passages within individual lines. Although some variability of the mean fluorescence intensity, much likely due to copy number variations and / or integration-specific effects, was observed between independent lines, we were able to establish several double- and triple-transgenic (Orban *et al.*, 2009)lines that maintained their transgene expression ubiquitously and constitutively without applying any selection pressure after clone picking. Expression of multiple transgenes did not interfere with pluripotency marker expression as well as the ability to differentiate into derivatives of all the three germ layers. The differentiation potential was comparable to that of the maternal cell lines. This point is worthwhile highlighting since culture adaption, which is usually required during generation of transgenic cell lines has been reported to alter culture and differentiation characteristics (Enver *et al.*, 2005; Catalina *et al.*, 2008).

14

Besides stable long term transgene expression in undifferentiated hPSCs, also the stability of transgene expression in differentiated derivatives of transgenic hPSC clones is of special interest for various applications. The frequently observed high levels of transgene silencing during differentiation is known to depend on the vector design and especially the promoter used. Typically, even transgenes that are highly and stably expressed in undifferentiated PSCs are silenced to a considerable extent during differentiation. Notably, cell type-dependent variations in the expression levels of the specific transcription factors required, as well as epigenetic silencing can account for decreased transgene expression during differentiation (Hong *et al.*, 2007).

In our system, we have analysed several PSC clones, which show CAG-promoter dependent stable and uniform expression of eGFP from a second non-selectable co-integrated plasmid in undifferentiated cells, for transgene expression during differentiation. As reported for other selectable plasmids or lentiviral vectors with CAG-promoter-dependent transgene expression, all of the tested PSC clones showed mosaic expression of the GFP in the differentiated progeny. This was the case in αMHC promoter-NeoR enriched cardiomyocytes as well.

Whether the presence of different cardiomyocytes-subtypes (i.e. pacemaker-, atrial- or ventricular-like cells) or a heterogeneous myocyte maturation grade of the cardiomyocytes accounts for this result, or whether in our system transgene silencing during differentiation is a rather stochastic than strictly cell-type-dependent event is not clear at this point.

Finally, the overexpression of a NIS symporter as imaging tool in large animals was exemplarily selected as application of our novel technique for straightforward generation of multi-transgenic PSC lines. As proof of concept for use in clinically relevant animal models, Venus-nucmem/NIS-over expressing undifferentiated hiPSCs were injected intramyocardially into an isolated pig heart. We show that our transgenic cells can be detected by SPECT-CT *in situ* and subsequently identified by nuclear Venus expression in histological biopsies. This is an important step for efficient, unequivocal monitoring of cell survival and integration of stem cell derivatives in large animal models which is a key issue in the field (Chang *et al.*, 2006). Extensive experiments applying these cell lines for longitudinal monitoring of hPSC engraftment in a pig myocardial infarct model are under way.

To our knowledge, this is the first study demonstrating the generation of multi-transgenic hPSC lines expressing transgenes located on independent plasmids with only one selection marker. Our fast and efficient transfection technology using the Neon™ Transfection System

15

will also support targeting of transgenes into specific loci for gene modification via homologous recombination or for ubiquitous reporter gene expression from defined genomic sides such as the Rosa26 locus.

16

Author Disclosure Statement

No competing financial interests exist.

References

ACTON, P.D., and KUNG, H.F. (2003). Small animal imaging with high resolution single photon emission tomography. Nucl Med Biol **30**, 889-895.

AMIT, M., MARGULETS, V., SEGEV, H., SHARIKI, K., LAEVSKY, I., COLEMAN, R., and ITSKOVITZ-ELDOR, J. (2003). Human feeder layers for human embryonic stem cells. Biol Reprod **68**, 2150-2156.

BOECKER, W., BERNECKER, O.Y., WU, J.C., ZHU, X., SAWA, T., GRAZETTE, L., ROSENZWEIG, A., DEL MONTE, F., SCHMIDT, U., and HAJJAR, R.J. (2004). Cardiac-specific gene expression facilitated by an enhanced myosin light chain promoter. Mol Imaging **3**, 69-75.

BRAAM, S.R., DENNING, C., MATSA, E., YOUNG, L.E., PASSIER, R., and MUMMERY, C.L. (2008a). Feeder-free culture of human embryonic stem cells in conditioned medium for efficient genetic modification. Nat Protoc **3**, 1435-1443.

BRAAM, S.R., DENNING, C., and MUMMERY, C.L. (2010). Genetic manipulation of human embryonic stem cells in serum and feeder-free media. Methods Mol Biol **584**, 413-423.

BRAAM, S.R., DENNING, C., VAN DEN BRINK, S., KATS, P., HOCHSTENBACH, R., PASSIER, R., and MUMMERY, C.L. (2008b). Improved genetic manipulation of human embryonic stem cells. Nat Methods **5**, 389-392.

BRAAM, S.R., DENNING, C., MATSA, E., YOUNG, L.E., PASSIER, R., MUMMERY, C.L. (2008). Feeder-free culture of human embryonic stem cells in conditioned medium for efficient genetic modification. Nature Protocols **3**, 1435-1443.

CAO, F., XIE, X., GOLLAN, T., ZHAO, L., NARSINH, K., LEE, R.J., and WU, J.C. (2010). Comparison of gene-transfer efficiency in human embryonic stem cells. Mol Imaging Biol **12**, 15-24.

CATALINA, P., MONTES, R., LIGERO, G., SANCHEZ, L., DE LA CUEVA, T., BUENO, C., LEONE, P.E., and MENENDEZ, P. (2008). Human ESCs predisposition to karyotypic instability: Is a matter of culture adaptation or differential vulnerability among hESC lines due to inherent properties? Mol Cancer **7**, 76.

CHANG, G.Y., XIE, X., and WU, J.C. (2006). Overview of stem cells and imaging modalities for cardiovascular diseases. J Nucl Cardiol **13**, 554-569.

17

CHERRY, S.R., BINISZKIEWICZ, D., VAN PARIJS, L., BALTIMORE, D., and JAENISCH, R. (2000). Retroviral expression in embryonic stem cells and hematopoietic stem cells. Mol Cell Biol **20**, 7419-7426.

COSTA, M., DOTTORI, M., NG, E., HAWES, S.M., SOURRIS, K., JAMSHIDI, P., PERA, M.F., ELEFANTY, A.G., and STANLEY, E.G. (2005). The hESC line Envy expresses high levels of GFP in all differentiated progeny. Nat Methods **2**, 259-260.

COSTA, M., DOTTORI, M., SOURRIS, K., JAMSHIDI, P., HATZISTAVROU, T., DAVIS, R., AZZOLA, L., JACKSON, S., LIM, S.M., PERA, M., ELEFANTY, A.G., STANLEY, E.G. (2007). A method for genetic modification of human embryonic stem cells using electroporation. Nature Protocols **2**, 792-796.

DAI, W., FIELD, L.J., RUBART, M., REUTER, S., HALE, S.L., ZWEIGERDT, R., GRAICHEN, R.E., KAY, G.L., JYRALA, A.J., COLMAN, A., DAVIDSON, B.P., PERA, M., and KLONER, R.A. (2007). Survival and maturation of human embryonic stem cell-derived cardiomyocytes in rat hearts. J Mol Cell Cardiol **43**, 504-516.

ELLIS, J., and YAO, S. (2005). Retrovirus silencing and vector design: relevance to normal and cancer stem cells? Curr Gene Ther **5**, 367-373.

ENVER, T., SONEJI, S., JOSHI, C., BROWN, J., IBORRA, F., ORNTOFT, T., THYKJAER, T., MALTBY, E., SMITH, K., ABU DAWUD, R., JONES, M., MATIN, M., GOKHALE, P., DRAPER, J., and ANDREWS, P.W. (2005). Cellular differentiation hierarchies in normal and culture-adapted human embryonic stem cells. Hum Mol Genet **14**, 3129-3140.

GRAICHEN, R., XU, X., BRAAM, S.R., BALAKRISHNAN, T., NORFIZA, S., SIEH, S., SOO, S.Y., THAM, S.C., MUMMERY, C., COLMAN, A., ZWEIGERDT, R., and DAVIDSON, B.P. (2008). Enhanced cardiomyogenesis of human embryonic stem cells by a small molecular inhibitor of p38 MAPK. Differentiation **76**, 357-370.

HAAS, D.L., CASE, S.S., CROOKS, G.M., and KOHN, D.B. (2000). Critical factors influencing stable transduction of human CD34(+) cells with HIV-1-derived lentiviral vectors. Mol Ther **2**, 71-80.

HAASE, A., OLMER, R., SCHWANKE, K., WUNDERLICH, S., MERKERT, S., HESS, C., ZWEIGERDT, R., GRUH, I., MEYER, J., WAGNER, S., MAIER, L.S., HAN, D.W., GLAGE, S., MILLER, K., FISCHER, P., SCHÖLER, H.R., MARTIN, U. (2009). Generation of Induced Pluripotent Stem cells from Human Cord Blood. Cell Stem Cell **5**, 434-441.

HOFFMAN, L.M., and CARPENTER, M.K. (2005). Characterization and culture of human embryonic stem cells. Nat Biotechnol **23**, 699-708.

HONG, S., HWANG, D.Y., YOON, S., ISACSON, O., RAMEZANI, A., HAWLEY, R.G., and KIM, K.S. (2007). Functional analysis of various promoters in lentiviral vectors at different stages of in vitro differentiation of mouse embryonic stem cells. Mol Ther **15**, 1630-1639.

HUBER, I., ITZHAKI, I., CASPI, O., ARBEL, G., TZUKERMAN, M., GEPSTEIN, A., HABIB, M., YANKELSON, L., KEHAT, I., and GEPSTEIN, L. (2007). Identification and selection of cardiomyocytes during human embryonic stem cell differentiation. Faseb J **21**, 2551-2563.

JANG, J.E., SHAW, K., YU, X.J., PETERSEN, D., PEPPER, K., LUTZKO, C., and KOHN, D.B. (2006). Specific and stable gene transfer to human embryonic stem cells using pseudotyped lentiviral vectors. Stem Cells Dev **15**, 109-117.

KELM, J.M., and FUSSENEGGER, M. (2010). Scaffold-free cell delivery for use in regenerative medicine. Adv Drug Deliv Rev **62**, 753-764.

KITA-MATSUO, H., BARCOVA, M., PRIGOZHINA, N., SALOMONIS, N., WEI, K., JACOT, J.G., NELSON, B., SPIERING, S., HAVERSLAG, R., KIM, C., TALANTOVA, M., BAJPAI, R., CALZOLARI, D., TERSKIKH, A., MCCULLOCH,

18

A.D., PRICE, J.H., CONKLIN, B.R., CHEN, H.S., and MERCOLA, M. (2009). Lentiviral vectors and protocols for creation of stable hESC lines for fluorescent tracking and drug resistance selection of cardiomyocytes. PLoS One **4**, e5046.

KLUG, M.G., SOONPAA, M.H., KOH, G.Y., and FIELD, L.J. (1996). Genetically selected cardiomyocytes from differentiating embronic stem cells form stable intracardiac grafts. J Clin Invest **98**, 216-224.

KNOERZER, W., BINDER, H.P., SCHNEIDER, K., GRUSS, P., MCCARTHY, J.E., and RISAU, W. (1989). Expression of synthetic genes encoding bovine and human basic fibroblast growth factors (bFGFs) in Escherichia coli. Gene **75**, 21-30.

KNOP, M., BARR, F., RIEDEL, C.G., HECKEL, T., and REICHEL, C. (2002). Improved version of the red fluorescent protein (drFP583/DsRed/RFP). Biotechniques **33**, 592, 594, 596-598 passim.

KUSTIKOVA, O., FEHSE, B., MODLICH, U., YANG, M., DULLMANN, J., KAMINO, K., VON NEUHOFF, N., SCHLEGELBERGER, B., LI, Z., and BAUM, C. (2005). Clonal dominance of hematopoietic stem cells triggered by retroviral gene marking. Science **308**, 1171-1174.

LIEW, C.G., DRAPER, J.S., WALSH, J., MOORE, H., and ANDREWS, P.W. (2007). Transient and stable transgene expression in human embryonic stem cells. Stem Cells **25**, 1521-1528.

LIU, J., JONES, K.L., SUMER, H., and VERMA, P.J. (2009). Stable transgene expression in human embryonic stem cells after simple chemical transfection. Mol Reprod Dev **76**, 580-586.

LIVAK, K.J., and SCHMITTGEN, T.D. (2001). Analysis of relative gene expression data using real-time quantitative PCR and the 2(-Delta Delta C(T)) Method. Methods **25**, 402-408.

MA, Y., RAMEZANI, A., LEWIS, R., HAWLEY, R.G., and THOMSON, J.A. (2003). High-level sustained transgene expression in human embryonic stem cells using lentiviral vectors. Stem Cells **21**, 111-117.

MAURITZ, C., MARTENS, A., ROJAS, S.V., SCHNICK, T., RATHERT, C., SCHECKER, N., MENKE, S., GLAGE, S., ZWEIGERDT, R., HAVERICH, A., MARTIN, U., and KUTSCHKA, I. (2011). Induced pluripotent stem cell (iPSC)-derived Flk-1 progenitor cells engraft, differentiate, and improve heart function in a mouse model of acute myocardial infarction. Eur Heart J **32**, 2634-2641.

MOORE, J.C., ATZE, K., YEUNG, P.L., TORO-RAMOS, A.J., CAMARILLO, C., THOMPSON, K., RICUPERO, C.L., BRENNEMAN, M.A., COHEN, R.I., and HART, R.P. (2010). Efficient, high-throughput transfection of human embryonic stem cells. Stem Cell Res Ther **1**, 23.

MOORE, J.C., VAN LAAKE, L.W., BRAAM, S.R., XUE, T., TSANG, S.Y., WARD, D., PASSIER, R., TERTOOLEN, L.L., LI, R.A., and MUMMERY, C.L. (2005). Human embryonic stem cells: genetic manipulation on the way to cardiac cell therapies. Reprod Toxicol **20**, 377-391.

NORRMAN, K., FISCHER, Y., BONNAMY, B., WOLFHAGEN SAND, F., RAVASSARD, P., and SEMB, H. (2010). Quantitative comparison of constitutive promoters in human ES cells. PLoS One **5**, e12413.

ODORICO, J.S., KAUFMAN, D.S., and THOMSON, J.A. (2001). Multilineage differentiation from human embryonic stem cell lines. Stem Cells **19**, 193-204.

OKITA, C., SATO, M., and SCHROEDER, T. (2004). Generation of optimized yellow and red fluorescent proteins with distinct subcellular localization. Biotechniques **36**, 418-422, 424.

OLMER, R., HAASE, A., MERKERT, S., CUI, W., PALECEK, J., RAN, C., KIRSCHNING, A., SCHEPER, T., GLAGE, S., MILLER, K., CURNOW, E.C.,

19

HAYES, E.S., and MARTIN, U. (2010). Long term expansion of undifferentiated human iPS and ES cells in suspension culture using a defined medium. Stem Cell Res **5**, 51-64.

ORBAN, T.I., APATI, A., NEMETH, A., VARGA, N., KRIZSIK, V., SCHAMBERGER, A., SZEBENYI, K., ERDEI, Z., VARADY, G., KARASZI, E., HOMOLYA, L., NEMET, K., GOCZA, E., MISKEY, C., MATES, L., IVICS, Z., IZSVAK, Z., and SARKADI, B. (2009). Applying a "double-feature" promoter to identify cardiomyocytes differentiated from human embryonic stem cells following transposon-based gene delivery. Stem Cells **27**, 1077-1087.

PALECEK, J., ZWEIGERDT, R., OLMER, R., MARTIN, U., KIRSCHNING, A., and DRAGER, G. (2011). A practical synthesis of Rho-Kinase inhibitor Y-27632 and fluoro derivatives and their evaluation in human pluripotent stem cells. Org Biomol Chem **9**, 5503-5510.

PANNELL, D., and ELLIS, J. (2001). Silencing of gene expression: implications for design of retrovirus vectors. Rev Med Virol **11**, 205-217.

PHILIPPE, S., SARKIS, C., BARKATS, M., MAMMERI, H., LADROUE, C., PETIT, C., MALLET, J., and SERGUERA, C. (2006). Lentiviral vectors with a defective integrase allow efficient and sustained transgene expression in vitro and in vivo. Proc Natl Acad Sci U S A **103**, 17684-17689.

PICHON, C., BILLIET, L., and MIDOUX, P. (2010). Chemical vectors for gene delivery: uptake and intracellular trafficking. Curr Opin Biotechnol **21**, 640-645.

RITNER, C., WONG, S.S., KING, F.W., MIHARDJA, S.S., LISZEWSKI, W., ERLE, D.J., LEE, R.J., and BERNSTEIN, H.S. (2011). An engineered cardiac reporter cell line identifies human embryonic stem cell-derived myocardial precursors. PLoS One **6**, e16004.

SCHINZEL, R.T., AHFELDT, T., LAU, F.H., LEE, Y.K., COWLEY, A., SHEN, T., PETERS, D., LUM, D.H., and COWAN, C.A. (2011). Efficient culturing and genetic manipulation of human pluripotent stem cells. PLoS One **6**, e27495.

SUN, N., LEE, A., and WU, J.C. (2009). Long term non-invasive imaging of embryonic stem cells using reporter genes. Nat Protoc **4**, 1192-1201.

WATANABE, K., UENO, M., KAMIYA, D., NISHIYAMA, A., MATSUMURA, M., WATAYA, T., TAKAHASHI, J.B., NISHIKAWA, S., NISHIKAWA, S., MUGURUMA, K., and SASAI, Y. (2007). A ROCK inhibitor permits survival of dissociated human embryonic stem cells. Nat Biotechnol **25**, 681-686.

WURM, M., GROSS, B., SGODDA, M., STANDKER, L., MULLER, T., FORSSMANN, W.G., HORN, P.A., BLASCZYK, R., and CANTZ, T. (2011). Improved lentiviral gene transfer into human embryonic stem cells grown in co-culture with murine feeder and stroma cells. Biol Chem.

XIA, X., ZHANG, Y., ZIETH, C.R., and ZHANG, S.C. (2007). Transgenes delivered by lentiviral vector are suppressed in human embryonic stem cells in a promoter-dependent manner. Stem Cells Dev **16**, 167-176.

XU, X.Q., GRAICHEN, R., SOO, S.Y., BALAKRISHNAN, T., RAHMAT, S.N., SIEH, S., THAM, S.C., FREUND, C., MOORE, J., MUMMERY, C., COLMAN, A., ZWEIGERDT, R., and DAVIDSON, B.P. (2008a). Chemically defined medium supporting cardiomyocyte differentiation of human embryonic stem cells. Differentiation **76**, 958-970.

XU, X.Q., ZWEIGERDT, R., SOO, S.Y., NGOH, Z.X., THAM, S.C., WANG, S.T., GRAICHEN, R., DAVIDSON, B., COLMAN, A., and SUN, W. (2008b). Highly enriched cardiomyocytes from human embryonic stem cells. Cytotherapy 10, 376-389.

1
2
3
4
5
6
7
8
9
10
11
12
13
14
15
16
17
18
19
20
21
22
23
24
25
26
27
28
29
30
31
32
33
34
35
36
37
38
39
40
41
42
43
44
45
46
47
48
49
50
51
52
53
54
55
56
57
58
59
60

XU, X.Q., ZWEIGERDT, R., SOO, S.Y., NGOH, Z.X., THAM, S.C., WANG, S.T., GRAICHEN, R., DAVIDSON, B., COLMAN, A., SUN, W. (2008). Highly enriched cardiomyocytes from human embryonic stem cells. Cytotherapy 10, 376-389.

YAO, S., SUKONNIK, T., KEAN, T., BHARADWAJ, R.R., PASCERI, P., and ELLIS, J. (2004). Retrovirus silencing, variegation, extinction, and memory are controlled by a dynamic interplay of multiple epigenetic modifications. Mol Ther 10, 27-36.

ZIELLO, J.E., HUANG, Y., and JOVIN, I.S. (2010). Cellular endocytosis and gene delivery. Mol Med 16, 222-229.

ZWAKA, T.P., and THOMSON, J.A. (2003). Homologous recombination in human embryonic stem cells. Nat Biotechnol 21, 319-321.

WURM, M., GROSS, B., SGODDA, M., STANDKER, L., MULLER, T., FORSSMANN, W.G., HORN, P.A., BLASCZYK, R., and CANTZ, T. (2011). Improved lentiviral gene transfer into human embryonic stem cells grown in co-culture with murine feeder and stroma cells. Biol Chem.

21

Figure legends

Figure 1. Transfection of hPSCs resulted in a highly viable cell population efficiently expressing different reporter genes. A: Vectors used for the generation of stable transgenic hPSC cell lines: pCAGGS2 and pCAG_RedStar_nucmem constitutively expressing eGFP, or the codon-optimized red GFP variant RedStar fused to nuclear membrane localization signal, respectively, under control of the chicken beta-actin (CAG) promoter; the bicistronic vector pCAG_rNIS_IRES2_Venus_nucmem containing the rat sodium iodide symporter (rNIS) linked via internal ribosomal entry side (IRES2) to the yellow GFP variant Venus_nucmem, both driven by the CAG promoter; αMHCneoPGKhygro with a hygromycin resistance constitutively expressed under the phosphoglycerate kinase (PGK) promoter together with the neomycin resistance under control of the αMHC (MYHC6) promoter for cardiomyocytes-specific expression. **B:** transfection efficiencies 48hrs post-microporation were determined for pCAGGS2 and pCAG_RedStar_nucmem via flow cytometry analysis. An average of 44 ± 4,8 eGFP^{pos} and 63 ± 12,7 RedStar^{pos} cells could be detected. **C:** Proliferation of surviving cells compensated microporation-related cell death roughly 48 hrs after transfection reaching the initial cell number (1.5 x 10^6) used for electroporation (89 ± 21,5 % of the initial cell number for eGFP vs. 100 ±20 % in case of RedStar).

Figure 2. A protocol of efficient and reliable electroporation-based generation of multi-transgenic hPSC clones. A: Timeline of clone generation: hPSCs used for transgenic modification were cultured under hPSC standard feeder-based culture conditions with a regular passaging once a week. Notably, there was no necessity for any feeder-free pre-adaption before setting the transfection experiments. For

transfection the cells were dissociated into single cells, and 1.5 x 10^6 cells were

transfected with the corresponding plasmid combinations. 3 days post-modification,

transfection efficiency was determined via flow cytometry. Hygromycin was added to

select for stable integrants in parallel cultures. After 7-10 days hygromycin-resistant

colonies became visible. On day 14, colonies were picked and further expanded

clonally. **B:** Efficiency of stable transgenesis in terms of total clone numbers and

percent of multi-transgenic clones per total clones (**C.**). An average of 74 ± 22.8

independently appearing clones were generated per 1.5 x 10^6 cells. With 16 ± 5,5

appearing colonies (~ 30% of hygromycin-resistant clones), the generation of

eGFP[pos] clones was more effective than the generation of RedStar[pos] clones (~ 6% of

the hygromycin-resistant clones) or eGFP[pos] / RedStar[pos] clones (6 ± 2; 10% of the

hygromycin-resistant clones).

**Figure 3. Morphology and eGFP expression of up-coming multi-transgenic
hiPSC clones. A:** Appearance of multi-transgenic hiPSC cell clones. Up-coming

stably transfected double-transgenic hPSC colony 10 days after hPSC modification

with αMHCneoPGKhygro together with pCAGGS2 (left). Apparent dark edges (white

arrow) are due pen-marking of hygromycin-resistant colonies that co-express eGFP.

eGFP[pos] hPSC clones were further cultivated under standard-culture conditions on

feeder-cells and acquired typical hPSC morphology. Exemplarily depicted is hPSC

αMHCneoPGKhygro_pCAGGS2 clone 2 in Passage 59, 12 passages after

transfection (right). **B:** All eGFP[pos] clones were picked and analyzed via overlapping

PCR primers for full integrity of the selection vector αMHCneoPGKhygro. Clones with

only partial integration of the transgenes (~20 %) were deleted from further

experiments. **C:** Established clones show variances in their eGFP-expression

intensity. Five established hPSC αMHCneoPGKhygro_CBAeGFP clones were

analyzed for their eGFP-expression. As opposed to four of the analyzed clones, one (clone 10) shows a mosaic in the eGFP-expression pattern ranging from very weak to strong expression. Scale bars 100µm.

Figure 4. Multi-transgenic hiPSC clones display the typical morphology of hPSCs and retain expression of pluripotency markers. A: hiPSC αMHCneoPGKhygro_CBAeGFP clone 2 in passage 68 stains positive for pluripotency associated markers OCT4, SSEA-3, SSEA-4 and TRA-1-60 (all in red). Nuclei are counter stained with DAPI (blue), green colour represents CBA promoter driven eGFP-expression. Scale bars 100µm.

Figure 5. CAG-promoter-driven transgene expression is partially down-regulated during differentiation of established hiPSC clones. A: Differentiation of hiPSC αMHCneoPGKhygro_CBAeGFP clone 2 in an EB- based approach resulted in partial down-regulation of the CAG-promoter-driven eGFP (see white arrow). Depicted are undifferentiated cells 14 Passages after picking (total passage 61, left), aggregated EBs on day 7 of differentiation (middle) and differentiated derivatives on day 14 of differentiation (right). Down-regulation effects could be hardly detected microscopically in the multi-layered floating EBs but became obvious after plating in the outgrowth of the differentiated cells. **B:** A more quantitative analysis of transgene expression in 3 individual clones during differentiation via flow cytometry revealed a general decrease of the proportion of eGFP^{pos} cells with clone-specific variations. Scale bars 100µm.

Figure 6. Differentiated hPSC-derivatives show mosaic expression of fluorescence reporter transgenes in triple-transgenic clones. A: Multi-transgenic

hPSC clones stably express cytoplasmatic eGFP and nuclear RedStar. Exemplarily depicted is hiPSC αMHCneoPGKhygro_CBAeGFP_RedStar_nucmem clone 6, 8 passages after clonal selection cultivated under standard culture conditions on feeder-cells. **B:** Differentiated cells from the same multi-transgenic clone on day 14 of differentiation. Although both fluorescence reporters still co-expressed in most of the differentiated cells, a minority of cells has lost either eGFP RedStar (white arrows) expression. **C:** Flow cytometry revealed stable transgene expression during ongoing differentiation for CAG promoter-driven fluorescence reporter genes ranging from 99.4% ± 0.31 eGFP^{pos} cells (99% ± 3,17 RedStar^{pos} cells) in the undifferentiated cultures to 95.7% ± 1.69% eGFP^{pos} cells (95% ± 2 RedStar^{pos} cells) in day 14 differentiations. Scale bars 100µm.

Figure 7. Enrichment of multi-transgenic hiPSC-derived cardiomyocytes based on G418-selection. hiPSC αMHCneoPGKhygro_CBAeGFP clone 2 was differentiated in an EB- based serum-free approach leading to various cell lineages, among them beating clusters of hPSC-derived CMs. **A:** G418-selection resulted in a highly enriched cardiac cell population with all cells positively stained for the cardiomyocyte marker Troponin T (cTN T, red). Nuclei are counter stained with DAPI (blue). **B:** Fluorescence reporter transgene down-regulation as described in figure 6 was also observed in the hiPCS-derived myocytes. αMHC-NeoR-enriched heart-cells showed a mixture of eGFP[pos] and eGFP cells, however most of the cells kept eGFP-expression. Scale bars 100µm.

Figure 8. Transgenic NIS expression enables in situ imaging of multi-transgenic hiPSCs

A: Established hiPSC αMHCneoPGKhygro_pCAG-rNIS_IRES2_Venus_nucmem clone expressing the rat sodium iodide symporter (rNIS) and the nuclear yellow GFP variant Venus (green). **B:** Three independent rNIS clones were analysed by qRT-PCR for the expression of the transgenic rat sodium iodide symporter (rNIS) and analysed relative to β-Actin. **C:** ^{123}I-pre-labelled NIS[pos]-hPSCs were injected *ex vivo* into pig hearts. Pig hearts were placed under a dissected pig chest in order to simulate *in vivo* imaging after clinical cell transplantation. After injection of pre-labelled mutli-trangenic hiPSCs, the heart was scanned with a Hybrid SPECT-CT (Discovery NM 570C, GE, Healthcare). Depicted are SPECT-CT images of pig hearts in the coronal and sagital view after injection of 5x10^{6} NIS[pos]-hiPSCs demonstrating tracer signal at the site of cell injection. **D:** Detection of rNIS expressing cells using an anti-GFP antibody knowing to cross-react with Venus as a yellow GFP variant (green). Immunostainings were performed after cell injection into swine left ventricle *in vitro*. Heart-tissue was visualized using an anti-Troponin T antibody (cTN T, red). Nuclei are counter stained with DAPI (blue). Scale bars 100µm. Venus^{pos} cells were detected along the presumed injection channel. Notably, fixation and immunhistological treatment led to a cytoplasmatic staining pattern of the otherwise nuclear Venus. This was in contrast to the expression pattern known from viable cells that is strictly restricted to the nucleus (shown in A).

1
2
3
4
5
6
7
8
9
10
11
12
13
14
15
16
17
18
19
20
21
22
23
24
25
26
27
28
29
30
31
32
33
34
35
36
37
38
39
40
41
42
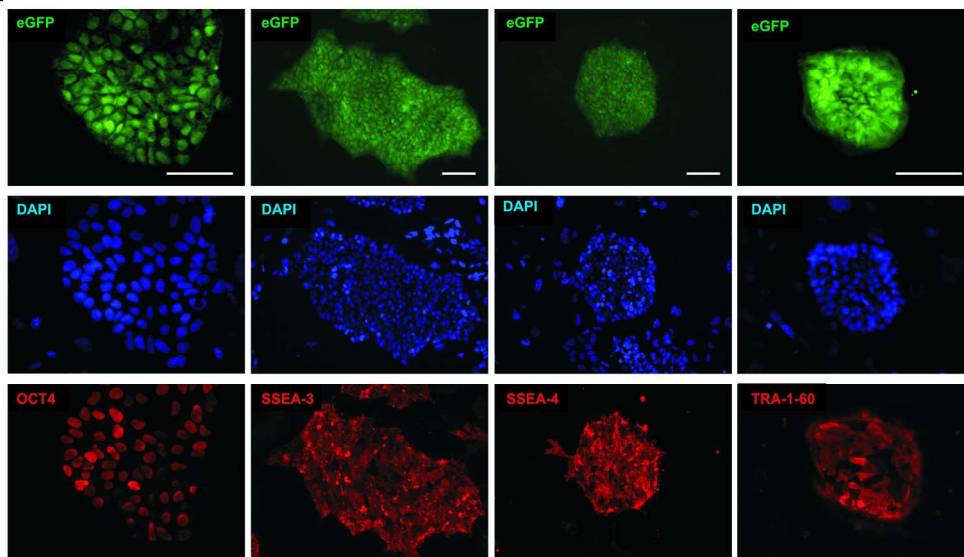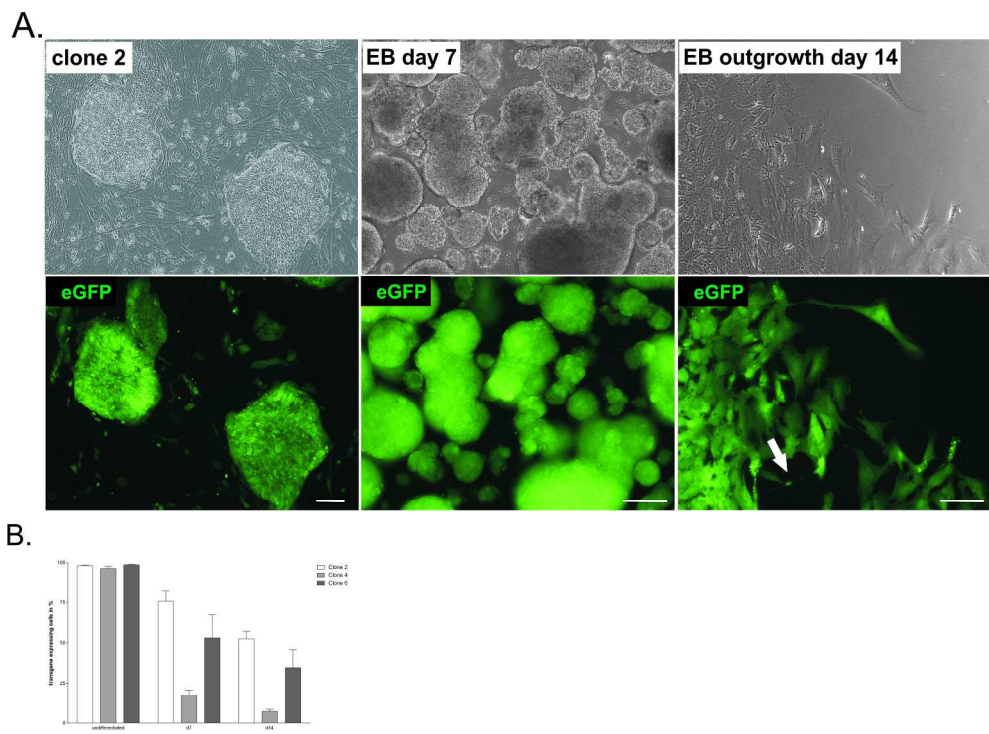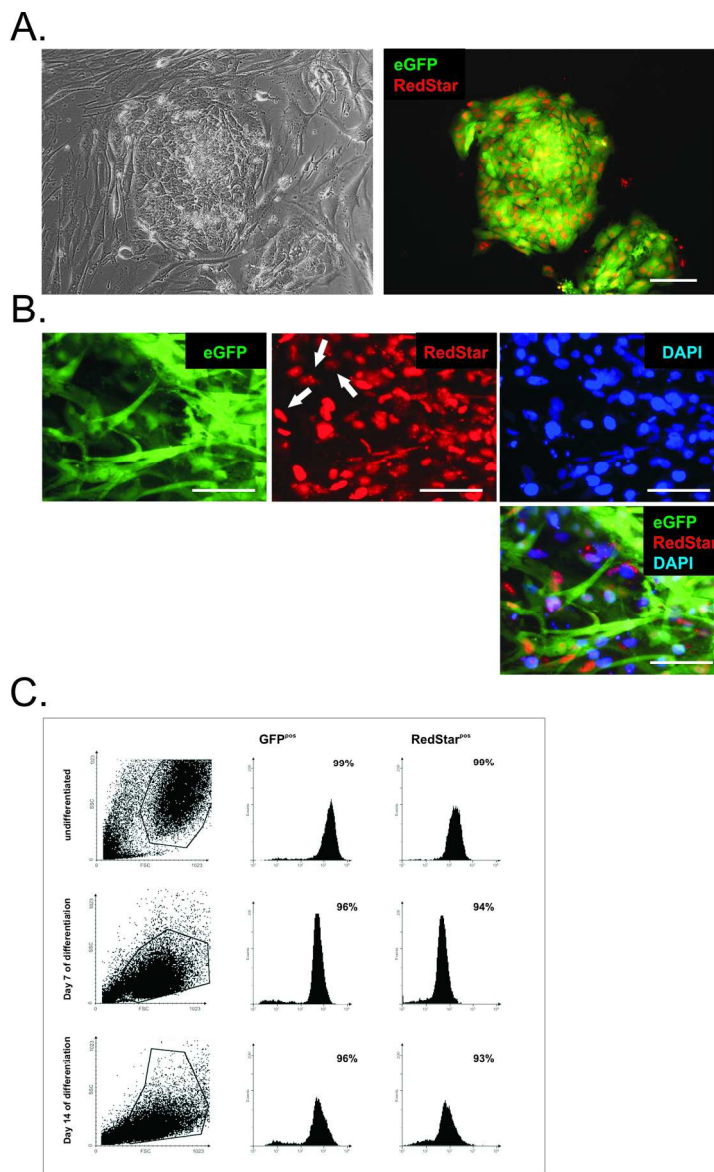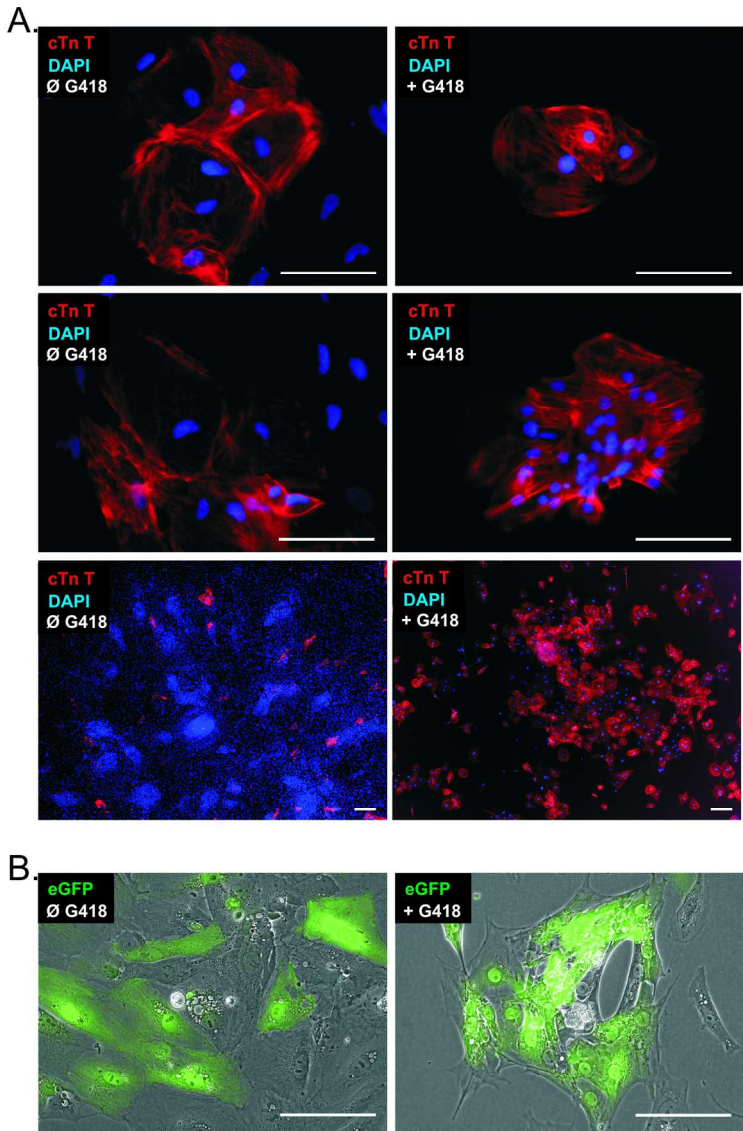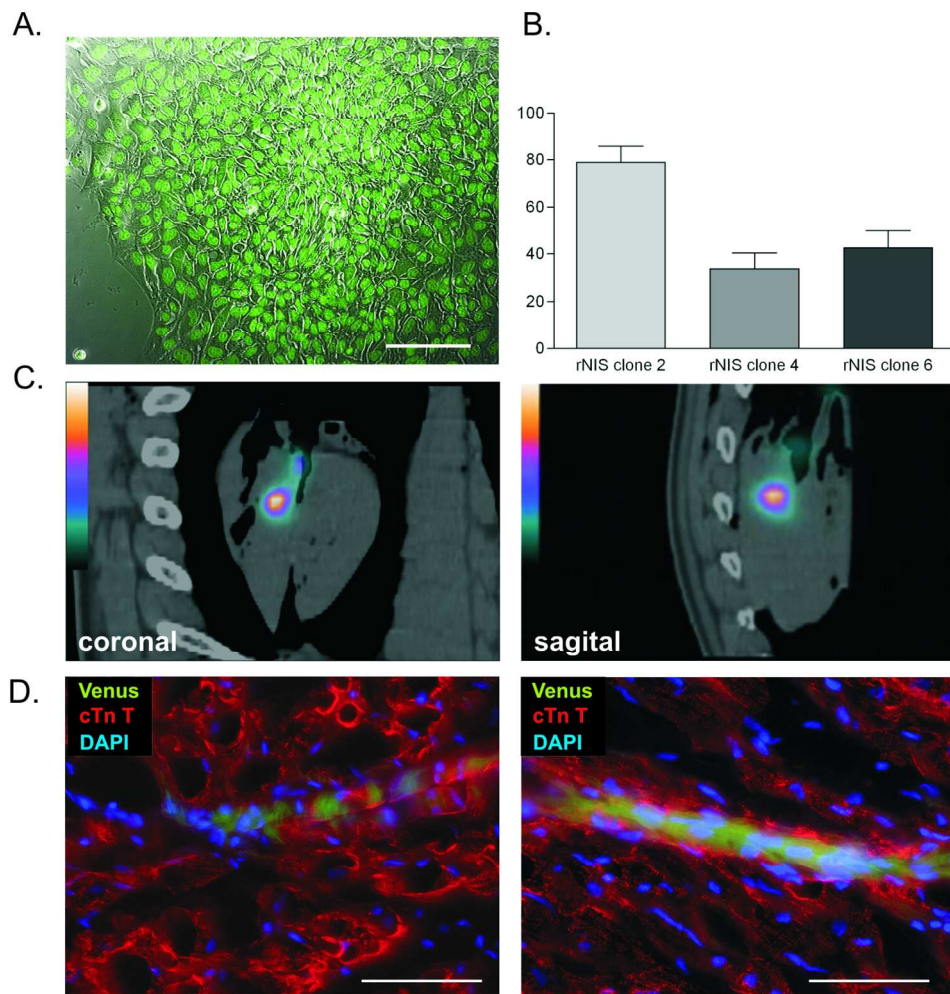43
44
45
46
47
48
49
50
51
52
53
54
55
56
57
58
59
60
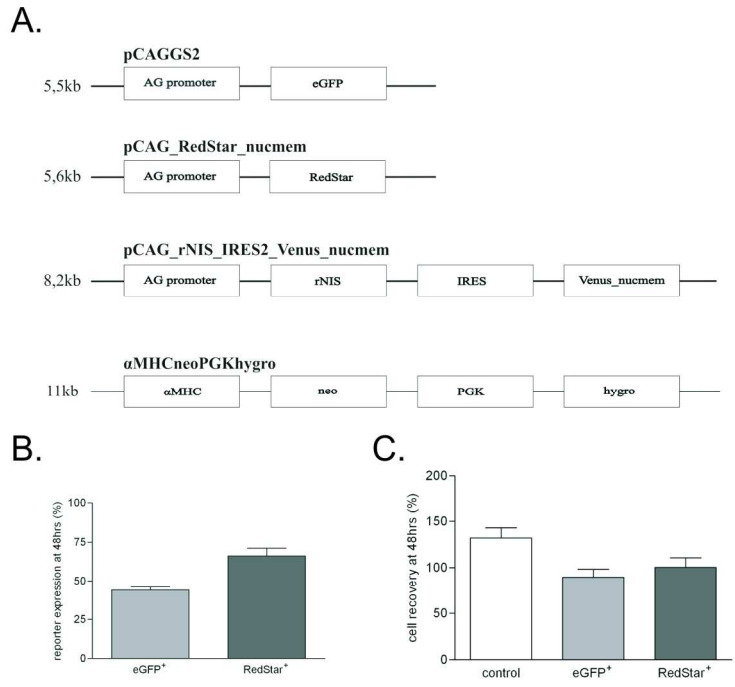
Figure 1

246x189mm (200 x 200 DPI)

1
2
3
4
5
6
7
8
9
10
11
12
13
14
15
16
17
18
19
20
21
22
23
24
25
26
27
28
29
30
31
32
33
34
35
36
37
38
39
40
41
42
43
44
45
46
47
48
49
50
51
52
53
54
55
56
57
58
59
60
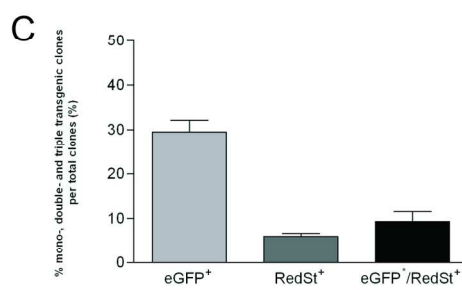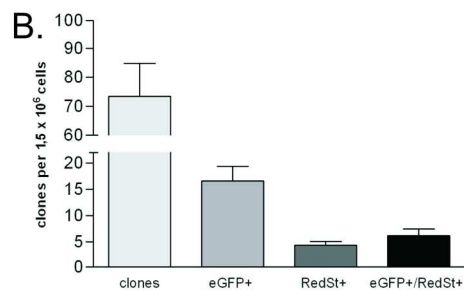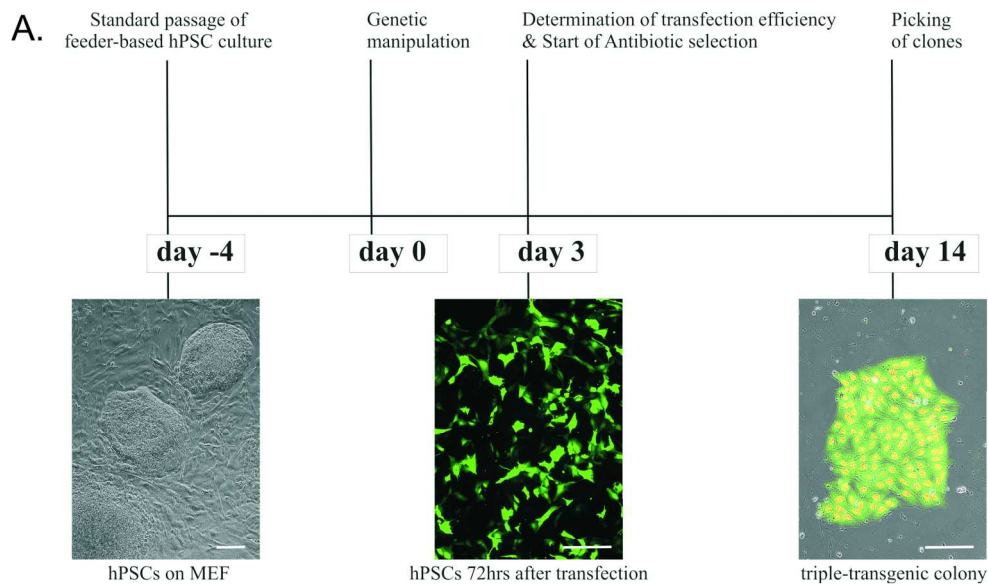
Figure 2

239x226mm (199 x 199 DPI)

1
2
3
4
5
6
7
8
9
10
11
12
13
14
15
16
17
18
19
20
21
22
23
24
25
26
27
28
29
30
31
32
33
34
35
36
37
38
39
40
41
42
43
44
45
46
47
48
49
50
51
52
53
54
55
56
57
58
59
60
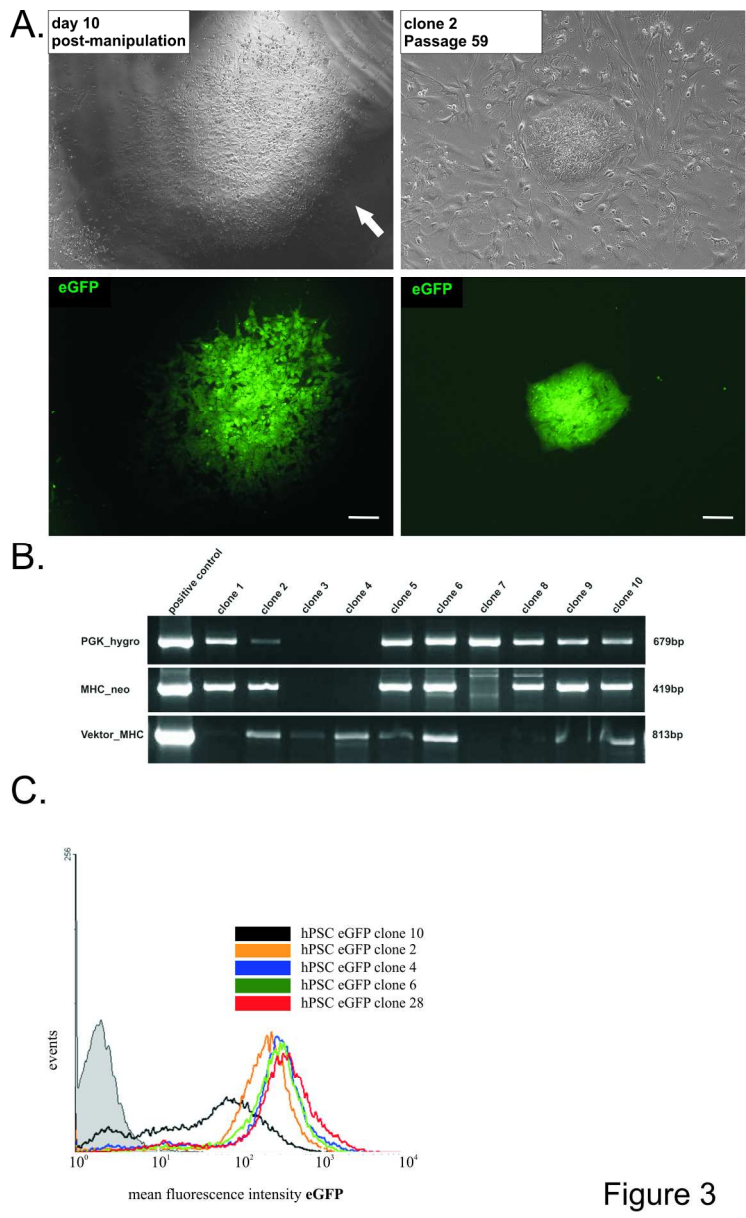
Figure 3

200x326mm (200 x 200 DPI)

1
2
3
4
5
6
7
8
9
10
11
12
13
14
15
16
17
18
19
20
21
22
23
24
25
26
27
28
29
30
31
32
33
34
35
36
37
38
39
40
41
42
43
44
45
46
47
48
49
50
51
52
53
54
55
56
57
58
59
60

A.

Figure 4

290x190mm (200 x 200 DPI)

Figure 5

292x227mm (200 x 200 DPI)

Figure 6

180x302mm (200 x 200 DPI)

Figure 7

183x291mm (200 x 200 DPI)

Figure 8

204x239mm (200 x 200 DPI)

Table 1 Overview on the generated stable clone stable transgenic hESC/hiPSC clones

Stem Cell line	Cultivation	Single or multi-transgenic	Vectors	Frequency of stable integrants
hCB iPS Clone 2	MEF	Mono-transgenic	αMHCneoPGKhygro	3×10^{-4} (n=7)
hCB iPS Clone 2	MEF	Double-transgenic	αMHCneoPGKhygro + pCAG eGFP	$6,5 \times 10^{-4}$ (n=7)
hCBiPS Clone 2	MEF	Double-transgenic	αMHCneoPGKhygro pCAG RedStar nuc mem	$1,3 \times 10^{-5}$ (n=6)
hCBiPS Clone 2	MEF	Triple-transgenic	αMHCneoPGKhygro pCAG eGFP pCAG RedStar nuc mem or pCAG eGFP	$2,3 \times 10^{-5}$ (n=6) $2,5 \times 10^{-5}$ (n=4)
hFF IPS Clone 4	MEF	Mono-transgenic	αMHCneoPGKhygro	1.9×10^{-5} (n=10)
hFF IPS Clone 4	MEF	Double-transgenic	αMHCneoPGKhygro + pCAG eGFP	$8,7 \times 10^{-5}$ (n=9)
hES3	hFF/MEF	Mono-transgenic	αMHCneoPGKhygro	$7,5 \times 10^{-5}$ (n=1)
hCB iPS Clone 2	Feeder-independent Suspension	Mono-transgenic	αMHCneoPGKhygro	$3,7 \times 10^{-4}$ (n=4)

Table S1. Sequences of oligonucleotides used for analysis of the full integrity of αMHCneoPGKhygro

Primer name	Position	Annealing temperature	Product size	Sequence (5' – 3')
αMHC_neo sense	5157	55°C	419bp	cgg cac tct tag caa acc tc
αMHC-neo ras I	5576			ctc gct ctg cag ttc att ca
αMHC_neo sense	5157	55°c	717bp	cgg cac tct tag caa acc tc
αMHC-neo ras II	5874			gat gct ctt cgt cca gat ca
PGK-hygro sense	6669	55°C	665bp	tag cag ctt tgc tcc ttc g
PGK-hygro ras I	7334			act gac ggt gtc gtc cat c
PGK-hygro sense	6669	55°C	679bp	tag cag ctt tgc tcc ttc g
PGK-hygro ras II	7348			tcc atc aca gtt tgc cag tg

PCR program used together with primers listed in table S1

94°C   1 minute

94°C   1minute
55°C   1minute   35 cycles
72°C   90seconds

72°C   10minutes

4°C   endlessly

1
2
3
4
5
6
7
8
9
10
11
12
13
14
15
16
17
18
19
20
21
22
23
24
25
26
27
28
29
30
31
32
33
34
35
36
37
38
39
40
41
42
43
44
45
46
47
48
49
50
51
52
53
54
55
56
57
58
59
60

Table S2. Sequences of oligonucleotides used for quantitative real-time RT-PCR.

Primer name	Target	Position	Annealing temperature	Product size	Sequence (5' – 3')
ß-actin RT sense	GI 168480144	1028	60°C	176bp	ATTGCCGACAGGATGCAGAA
ß-actin RT ras		1165			GGGCCGGACTCGTCATACTC
rNIS sense	GI U60282.1	1193	60°C	168bp	ATGGCAGCTGTGACTGTGGA
rNIS ras		1361			TGAAGGAACCCTGGAGGACA

Publikation 2

Titel der Arbeit: „Transplantation and Tracking of Human Induced Pluripotent Stem Cells in a Pig Model of Myocardial Infarction: Assessment of Cell Survival, Engraftment and Distribution by Hybrid Single Photon Emission Computed Tomography/Computed Tomography of Sodium Iodide Symporter Trangene Expression"

Autoren: **Templin C**, Zweigerdt R, Schwanke K, Olmer R, Ghadri JR, Emmert M, Müller E, Küest SM, Cohrs S, Schibli R, Kronen P, Hilbe M, Strunk D, Haverich A, Hoerstrup SP, Lüscher TF, Kaufmann PA, Landmesser U, Martin U.

Publikationsorgan: Circulation 2012 Jul 24;126(4):430-9.

eigener Beitrag: - Studienidee und Studiendesign

- *In vitro* Versuche zur Jodaufnahme und -abgabe

- *In vitro* Radiotoxizitäts-Assay ^{125}I markierter NIS$^+$-hiPSCs

- Versuche zur Bestimmung des SPECT Detektionslimits von NIS$^+$-hiPSCs in *ex vivo* Schweineherzen

- Zellkultur und Labeling der NIS$^+$-hiPSCs mit Radiotracern

- Induktion des experimentellen Myokardinfarktes durch intrakoronare Ballonokklusion bei allen Versuchstieren

- NOGA-Mapping des linksventrikulären Myokards bei allen Versuchstieren

- Intramyokardiale Stammzellapplikation mittels MyoStar-Injektions-katheter bei allen Versuchstieren

- Intrakoronare Applikation des Radiotracers

- SPECT-CT-Untersuchungen bei allen Versuchstieren

- Quantifizierung der SPECT Signale durch VOI Analysen

- Autopsie aller Versuchstiere und Gewebepräparation

- histologische Aufarbeitung der Gewebe

- Analyse und Interpretation der Daten

- Schreiben des Manuskriptes

Circulation

American Heart Association

Transplantation and Tracking of Human-Induced Pluripotent Stem Cells in a Pig Model of Myocardial Infarction : Assessment of Cell Survival, Engraftment, and Distribution by Hybrid Single Photon Emission Computed Tomography/Computed Tomography of Sodium Iodide Symporter Transgene Expression

Christian Templin, Robert Zweigerdt, Kristin Schwanke, Ruth Olmer, Jelena-Rima Ghadri, Maximilian Y. Emmert, Ennio Müller, Silke M. Küest, Susan Cohrs, Roger Schibli, Peter Kronen, Monika Hilbe, Andreas Reinisch, Dirk Strunk, Axel Haverich, Simon Hoerstrup, Thomas F. Lüscher, Philipp A. Kaufmann, Ulf Landmesser and Ulrich Martin

The online version of this article, along with updated information and services, is located on the World Wide Web at:
http://circ.ahajournals.org/content/126/4/430

Data Supplement (unedited) at:
http://circ.ahajournals.org/content/suppl/2012/06/29/CIRCULATIONAHA.111.087684.DC1.html

Imaging

Transplantation and Tracking of Human-Induced Pluripotent Stem Cells in a Pig Model of Myocardial Infarction

Assessment of Cell Survival, Engraftment, and Distribution by Hybrid Single Photon Emission Computed Tomography/Computed Tomography of Sodium Iodide Symporter Transgene Expression

Christian Templin, MD; Robert Zweigerdt, PhD; Kristin Schwanke, PhD; Ruth Olmer, PhD; Jelena-Rima Ghadri, MD; Maximilian Y. Emmert, MD; Ennio Müller; Silke M. Küest, MD; Susan Cohrs, PhD; Roger Schibli, PhD; Peter Kronen, DVM; Monika Hilbe, DVM; Andreas Reinisch, MD, PhD; Dirk Strunk, MD; Axel Haverich, MD; Simon Hoerstrup, MD, PhD; Thomas F. Lüscher, MD; Philipp A. Kaufmann, MD; Ulf Landmesser, MD*; Ulrich Martin, PhD*

Background—Evaluation of novel cellular therapies in large-animal models and patients is currently hampered by the lack of imaging approaches that allow for long-term monitoring of viable transplanted cells. In this study, sodium iodide symporter (NIS) transgene imaging was evaluated as an approach to follow in vivo survival, engraftment, and distribution of human-induced pluripotent stem cell (hiPSC) derivatives in a pig model of myocardial infarction.

Methods and Results—Transgenic hiPSC lines stably expressing a fluorescent reporter and NIS (NIS^pos-hiPSCs) were established. Iodide uptake, efflux, and viability of NIS^pos-hiPSCs were assessed in vitro. Ten (±2) days after induction of myocardial infarction by transient occlusion of the left anterior descending artery, catheter-based intramyocardial injection of NIS^pos-hiPSCs guided by 3-dimensional NOGA mapping was performed. Dual-isotope single photon emission computed tomographic/computed tomographic imaging was applied with the use of ^{123}I to follow donor cell survival and distribution and with the use of ^{99m}TC-tetrofosmin for perfusion imaging. In vitro, iodide uptake in NIS^pos-hiPSCs was increased 100-fold above that of nontransgenic controls. In vivo, viable NIS^pos-hiPSCs could be visualized for up to 15 weeks. Immunohistochemistry demonstrated that hiPSC-derived endothelial cells contributed to vascularization. Up to 12 to 15 weeks after transplantation, no teratomas were detected.

Conclusions—This study describes for the first time the feasibility of repeated long-term in vivo imaging of viability and tissue distribution of cellular grafts in large animals. Moreover, this is the first report demonstrating vascular differentiation and long-term engraftment of hiPSCs in a large-animal model of myocardial infarction. NIS^pos-hiPSCs represent a valuable tool to monitor and improve current cellular treatment strategies in clinically relevant animal models. (***Circulation***. 2012;126:430-439.)

Key Words: imaging ■ induced pluripotent stem cells ■ iPS cell ■ myocardial infarction in pig ■ sodium iodide symporter (NIS)

Stem cell–based therapies are being actively explored as a potentially innovative therapeutic strategy for various genetic and acquired diseases. Recently, the possibility of reprogramming human somatic cells into human-induced pluripotent stem cells (hiPSCs) that are able to differentiate into all cell lineages present in the heart[1–4] has opened novel opportunities for myocardial repair. With respect to the potential therapeutic application of pluripotent stem cell derivatives, major progress

has been achieved concerning scalable cell production[5,6] and more efficient and specific differentiation into cell types of interest.[7]

Editorial see p 388
Clinical Perspective on p 439

However, there are still major hurdles and risks to overcome with regard to PSC-based heart repair. These include safety risks, especially the potential of teratoma and tumor formation,[2] low cell retention and engraftment rates,[8–11] and the general question of whether engraftment of hiPSCs after simple intramyocardial cell injection leads to formation of functional tissue, such as de novo vasculature or myocardium, and results in significant clinical benefits.[12] Although some of these issues can be addressed in vitro or in appropriate small-animal models, others will require exploration in large-animal models, which are more similar to humans.[13] Transplanted human cardiomyocytes, for example, are unlikely to fully functionally integrate with rodent myocardium because of highly dissimilar beating rates.[11] Therefore, meaningful assessment of human cells for heart repair must be demonstrated in large-animal models such as dogs, pigs, or monkeys.[13]

Clearly, advanced imaging technologies allowing for longitudinal tracking of cellular grafts and ideally enabling monitoring of donor cell survival, proliferation, distribution, or even differentiation are crucial for (pre)clinical evaluation of novel cell-based therapeutics.[14] At present, transgene-based imaging approaches that fulfill these requirements are mainly restricted to far-red fluorescence reporters or photon-emitting technologies, in particular those based on luciferase expression. Unfortunately, limited tissue penetration restricts application of these technologies to small-animal models only.[15]

Most previous large-animal studies applied magnetic resonance imaging technology to detect nanoparticle-labeled cells.[16] The main disadvantage of this approach is the inability to discriminate vital donor cells from nanoparticle-loaded cell debris or the recipient's cells such as macrophages, which can actively incorporate cell debris and released nanoparticles by phagocytosis.[16] In other studies, direct radionuclide labeling of cells was performed (eg, through [^{18}F]FDG, In^{111} oxine, ^{64}Cu-PTSM, or ^{99m}Tc-hexamethylprophylene amine oxine).[16] Limitations of the latter techniques include isotope half-time– and label-retention–dependent loss of signal strength.[16] In addition, direct labeling strategies with nanoparticles or radionuclides, particularly for In^{111}, have been reported to affect (stem) cell vitality.[16]

In a first pilot study to overcome these critical drawbacks, herpes simplex virus thymidine kinase–mediated phosphorylation of [^{18}F]FHBG was evaluated as a transgene-based imaging approach in large animals,[17,18] but detection of transplanted cells was reported several hours after cell injection only.

Another promising approach has been developed recently,[19] which permits detection of viable transplanted cells by positron emission tomography (PET) or single photon emission computed tomography (SPECT) after iodide (^{123}I) or ^{99m}Tc radiotracer administration. This technology relies on the expression of a transgenic sodium iodide symporter (NIS)[20] in transplanted donor cells. Physiological expression of NIS in the adult organism is restricted to the thyroid,

stomach, choroids plexus, and salivary gland and is not detectable in limbs, brain, or other internal organs such as the heart.[20] NIS-mediated iodide accumulation in the thyroid is an active transport process that occurs at the basolateral plasma membrane of the thyroid follicular cells against the iodide electrochemical gradient stimulated by thyroid-stimulating hormone and can be specifically inhibited by perchlorate. Clinically, NIS expression provides the basis for the effective diagnostic of thyroid cancer and its metastases by iodide isotope administration.[20]

The technology provides important advantages with respect to clinical application for longitudinal tracking of stem cell grafts. This includes the lack of immunogenicity of the human NIS transgene and the fact that SPECT scanning of radiotracers such as ^{99m}Tc and ^{123}I is widely available at relatively low cost and is approved by responsible regulatory authorities such as the Food and Drug Administration. Moreover, recent progress in quantification of tracer signals with the use of clinical SPECT systems[21] emphasizes the potential of this approach for tracking cellular transplants in large animals and patients. To date, however, the strategy was evaluated only in a small-animal model focused on detection of acute cell retention after administration of cardiac derived stem cells.[19]

In the present study, we demonstrate the applicability of this technology for in vivo monitoring of cellular grafts in a pig model of myocardial infarction. SPECT/computed tomographic (CT) imaging results revealed successful in vivo donor cell labeling by intracoronary iodide administration 5 days or 12/15 weeks after intramyocardial cell transplantation. These data were confirmed by immunohistochemistry on harvested tissue, providing unequivocal evidence for long-term survival, engraftment, and differentiation of transplanted hiPSC derivatives.

Methods

Culture of hiPSCs

Conventional culture of hiPSCs was performed as described previously.[1] Mass cell generation of NIS transgenic hiPSCs (NIS^{pos}-hiPSCs) in suspension cultures was performed as described previously.[5,6]

Generation of NIS^{pos}-hiPSC Lines

See the online-only Data Supplement for details of NIS^{pos}-hiPSC lines.

Characterization of NIS^{pos}-hiPSCs

See Figure 1 and the online-only Data Supplement for details.

Iodide Uptake and Efflux

See the online-only Data Supplement for details.

Ex Vivo Cardiac SPECT/CT Imaging

For assessing the SPECT/CT detection limit in terms of prelabeled NIS^{pos}-hiPSCs, cells were incubated for 90 minutes with 1 MBq ^{123}I per 1×10^6 cells. After vigorous washing, serial cell dilutions comprising a total of 1×10^4, 1×10^5, 5×10^5, 1×10^6, 3×10^6, 6×10^6, or 1.2×10^7 labeled cells were injected into the lateral and septal walls of the left ventricle. The ^{123}I signal was visualized through a dual-detector hybrid SPECT/CT scanner (Infinia Hawkeye, GE Healthcare). To mimic in vivo imaging, heart-derived ^{123}I signals were recorded through a dissected pig chest that was placed above the heart to mimic signal attenuation.
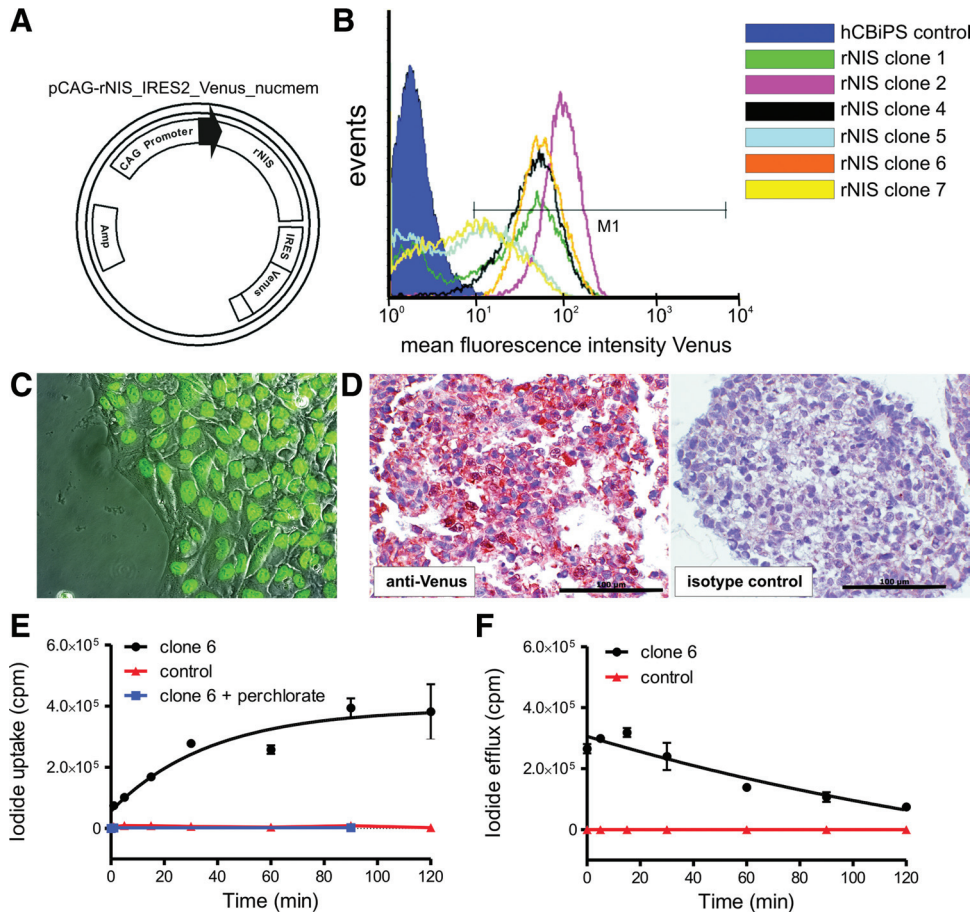
Figure 1. Generation and functional characterization of sodium iodide symporter transgenic human induced pluripotent stem cells (NIS^{pos}-hiPSCs). **A**, Map of the bicistronic vector pCAG_rNIS_IRES2_Venus_nucmem used for the generation of transgenic hiPSC clones. **B**, Fluorescence-activated cell sorting analysis of Venus expression in several independent rNIS^{pos}-hiPSC clones. Individual clones showed a stable level of transgene expression for up to 23 passages. **C**, Overlay of fluorescence and phase contrast image revealing the expected nuclear Venus localization of a typical NIS^{pos}-hiPSC colony cultured on Matrigel (clone 6, 6 passages after clonal selection). **D**, Detection of Venus by immunohistochemistry on a section of paraformaldehyde-fixed NIS^{pos}-hiPSC aggregates derived from suspension culture and the respective isotope control. For immunostaining, an anti-green fluorescent protein antibody was used, which cross-reacts with the yellow green fluorescent protein variant Venus. Notably, fixation and immunohistochemistry treatments lead to an apparently cytoplasmic Venus-specific staining, which is in contrast to the direct Venus fluorescence in viable cells that is strictly restricted to the nuclear membrane, as shown in **C**. **E**, Kinetics of ^{125}I uptake by NIS^{pos}-hiPSCs (clone 6), inhibition by 100 μmol/L perchlorate, and NIS^{neg}-hiPSC controls (mean±SEM, triplicate measurements). Iodide uptake reached a steady state within 90 minutes with a maximum concentration of ≈100-fold above background in negative controls. ^{125}I accumulation in NIS^{pos}-hiPSCs was completely abolished by perchlorate, suggesting specificity of the signal. **F**, Kinetics of iodide retention in NIS^{pos}-hiPSCs (mean±SEM, triplicate measurements). hCBiPS indicates human cord blood iPS.

Large-Animal Model

Female Landrace pigs (Large White Duroc, Sidler, Zurich, Switzerland; n=13; weight, 25–30 kg; aged 8–10 weeks) were investigated in the present study. Animals were immunosuppressed with cyclosporine A (Novartis Pharmaceuticals, East Hanover, NJ; 10 mg/kg body wt daily) and prednisolone (Pfizer, Zurich, Switzerland; 2.5 mg/kg body wt daily) starting 5 days before hiPSC transplantation until animals were euthanized. Furthermore, all animals received 2×400 mg/d dronedarone at the first preoperative and operative day and 2×200 mg/d from the first postoperative day until the end of the study. All procedures were approved by the responsible local authorities and performed according to the *Guide to the Care and Use of Experimental Animals* published by the US National Institutes of Health (National Institutes of Health publication 85–23, reviewed 1996). A detailed description of the study design is shown in Figure 2.

Induction of Myocardial Infarction

Myocardial infarction was created by inflating the balloon for 180 minutes in the mid segment of the left anterior descending coronary artery, followed by reperfusion. See the online-only Data Supplement for details.

Electromechanical Mapping

Three-dimensional NOGA mapping (Biologics Delivery Systems, Biosense Webster, Johnson & Johnson, Irwindale, CA) was performed 10±2 days after induction of myocardial infarction to assess electrophysiological tissue viability patterns and wall motion abnormalities. The catheter was placed through the right carotid sheath across the aortic valve into the left ventricle. By navigating the catheter along the endocardium, the local intracardiac electrogram together with the wall motion was recorded from its tip at multiple endocardial sites, and detailed 3-dimensional electromechanical maps of the left ventricle were generated. The unipolar voltage values were color coded (visualizing infarct zones as red and viable tissue as green to purple) and superimposed on the 3-dimensional geometry of the map. NOGA mapping and injections were performed as described previously.[22]
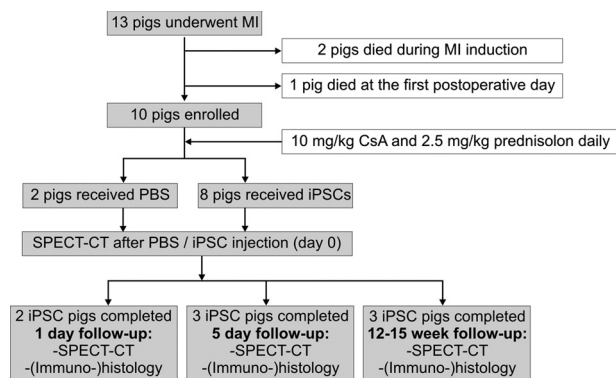
Figure 2. Study design. MI indicates myocardial infarction; CsA, cyclosporine A; PBS, phosphate-buffered saline; SPECT-CT, single photon emission computed tomography/computed tomography; and iPSCs, induced pluripotent stem cells.

Intramyocardial Cell Injections

hiPSCs (1×10^8) were labeled with 100 MBq of ^{123}I (1 MBq$=1 \times 10^6$ cells) for 90 minutes before cell injection. Subsequently, cells were washed twice in phosphate-buffered saline and were resuspended in phosphate-buffered saline as the delivery medium, which was supplemented with fluorospheres (Molecular Probes) to enable unequivocal identification of the cell injection sites under ultraviolet light during tissue sampling in euthanized animals (Figure I in the online-only Data Supplement). Cell injection was performed with an 8F MyoStar injection catheter (Biosense-Webster) with a 27-gauge needle, as follows: Three sites each with 8 single 250-μL injections were selected (left ventricle anterior wall: 50 million control cells [human mesenchymal stem cells {MSCs}]; lateral and septal wall: 50 million NIS^{pos}-hiPSCs or 50 million NIS^{pos}-hiPSCs mixed with 50 million human MSCs). Control animals received phosphate-buffered saline injections at corresponding injection sites. Exact positions of individual injection sites were documented by NOGA mapping.

CT Angiography

For cardiac CT angiography, 1 mL/kg body wt iodixanol (Visipaque 320 mg/mL; GE Healthcare, Bucks, UK) at a flow rate of 4 to 5 mL/s followed by 50 mL saline solution was injected into the ear vein via a 20-gauge catheter. All scans were performed with the 64-detector CT component (LightSpeed VCT, GE Healthcare) of a SPECT/CT scanner with prospective ECG triggering, as established and described in detail previously.[23] Images were analyzed on an external workstation (AW 4; GE Healthcare).

Full-body CT scanning was performed on the same CT scanner with the use of 100 mL iodixanol.

SPECT Imaging

For assessment of myocardial perfusion, ^{99m}TC (10 MBq/kg) was injected into the ear vein, and images were acquired over 5 minutes on the SPECT part of a hybrid SPECT/CT scanner (Discovery NM CT 570c, GE Healthcare) integrating a 64-slice CT device and a cadmium-zinc-telluride gamma camera. The cadmium-zinc-telluride camera has been extensively described recently.[24,25] Briefly, it is a gamma detector with a pinhole collimator and 19 stationary detector modules positioned around the chest. For perfusion imaging, a symmetrical energy window at 140 keV ($\pm 5\%$) was used, and for dual peak acquisition with ^{123}I, a window at 159 keV ($\pm 5\%$) was added.

For mid-term (5 days after transplantation) and long-term (12–15 weeks after transplantation) detection of transplanted hiPSCs, we performed intracoronary injection of ^{123}I into each main coronary artery (left anterior descending, left circumflex, right coronary arteries) with the use of an over-the-wire balloon catheter during 3 coronary occlusions, each lasting 2 to 3 minutes. Between occlu-

sions, the coronary artery was reperfused for 2 minutes. Afterward, animals underwent SPECT/CT imaging as described above.

See Figure II in the online-only Data Supplement for details.

(Immuno)Histological Analysis

See details in the online-only Data Supplement.

Results

Functional NIS Expression in Transgenic hiPSC Clones

hiPSCs (clone hCBiPSC2)[1] were cotransfected with the bicistronic vector pCAG_rNIS_IRES2_Venus_nucmem (Figure 1A) and the plasmid αMHCneoPGKhygro,[26] enabling selection of hygromycin-resistant transgenic cell clones. Six independent Venus^{pos} clones (designated rNIS clones 1, 2, 4, 5, 6, 7) were analyzed for stability of transgene expression. Flow cytometry and fluorescence microscopy revealed robust and stable Venus expression for up to 23 passages with line-specific variations (Figure 1B and 1C). Venus-specific immunohistological assessment was also performed on paraffin sections of suspension culture–derived cell aggregates and differentiated cells in embryoid bodies. In contrast to the expected Venus fluorescence signal in the nucleus of viable cells (Figure 1C), cytoplasmic staining was noted after fixation and immunohistochemistry (Figure 1D, left); however, staining specificity was proven by isotype (Figure 1D, right) and nontransgenic cell controls (data not shown). Quantitative reverse transcription polymerase chain reaction revealed coexpression of the NIS transgene in Venus-expressing clones (data not shown). Venus protein expression was demonstrated in undifferentiated as well as differentiated cells of the NIS^{pos}-hiPSC clone 6, including hiPSC-derived CD31^{pos} endothelial cells (Figure III in the online-only Data Supplement). Further analyses and all cell transplantation experiments were conducted with the use of the NIS^{pos}-hiPSC clone 6.

Transgenic cells and control hiPSCs were analyzed for NIS-specific iodide uptake by in vitro incubation with ^{125}I, an isotope with a half-life of 13 hours. Intracellular labeling efficiency depends on the effective half-life of an applied isotope and the kinetics of the respective isotope accumulation of the cells. ^{125}I uptake in NIS^{pos}-hiPSCs reached a plateau after $\approx$90 minutes. After vigorous washing, ^{125}I accumulation was $\approx$100 times higher than for nontransgenic hiPSC control cells (Figure 1E). Importantly, iodide uptake was completely blocked by the specific NIS inhibitor perchlorate. Typically, the majority of accumulated ^{125}I was released to the medium within 2 hours (Figure 1F). Notably, neither NIS expression nor radiolabeling of NIS^{pos}-hiPSCs affected cell viability (Figure IV in the online-only Data Supplement).

Successful SPECT/CT-Based Detection of Down to 1×10^5 ^{123}I-Labeled NIS^{pos}-hiPSCs in Explanted Pig Hearts

Ex vivo cardiac SPECT/CT was performed to determine the detection limit for ^{123}I-prelabeled NIS^{pos}-hiPSCs after intramyocardial cell injection. Equal volumes of a serial dilution of labeled cells were applied. As shown in Figure 3, SPECT/CT enabled detection of a minimum of 1×10^5 cells injected into explanted pig hearts. Notably, ^{123}I tracer uptake
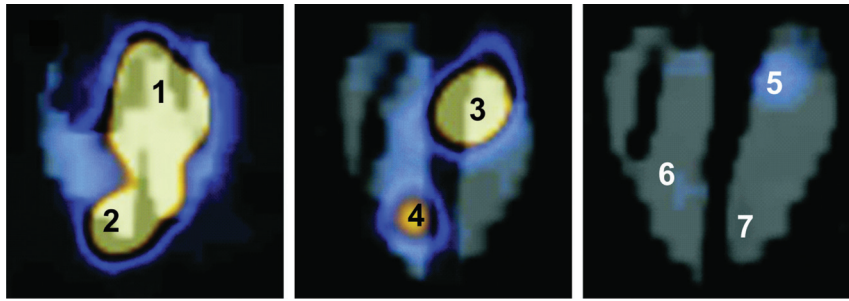
Figure 3. Ex vivo single photon emission computed tomography/computed tomography of pig hearts transplanted with sodium iodide symporter transgenic human induced pluripotent stem cells (NIS^{pos}-hiPSCs). ^{123}I-prelabeled NIS^{pos}-hiPSCs were transplanted into pig hearts ex vivo to determine the minimal number of detectable NIS^{pos}-hiPSCs. Depicted are single photon emission computed tomographic images of pig hearts after injections of equal volumes with different amounts of cells as indicated: $1=1.2\times10^7$; $2=6\times10^6$; $3=3\times10^6$; $4=1\times10^6$; $5=5\times10^5$; $6=1\times10^5$; $7=1\times10^4$. Injected NIS^{pos}-hiPSCs were detectable down to 1×10^5 cells.

was detected through a dissected pig chest that had been placed above the heart to mimic signal attenuation in vivo. On the basis of these results, 5×10^7 prelabeled NIS^{pos}-hiPSCs were subsequently applied in vivo per injection area with a hypothetical detection threshold of ≈2% persistent cells.

Prelabeled NIS^{pos}-hiPSCs Were Detected for up to 5 Hours After Catheter-Based Intramyocardial Delivery Into Distinct Regions of Infarcted Hearts

As indicated in the study design (Figure 2), myocardial infarction was induced in 13 animals, 10 of which were enrolled in the study. Ten days after transient occlusion of the left anterior descending coronary artery, SPECT/CT imaging revealed perfusion defects in the apex and mid segment of the anterior and septal walls in all treated animals (Figure 4, line 1). This was also confirmed by NOGA mapping demonstrating loss of electric activity at the apicoseptal, apicobasal, and apicolateral myocardial regions (red color). Brown points represent the locations of the NOGA-guided intramyocardial injections at the border zone of infarction (Figure 4, line 2, and Figure V in the online-only Data Supplement). One to 3 hours after injection of ^{123}I-prelabeled NIS^{pos}-hiPSCs (5×10^7 hiPSCs or 5×10^7 hiPSCs coadministered with 5×10^7 human MSCs, respectively, per injection area), intensive ^{123}I signals were detected by SPECT/CT imaging in the septal and lateral walls of the left ventricle, corresponding exactly to the injection site as recorded by NOGA mapping. As expected, ^{123}I-treated control cells injected into a separate region of the same heart did not result in a detectable SPECT signal (Figure 4, line 3). Notably, MSC coadministration considerably increased signal intensity, suggesting improved hiPSC retention in the myocardium after transplantation (Figure 4 and Video I in the online-only Data Supplement). The signal intensity was highest in the first hour after cell transplantation and diminished successively. At 3 to 5 hours after injection, signal intensity was substantially reduced (Figure VI in the online-only Data Supplement) and became undetectable after 24 hours (data not shown). Imaging of control animals treated with phosphate-buffered saline did not show any SPECT signal (data not shown). As expected, immunohistological staining of tissue sections of the region where NIS^{pos}-hiPSCs and human MSCs had been coinjected showed an injection channel filled with rounded cells containing a fraction of

Venus^{pos} and OCT4^{pos} cells (Figure 4). A semiquantitative analysis of the obtained ^{123}I signals in the 2 pigs that had been euthanized after day 1 follow-up demonstrated that the NIS^{pos}-hiPSCs cotransplanted with MSCs gave a 6.8-fold/ 1.7-fold stronger ^{123}I signal than the separately transplanted NIS^{pos}-hiPSC cells (Figure VII in the online-only Data Supplement). No detectable ^{123}I activity was associated with the transplanted NIS^{neg} control cells (Table I in the online-only Data Supplement).

Long-Term Detection of Engrafted NIS^{pos}-hiPSC Derivatives for up to 15 weeks by SPECT/CT Imaging After Intracoronary Iodide Administration

For detection of transplanted NIS^{pos}-hiPSC derivatives at 5 days and 12 to 15 weeks after intramyocardial cell injection, ^{123}I was infused by intracoronary injection into the left anterior descending, left circumflex, and right coronary arteries. One hour after tracer injection, the resulting ^{123}I signals were assessed. As expected, on SPECT/CT scanning, a very strong uptake was observed in the thyroid, whereas a weaker uptake was detected in the stomach (data not shown). Interestingly, in the heart, ^{123}I signals were detected exclusively in regions where NIS^{pos}-hiPSCs had been cotransplanted with human MSCs (Figure 5). In independent hearts, ^{123}I accumulation was detected either in the lateral heart region or in the septal left ventricular wall, always correlating with the area of NIS^{pos}-hiPSC/MSC coinjection. In contrast, no ^{123}I signal could be detected in regions where only NIS^{pos}-hiPSCs or control cells had been injected.

In vitro coculture experiments under hypoxic conditions were performed to investigate whether antiapoptotic effects of MSCs might support the survival of NIS-hiPSCs. Interestingly, MSCs significantly decreased the rate of NIS-hiPSC apoptosis. This effect was dependent of both secreted factors and cell-cell contact (Figure VIII in the online-only Data Supplement).

After SPECT/CT, hearts were euthanized for tissue sample analysis. In correlation with SPECT/CT imaging and NOGA mapping of myocardial infarction, histological analyses of respective heart regions (collected 5 days and 15 weeks after cell transplantation) revealed typical signs of infarction and subsequent fibrosis, including widespread replacement of myocardium by loose to densely arranged cells with fibroblast
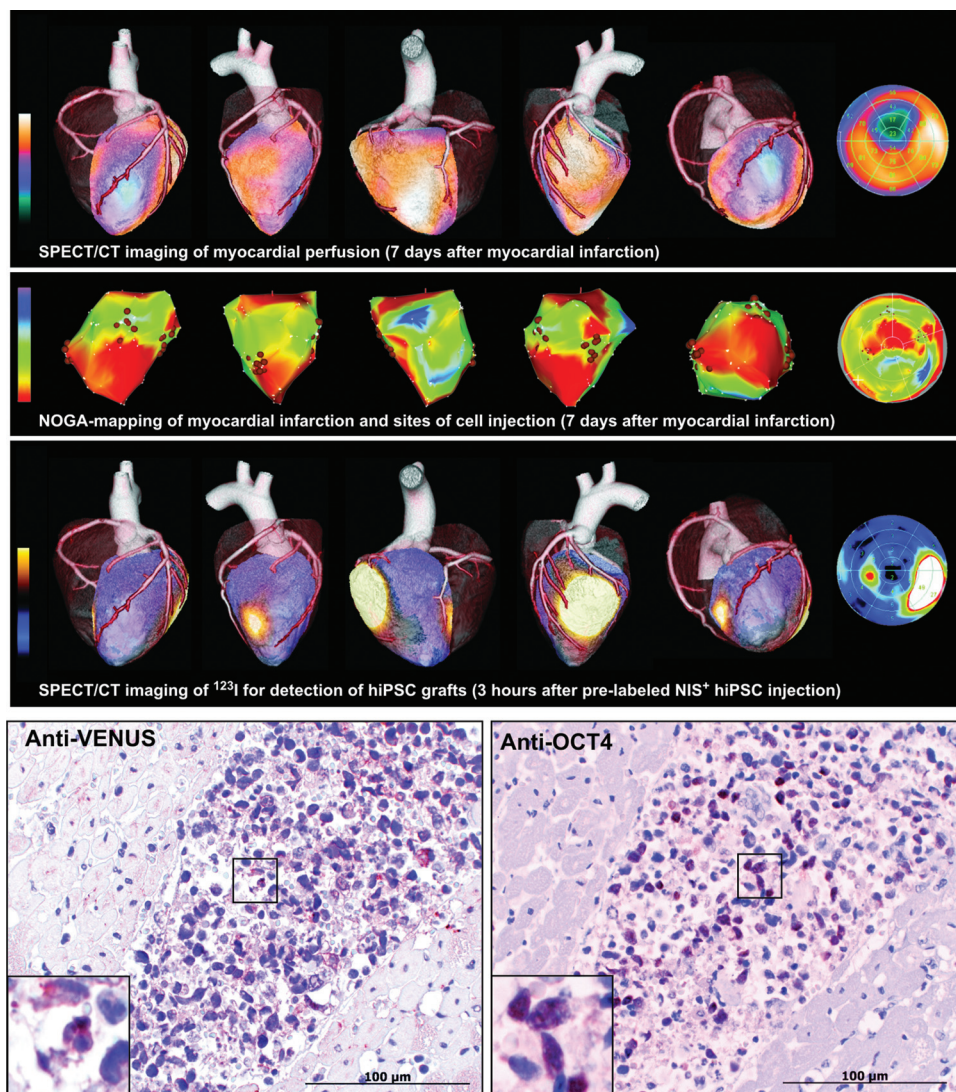
Figure 4. In vivo cardiac hybrid single photon emission computed tomography/computed tomography (SPECT/CT) demonstrates successful induction of myocardial infarction and suggests long-term survival of sodium iodide symporter transgenic human induced pluripotent stem cell (NIS[pos]-hiPSC) grafts. Representative images of a heart of 1 of 3 recipient animals that were euthanized 6 hours after cell injection are shown. Line 1: SPECT/CT in vivo imaging of the left ventricle demonstrates a loss of myocardial perfusion (blue) in the anteroapical and septal walls after occlusion of the left anterior descending coronary artery. Noninfarcted myocardium appears orange colored, indicating normal [99m]TC-tetrofosmin uptake. Line 2: Three-dimensional NOGA mapping of the left ventricle recorded during cell injection. NOGA colors represent unipolar voltage values: red=scar, green to blue=viable tissue. Cell injection sites in the lateral (NIS[pos]-hiPSCs+mesenchymal stem cells), septal (NIS[pos]-hiPSCs), and anterior (nontransgenic mesenchymal stem cells) walls are shown as brown dots. Line 3: SPECT/CT imaging of left ventricle 1 hour after catheter-based intramyocardial cell injection demonstrating intense ^{123}I signals (yellow) in the lateral and septal walls that correspond exactly to the injection sites (each injection area 5×10^7 hiPSCs), as recorded by NOGA mapping; control cells did not result in a detectable radiotracer signal (anterior wall). Coadministration of mesenchymal stem cells markedly increased signal intensity (lateral wall). Immunohistochemistry: Depicted are immunohistological sections of the lateral ventricle wall showing a cell injection channel 6 hours after cell application filled with cotransplanted human mesenchymal stem cells and Venus[pos] NIS[pos]-hiPSCs stained for Venus and OCT4 (each with brown color).

phenotype, and moderate presence of granulocytes and lymphocytes. Immunohistochemistry confirmed persistent engraftment of NIS[pos]-hiPSCs. Anti-Venus–specific staining demonstrated the presence of Venus[pos] hiPSC derivatives 5 days and 12/15 weeks after cell injection. Notably, after 12/15 weeks, the histological images suggest that hiPSC derivatives had adopted an endothelial phenotype lining numerous vessels in the injected heart regions (Figure 5, right, and Figure IX in the online-only Data Supplement). Complementing semiquantitative analyses on the capillary densities of the respective heart regions suggested an increased capillary density in the regions of NIS[pos]-

hiPSC-MSC versus NIS[pos]-hiPSC injection (Figure X in the online-only Data Supplement). Interestingly, in contrast to analysis 5 hours after cell administration, no OCT4-specific cell staining could be detected at 5 days or 12/15 weeks (data not shown). In addition, no teratoma or other obvious tumor formation was detected in the euthanized recipient animals during autopsy.

Discussion

The availability of transgene-based imaging technologies in large animals that enable nontoxic, specific, sensitive, non-
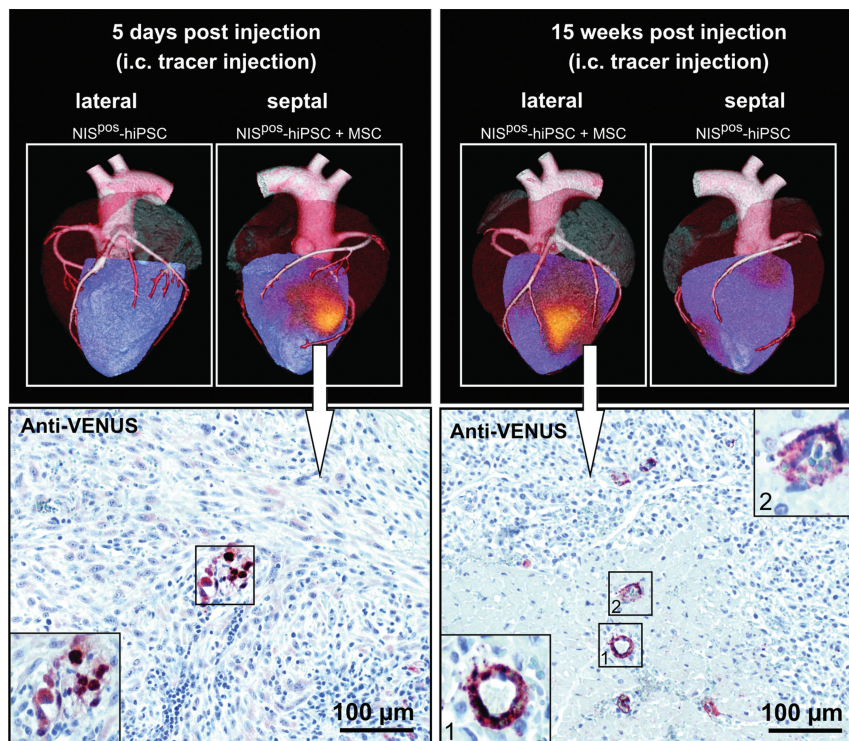
Figure 5. In vivo single photon emission computed tomography/computed tomography (SPECT/CT) imaging of long-term surviving derivatives of sodium iodide symporter transgenic human induced pluripotent stem cells (NIS^{pos}-hiPSCs) in pig hearts after 5 days and 15 weeks, respectively. Non-prelabeled NIS^{pos}-hiPSCs (each site 5×10^7 cells) could be detected in mid-term (5 days) and long-term follow-up (15 weeks) $\approx$1 hour after intracoronary (i.c.) ^{123}I injection. Immunohistochemical staining of tissue sections of corresponding areas of the left ventricular wall confirmed the presence of Venus^{pos} (stained with cross-reacting anti-green fluorescent protein antibody) NIS^{pos}-hiPSC derivatives. Notably, the vast majority of Venus^{pos} iPSC derivatives were found to represent endothelial cells integrated into the cardiac vasculature 15 weeks after cell transplantation. No OCT4^{pos} cells could be detected (data not shown). The ^{123}I signal intensities as determined by volume of interest analysis of the respective animals shown are as follows: 5 days after injection animal, volume of interest$=4.3\times10^5$ counts (septal region$=$NIS^{pos}-hiPSC+mesenchymal stem cell [MSC] injection); 15 weeks after injection animal, volume of interest$=1.8\times10^5$ counts (lateral region$=$NIS^{pos}-hiPSC+MSC injection).

invasive, and serial long-term imaging of viable grafts is of utmost importance for preclinical evaluation of stem cell–based therapies.

In the present study, we have established a reporter gene approach that enables in vivo monitoring of long-term survival of hiPSC derivatives in a pig model of myocardial infarction. Notably, this is the first report demonstrating the feasibility of repeated longitudinal in vivo imaging of cell viability, proliferation, and tissue distribution of cellular grafts in internal organs of large animals.

Similar to luciferase imaging in small animals, viable cells expressing NIS are able to accumulate ^{123}I and to evoke a detectable SPECT signal, thereby preventing false-positive detection of dead cells, cellular debris–bound label, or phagocytosing macrophages. Although the ratio of the intensity of the specific ^{123}I signal in our NIS^{pos}-hiPSCs compared with NIS^{neg}-hiPSCs as determined in vitro is lower than the typical signal-to-background ratio in the case of luciferase reporter systems, long-term surviving NIS^{pos}-hiPSC derivatives evoked a ^{123}I signal of considerable intensity in the areas of intramyocardial cell injection. This may be explained by the relatively low absorption of the ^{123}I signal through soft and hard tissue and is in contrast to the very limited tissue penetration of luciferin-emitted light, which, even in small animals with low tissue thickness, leads to significant loss of signal.

Ex vivo injection of ^{123}I-labeled NIS^{pos}-hiPSCs revealed a detection limit of $\approx1\times10^5$ cells in isolated pig hearts. Because ^{123}I signals were recorded through an isolated pig chest, one can expect signal intensities in vivo in the same range as those detected in hearts assessed ex vivo. Although not directly comparable, because (1) lentiviral vectors and another tracing approach were used; (2) another stem cell type, namely, cardiac stem cells, was applied; and (3) signal retention through pig chest is slightly different from retention through rat chest, the determined detection limit is in the same range as for cell transplantation into rat hearts. Here, Terrovitis et al[19] estimated 1.5×10^5 as the minimal detectable cell number. Further advantages of human NIS-SPECT versus herpes simplex virus thymidine kinase–PET imaging are wide availability of the necessary tracers, lack of need for specialized radiosynthesis facilities, and lack of immunogenicity of the human NIS, which may be of critical importance for long-term monitoring in particular.

Obviously, SPECT imaging of NIS-expressing cell grafts has limitations. As is the case with every in vivo imaging approach, there is a detection limit in terms of a minimal detectable number of cells. Certainly, we cannot exclude distribution of single undifferentiated or differentiated hiPSC derivatives to other organs. Indeed, only if a critical number of cells accumulates or is reached as a result of local prolifera-

tion, or the minimal detection limit at a specific site is achieved, can NIS-expressing engrafted cells be detected. Nevertheless, in our experiments, we were not able to detect any ^{123}I signals outside the heart despite the naturally NIS-expressing tissue sites. Autopsies of the euthanized animals 12 to 15 weeks after cell infusion confirmed these results and did not reveal any sign of tumor or teratoma formation. Together with the absence of OCT4^{pos} cells 12 to 15 weeks after cell transplantation, as analyzed by immunohistochemistry, this raises the question of whether the high incidence of teratomas observed in immunoincompetent mice is actually indicative of clinical applications or is rather an artifact of species incompatibilities that prevent natural control of cell proliferation in the specific tissue niches. Another potential explanation for the obvious absence of undifferentiated cells and the observed parallel persistence of differentiated vascular NIS[pos]-hiPSC derivatives might be the applied immunosuppressive protocol consisting of relatively high doses of cyclosporine A and prednisolone. In general, the long-term persistence of hiPSC-derived endothelial cells indicates the efficacy of our immunosuppressive protocol, at least in terms of T-cell reactivity toward differentiated iPSC derivatives. However, there is evidence that cyclosporine A is not effective toward natural killer cells,[27] which might lead to selective natural killer cell–based erasure of undifferentiated PSCs.[28] In the case of prednisolone, recent data suggest that inhibition of natural killer cells depends on the mode of activation, thereby indicating that prednisolone treatment might also not fully prevent natural killer–mediated killing of undifferentiated hiPSCs.[29]

Another limitation of this imaging technology is the physiological expression of NIS in the thyroid, stomach, choroid plexus, and salivary gland. Because the signals from these organs are strong, they may cover up weak signals from adjacent organs. For instance, although it does not pose a problem in larger animals such as the pig, the strong thyroid signal may interfere with close-by cardiac tracer signals in mice. In addition, the stomach background signal may interfere with tracer signals in the upper abdomen.

Of course, there is room for further improvement. Higher levels of NIS[pos] expression in optimized vector systems and selected stable cell clones may lead to further increase of ^{123}I accumulation compared with NIS^{neg} control cells. In addition, we currently do not know whether potential silencing effects during in vivo differentiation of the transplanted NIS[pos]-hiPSCs may have diminished NIS expression in our experiments and whether expression systems with reduced silencing can lead to further increase of the ^{123}I signal.

As mentioned above, immunohistochemical staining of myocardial tissue sections harvested 5 days and 12 to 15 weeks after cell application showed no OCT4^{pos} cells in the areas of previous cell infusion. Instead, Venus[pos] NIS[pos]-hiPSC derivatives with endothelial phenotype were detected, which contributed to the intramyocardial vasculature. Notably, the utilized CAG promoter–driven NIS does not allow following differentiation events through SPECT imaging. However, this could be realized by placing NIS under the control of cell type–specific promoters, for instance, the OCT4 promoter[5] or the cardiomyocyte-specific α-myosin heavy chain promoter.[30]

Of importance for future clinical application of this technology will be the use of well-characterized transgenic cell clones with defined transgene integration through zinc finger or transcription activator-like effector (TALE) nuclease,[31] for instance, in safe harbor sites such as adeno-associated virus integration site 1,[31] thereby diminishing risks of insertional mutagenesis and carcinogenesis. Importantly, it must be assessed whether the required level of radiation can be reduced: Although the applied ^{123}I dose is on a level similar to that clinically applied for standard tumor therapies, it is far higher than for routine thyroid diagnostics, thereby prohibiting clinical application of the developed approach at this stage. Furthermore, and although the conducted minimal invasive cell application by intramyocardial hiPSC injection is of high clinical relevance, it must be evaluated whether similar or even higher sensitivities and signal-to-noise ratios can be obtained in case of global tracer delivery (eg, through the ear veins of the pig).

As a first application of the established technology for SPECT imaging of transgenic NIS expression, we have addressed the common problem of low cell survival and retention rates after cell transplantation.[8–10] Typically, after intramyocardial cell infusion, the majority of donor cells are directly flushed back through the injection channel[10,32] or do not survive the initial phase after transplantation.[9] To address this problem, Laflamme et al[8] recently described a novel prosurvival cocktail that can dramatically increase engraftment of transplanted human embryonic stem cell–derived cardiomyocytes in an athymic rat model. We have now investigated whether cotransplantation of human MSCs that release antiapoptotic factors[33] and express immunomodulatory properties[34] may improve the survival and engraftment of transplanted NIS[pos]-hiPSCs after xenotransplantation into pigs. Interestingly, SPECT imaging suggested a positive effect of the cotransplanted human MSCs even at 3 hours after cell infusion, showing a markedly stronger tracer uptake at the sites where NIS[pos]-hiPSCs had been cotransplanted with human MSCs than at the injection sites of pure NIS[pos]-hiPSCs. It is questionable whether this very early phenomenon can be explained through antiapoptotic effects. It is more likely that other factors, including MSC-mediated increased cell aggregation, which may favor engraftment and diminish the flushing out of transplanted cells, are responsible for this effect. However, in the mid and long terms (5 days and 12–15 weeks), NIS[pos]-hiPSCs could be detected exclusively at the site of coinjection, indicating an additional profound effect on long-term engraftment of NIS[pos]-hiPSCs. Certainly, deciphering the underlying mechanisms will require extensive additional investigations but will be of utmost importance to optimize MSC-supported survival of hiPSC derivatives.

Conclusions

This is the first study demonstrating the usefulness of the NIS for serial long-term tracking of survival, engraftment, and distribution of cellular grafts in a large-animal model in which SPECT/CT imaging was used. Moreover, for the first time we demonstrate long-term survival and differentiation of

hiPSCs in a preclinical pig model of myocardial infarction. The applied 3-dimensional hybrid imaging protocol enables combined assessment of cardiac anatomy and myocardial perfusion and monitoring of donor cell survival, proliferation, and distribution within 1 imaging modality.

Disclosures

None.

References

1. Haase A, Olmer R, Schwanke K, Wunderlich S, Merkert S, Hess C, Zweigerdt R, Gruh I, Meyer J, Wagner S, Maier LS, Han DW, Glage S, Miller K, Fischer P, Scholer HR, Martin U. Generation of induced pluripotent stem cells from human cord blood. *Cell Stem Cell*. 2009;5:434–441.
2. Mauritz C, Martens A, Rojas SV, Schnick T, Rathert C, Schecker N, Menke S, Glage S, Zweigerdt R, Haverich A, Martin U, Kutschka I. Induced pluripotent stem cell (iPSC)-derived flk-1 progenitor cells engraft, differentiate, and improve heart function in a mouse model of acute myocardial infarction. *Eur Heart J*. 2011;32:2634–2641.
3. Mauritz C, Schwanke K, Reppel M, Neef S, Katsirntaki K, Maier LS, Nguemo F, Menke S, Haustein M, Hescheler J, Hasenfuss G, Martin U. Generation of functional murine cardiac myocytes from induced pluripotent stem cells. *Circulation*. 2008;118:507–517.
4. Zhang SJ, Wu JC. Comparison of imaging techniques for tracking cardiac stem cell therapy. *J Nucl Med*. 2007;48:1916–1919.
5. Olmer R, Haase A, Merkert S, Cui W, Palecek J, Ran C, Kirschning A, Scheper T, Glage S, Miller K, Curnow EC, Hayes ES, Martin U. Long term expansion of undifferentiated human iPS and ES cells in suspension culture using a defined medium. *Stem Cell Res*. 2010;5:51–64.
6. Zweigerdt R, Olmer R, Singh H, Haverich A, Martin U. Scalable expansion of human pluripotent stem cells in suspension culture. *Nat Protoc*. 2011;6:689–700.
7. Murry CE, Keller G. Differentiation of embryonic stem cells to clinically relevant populations: lessons from embryonic development. *Cell*. 2008;132:661–680.
8. Laflamme MA, Chen KY, Naumova AV, Muskheli V, Fugate JA, Dupras SK, Reinecke H, Xu C, Hassanipour M, Police S, O'Sullivan C, Collins L, Chen Y, Minami E, Gill EA, Ueno S, Yuan C, Gold J, Murry CE. Cardiomyocytes derived from human embryonic stem cells in pro-survival factors enhance function of infarcted rat hearts. *Nat Biotechnol*. 2007;25:1015–1024.
9. Muller-Ehmsen J, Krausgrill B, Burst V, Schenk K, Neisen UC, Fries JW, Fleischmann BK, Hescheler J, Schwinger RH. Effective engraftment but poor mid-term persistence of mononuclear and mesenchymal bone marrow cells in acute and chronic rat myocardial infarction. *J Mol Cell Cardiol*. 2006;41:876–884.
10. Teng CJ, Luo J, Chiu RC, Shum-Tim D. Massive mechanical loss of microspheres with direct intramyocardial injection in the beating heart: implications for cellular cardiomyoplasty. *J Thorac Cardiovasc Surg*. 2006;132:628–632.
11. van Laake LW, Passier R, Doevendans PA, Mummery CL. Human embryonic stem cell-derived cardiomyocytes and cardiac repair in rodents. *Circ Res*. 2008;102:1008–1010.
12. Templin C, Luscher TF, Landmesser U. Cell-based cardiovascular repair and regeneration in acute myocardial infarction and chronic ischemic cardiomyopathy-current status and future developments. *Int J Dev Biol*. 2011;55:407–417.
13. Gandolfi F, Vanelli A, Pennarossa G, Rahaman M, Acocella F, Brevini TA. Large animal models for cardiac stem cell therapies. *Theriogenology*. 2011;75:1416–1425.
14. Bengel FM, Schachinger V, Dimmeler S. Cell-based therapies and imaging in cardiology. *Eur J Nucl Med Mol Imaging*. 2005;32(suppl 2):S404–S416.
15. de Almeida PE, van Rappard JR, Wu JC. In vivo bioluminescence for tracking cell fate and function. *Am J Physiol*. 2011;301:H663–H671.
16. Ruggiero A, Thorek DL, Guenoun J, Krestin GP, Bernsen MR. Cell tracking in cardiac repair: what to image and how to image. *Eur Radiol*. 2012;22:189–204.
17. Lee AS, Xu D, Plews JR, Nguyen PK, Nag D, Lyons JK, Han L, Hu S, Lan F, Liu J, Huang M, Narsinh KH, Long CT, de Almeida PE, Levi B, Kooreman N, Bangs C, Pacharinsak C, Ikeno F, Yeung AC, Gambhir SS, Robbins RC, Longaker MT, Wu JC. Preclinical derivation and imaging of autologously transplanted canine induced pluripotent stem cells. *J Biol Chem*. 2011;286:32697–32704.
18. Willmann JK, Paulmurugan R, Rodriguez-Porcel M, Stein W, Brinton TJ, Connolly AJ, Nielsen CH, Lutz AM, Lyons J, Ikeno F, Suzuki Y, Rosenberg J, Chen IY, Wu JC, Yeung AC, Yock P, Robbins RC, Gambhir SS. Imaging gene expression in human mesenchymal stem cells: from small to large animals. *Radiology*. 2009;252:117–127.
19. Terrovitis J, Kwok KF, Lautamaki R, Engles JM, Barth AS, Kizana E, Miake J, Leppo MK, Fox J, Seidel J, Pomper M, Wahl RL, Tsui B, Bengel F, Marban E, Abraham MR. Ectopic expression of the sodium-iodide symporter enables imaging of transplanted cardiac stem cells in vivo by single-photon emission computed tomography or positron emission tomography. *J Am Coll Cardiol*. 2008;52:1652–1660.
20. Dohan O, De la Vieja A, Paroder V, Riedel C, Artani M, Reed M, Ginter CS, Carrasco N. The sodium/iodide symporter (NIS): characterization, regulation, and medical significance. *Endocr Rev*. 2003;24:48–77.
21. Stodilka RZ, Blackwood KJ, Kong H, Prato FS. A method for quantitative cell tracking using SPECT for the evaluation of myocardial stem cell therapy. *Nucl Med Commun*. 2006;27:807–813.
22. Gyongyosi M, Dib N. Diagnostic and prognostic value of 3D NOGA mapping in ischemic heart disease. *Nat Rev Cardiol*. 2011;8:393–404.
23. Buechel RR, Husmann L, Herzog BA, Pazhenkottil AP, Nkoulou R, Ghadri JR, Treyer V, von Schulthess P, Kaufmann PA. Low-dose computed tomography coronary angiography with prospective electrocardiogram triggering: feasibility in a large population. *J Am Coll Cardiol*. 2011;57:332–336.
24. Buechel RR, Herzog BA, Husmann L, Burger IA, Pazhenkottil AP, Treyer V, Valenta I, von Schulthess P, Nkoulou R, Wyss CA, Kaufmann PA. Ultrafast nuclear myocardial perfusion imaging on a new gamma camera with semiconductor detector technique: first clinical validation. *Eur J Nucl Med Mol Imaging*. 2010;37:773–778.
25. Herzog BA, Buechel RR, Husmann L, Pazhenkottil AP, Burger IA, Wolfrum M, Nkoulou RN, Valenta I, Ghadri JR, Treyer V, Kaufmann PA. Validation of CT attenuation correction for high-speed myocardial perfusion imaging using a novel cadmium-zinc-telluride detector technique. *J Nucl Med*. 2010;51:1539–1544.
26. Xu XQ, Zweigerdt R, Soo SY, Ngoh ZX, Tham SC, Wang ST, Graichen R, Davidson B, Colman A, Sun W. Highly enriched cardiomyocytes from human embryonic stem cells. *Cytotherapy*. 2008;10:376–389.
27. Wai LE, Fujiki M, Takeda S, Martinez OM, Krams SM. Rapamycin, but not cyclosporine or fk506, alters natural killer cell function. *Transplantation*. 2008;85:145–149.
28. Drukker M, Benvenisty N. The immunogenicity of human embryonic stem-derived cells. *Trends Biotechnol*. 2004;22:136–141.
29. Chiossone L, Vitale C, Cottalasso F, Moretti S, Azzarone B, Moretta L, Mingari MC. Molecular analysis of the methylprednisolone-mediated inhibition of NK-cell function: evidence for different susceptibility of IL-2- versus IL-15-activated NK cells. *Blood*. 2007;109:3767–3775.
30. Xu XQ, Soo SY, Sun W, Zweigerdt R. Global expression profile of highly enriched cardiomyocytes derived from human embryonic stem cells. *Stem Cells*. 2009;27:2163–2174.
31. Hockemeyer D, Wang H, Kiani S, Lai CS, Gao Q, Cassady JP, Cost GJ, Zhang L, Santiago Y, Miller JC, Zeitler B, Cherone JM, Meng X, Hinkley

SJ, Rebar EJ, Gregory PD, Urnov FD, Jaenisch R. Genetic engineering of human pluripotent cells using TALE nucleases. *Nat Biotechnol*. 2011;29: 731–734.

32. Al Kindi A, Ge Y, Shum-Tim D, Chiu RC. Cellular cardiomyoplasty: routes of cell delivery and retention. *Front Biosci*. 2008;13: 2421–2434.

33. Wen Z, Zheng S, Zhou C, Wang J, Wang T. Repair mechanisms of bone marrow mesenchymal stem cells in myocardial infarction. *J Cell Mol Med*. 2011;15:1032–1043.

34. Shi M, Liu ZW, Wang FS. Immunomodulatory properties and therapeutic application of mesenchymal stem cells. *Clin Exp Immunol*. 2011;164: 1–8.

CLINICAL PERSPECTIVE

Cardiac cell replacement therapies may significantly extend current therapeutic options for various cardiac diseases. The recently developed induced pluripotent stem cells are considered a major breakthrough with respect to the development of novel regenerative therapies and combine the advantages of adult and embryonic stem cells, namely, the availability of an autologous, ethically nonproblematic cell source with high potential for proliferation and differentiation into all cell lineages of interest. However, evaluation of novel cellular therapies in preclinical large-animal models and patients is currently hampered by the lack of suitable imaging approaches that allow long-term monitoring of viable transplanted cells. The present study was therefore designed to evaluate sodium iodide symporter transgene imaging as a novel approach to follow human induced pluripotent stem cell derivatives in a pig model of myocardial infarction. For the first time, our study demonstrates the usefulness of a sodium iodide symporter transgene for longitudinal in vivo tracking of survival, engraftment, and distribution of cellular grafts in a large-animal model with the use of single photon emission tomographic/computed tomographic imaging. Moreover, for the first time we demonstrate long-term survival and differentiation of human induced pluripotent stem cells in a preclinical pig model of myocardial infarction. The applied 3-dimensional hybrid imaging protocol enables combined assessment of cardiac anatomy and myocardial perfusion and monitoring of donor cell survival, proliferation, and distribution within 1 imaging modality. The developed approach will contribute to further optimization of novel cardiovascular cell–based treatment strategies and is of utmost importance for careful in vivo monitoring of associated risks such as potential tumor or teratoma formation.

SUPPLEMENTAL MATERIAL

Supplemental Methods

Isolation, culture and characterisation of human MSCs

MSCs were isolated from human umbilical cord as previously described.[1] Large scale expansion was performed to produce sufficient cell numbers for large animal experimentation (i.e., > 1 x 10^8 per cord).[2] MSC purity of > 95%, and typical immune phenotype were confirmed by flow cytometry (**Supplemental Figure 11**) and aliquots of 1 x 10^7 – 2 x 10^8 MSCs per aliquot were cryopreserved until further use as described.[3]

Construction of the reporter plasmid pCAG_rNIS_IRES2_Venus_nucmem

For generation of transgenic hiPSC lines, a bicistronic vector pCAG_rNIS_IRES2_Venus_nucmem (**Figure 1A**) was constructed. The vector (size: 8287 bp) contains the rat sodium iodide symporter (NIS) cDNA driven by the ubiquitous chicken β-actin (CAG) promoter and Venus_nucmem, a yellow variant of green fluorescent protein coupled to a nuclear membrane localization signal,[4] also under control of the CAG promoter via an internal ribosomal entry site (IRES2).

The vector was constructed as follows: The rNIS was cloned from pDF202 via Eco RI / Xho I into pCAGGS2.[5] The fluorescence reporter gene eGFP was deleted from the vector backbone and replaced by the IRES2_Venus_nucmem fragment from pCAG_IRES2_Venus_nucmem (Venus nucmem was a kind gift from Timm Schröder, Munich) by Xho I /Bgl II digestion.

Generation of hiPSC lines transgenic for the sodium-iodide symporter

Stably NIS expressing double transgenic hiPSC lines were generated by transfecting 1.5 x 10^6 hiPSCs (Clone hCBiPS2)[6] with αMHCneoPGKhygro and pCAG_rNIS_IRES2_Venus_nucmem in equimolar amounts using the Neon™ transfection

1

system (Invitrogen). The vector αMHCneoPGKhygro was a kind gift from Loren Field (Indianapolis, USA). αMHCneoPGKhygro is a 10.9 kb construct carrying two selection cassettes: 1st. The hygromycin resistance gene controlled under the ubiquitously expressed phosphoglycerate kinase (PGK) promoter allowing for the establishment of stable integrants, and 2nd the neomycin resistance gene under the control of the heart-specific alpha myosin heavy chain (αMHC) promoter, allowing the selection of stem cell-derived cardiomyocytes. 72 hours after transfection stable integrants were selected by the addition of 200 µg / ml Hygromycin. Upcoming Hygromycin-resistant Venus[pos] colonies were manually picked 14 days after electroporation, transferred onto irradiated feeder cells and expanded clonally.

Analysis of NIS expression through quantitative reverse transcriptase real time PCR

For quantitative real-time PCR total RNA was prepared using the RNeasy Kit (Macherey-Nagel, Düren, Germany) and reverse transcribed with Superscript II (Invitrogen) using oligo dT primers according to manufacturer's instructions. qRT-PCR was performed in triplicate using a Mastercycler® ep *relaplex²* (Eppendorf, Hamburg, Germany) and the Absolute™ QPCR SYBR® Green Mix (ABgene, Epsom, Surrey, UK). The size of amplicons and absence of nonspecific products were controlled by melting curves. The relative changes in gene expression were analyzed via $2^{-\Delta\Delta Ct}$ in comparing the reporter gene expressing group related to the non-transgenic hiPSC clones in pluripotent as well as differentiating cells using Mastercycler® ep realplex Software Version 2.0 (Eppendorf). Expression levels of target genes were normalized to β-actin transcript levels. Data are given as mean ± SEM of normalized gene expression levels from three experiments.

Characterization of NIS[pos]-hiPSCs

Established transgenic clones were analysed for the expression of typical pluripotency markers via immunfluorescence staining and semi-quantitative RT-PCR. RT-PCR was also used to test for the full integrity of the selection plasmid αMHCneoPGKhygro. The stable expression of the fluorescence reporter gene Venus was monitored by flow cytometry, the

expression of the rNIS transgene was assessed via quantitative real time PCR (qRT-PCR) up to 23 passages in undifferentiated as well as in differentiating cells.

For flow cytometry, cells were washed once with Phosphate Buffered Saline (PBS) w/o Ca^{2+}/Mg^{2+} and trypsinized for three minutes at 37 °C to create a single-cell suspension 72 h post transfection. After centrifugation, cells were resuspended in PBS and stored on ice until analysis. Acquisition was performed on a FACSCalibur system (BD Biosience, USA) and the samples were analysed using BD CellQuest software (BD Biosience, USA). 25.000 cells were analysed per sample. Undifferentiated non-transgenic and differentiated non-transgenic hiPSCs served as controls for autofluorescence as well as for forward scatter (FSC) and side scatter (SSC) range.

Differentiation of hiPSCs and immunostaining of embryoid body sections

Embryoid Body (EB)-based differentiation was induced as previously described.[6] For immunhistological analysis EBs were harvested on day 21 of differentiation, washed once with PBS w/o Ca^{2+} and Mg^{2+}, embedded within OCT and stored at -80°C. Subsequently 10µm sections were generated using a microm cryostar HM 560 (Thermo Scientific, Waltham, Massachusetts, USA). Immunhistological stainings were performed as described in[7]. In brief, cryosections were fixed using 4% paraformaldehyde for 15 minutes at room temperatures followed by blocking with 5% donkey serum and 0,25% Triton X-100 (Sigma-Aldrich, Steinheim, Germany) diluted in Tris-buffered saline for 20 minutes at room temperature. Cryosections were incubated for 1 hour with primary antibodies (1:100 anti-CD31 mouse IgG, DAKO, Glostrup, Denmark, 1:100 anti-GFP goat IgG, Acris, Herford, Germany) at room temperature diluted in PBS w/o Ca^{2+} / Mg^{2+} with 1% bovine serum albumin, then rinsed 3 times with PBS w/o Ca^{2+} / Mg^{2+} and were subsequently incubated with secondary antibodies (donkey anti-mouse IgG DyLight®549-labeled, 1:200, and donkey anti-goat IgG Cy3-labeled, 1:100, both Jackson Immunoresearch Laboratories) for 30 minutes at room temperature. Afterwards cryosections were washed with PBS w/o Ca^{2+} / Mg^{2+},

3

counterstained with DAPI (Sigma-Aldrich) and analysed using an Axio Observer A1 fluorescence microscope (Zeiss, Göttingen, Germany).

Iodide uptake and efflux

Uptake: 1.5×10^6 cells / ml in growth medium were incubated with ^{125}I (5×10^5 cpm / ml) in a 50 ml Falcon tube at 37 ºC for the indicated time points. 100 µM perchlorate was added to block the iodine uptake. At each time point 1 ml cell suspension was washed rigorously and cell-bound radioactivity was counted in a gamma counter. All time points were performed in triplicates.

Efflux: After one hour of incubation with ^{125}I, half of the cells were thoroughly washed and resuspended in medium without iodine. Iodine activity in NIS^{pos}-hiPSCs was measured at different time points after removal of medium. The total cell bound radioactivity present at the initiation of the efflux measurements was considered as 100 %. Each time point was evaluated in triplicates.

Coculture experiments and Apoptosis Assay

Based on the hypothesis that MSCs have the potential to reduce apoptosis of iPSCs under hypoxic conditions coculture experiments were performed in order to test whether factors secreted by MSCs or direct cell-to-cell contact between MSCs and iPSCs can rescue iPSCs from apoptosis. MSCs were cultured as described with minor modifications.[1] In brief, MSC supernatants were obtained from cultures of confluent MSCs maintained under hypoxia (1% O$_2$) in alpha-modified minimum essential medium (α-MEM) supplemented with 1% pooled human platelet lysate (pHPL) for one week. The secreted factor-conditioned medium was harvested and filtered (0.22µm, Millipore) to remove cells and cell-derived particles. Separate cultures of two independent human umbilical cord-derived MSC lines (UC0069 and UC0084) were grown to confluence under regular ambient air oxygen conditions until confluent in 75 cm2 tissue culture flasks (vented cap; Corning). Six million iPSCs each were seeded on top of the MSCs. Equal aliquots were resuspended in freshly prepared a-MEM/10% pHPL or

4

MSC-conditioned medium. All cultures were maintained for 24h at 37°C under humidified 1% O_2 conditions. Cells were harvested after detachment with TrypLE (Invitrogen) for 3 minutes at 37°C, transferred on ice immediately and nonspecific antibody binding was blocked by adding 10% v/v normal sheep serum. AnnexinV-APC staining and 7-aminoactinomycin (7AAD) counterstaining was performed in Ca^{++}/Mg^{++}-containing buffer following manufacturers' instructions (BD Pharmingen) using titrated reagent concentration optimized for the target cells. MSCs and iPSCs were separated by their physical parameters (forward and sideward light scattering) combined with Venus fluorescence at 488nm excitation and 525 nm emission wavelengths together with Annexin-V-APC and 7AAD fluorescence using a Navios flow cytometer (Coulter). Data were analysed after doublet discrimination in a time of flight analysis using the Kaluza software (Coulter). Results were obtained from three analyses with two independent MSC donors for all different culture conditions. The percentage of apoptotic (Annexin-V-positive and 7AAD negative) iPSCs was determined and mean as well as standard deviation was determined before statistical analysis.

Induction of myocardial infarction

All interventional procedures were performed under general anaesthesia and electrocardiographic monitoring. Animals were pre-medicated with ketamine (5 - 10 mg / kg body weight), azaperone (2 - 3 mg / kg body weight) and atropine 0.1 % (0.02 - 0.05 mg / kg body weight) intramusculary. To facilitate intubation, anaesthesia was deepened with isoflurane 3 % and oxygen was given through a mask. Two venous ear catheters and one arterious tail catheter were placed. After intubation, anaesthesia was maintained with 1% isoflurane and oxygen at 1l / min and propofol was given as a constant infusion rate (1 mg / kg / h). At the beginning of the intervention animals received heparin (150 IE / kg body weight). A guiding catheter was placed into the sheath of the right carotid artery and advanced under fluoroscopic guidance (Siemens Multistar) into the left coronary arteries. After placement of the guide catheter, a 0.014" guidewire was used to deliver a 2.5 / 9 mm balloon catheter (8 atm) into the mid segment of the left ascending coronary artery. After

5

positioning of the balloon catheter, 300 mg of lidocain followed by 100 mg / h (intravenous) were administered. Myocardial infarction was created by inflating the balloon for 180 min, followed by reperfusion. Every 15 - 30 min a small amount of contrast was applied to check balloon inflation. The animals were treated with antibiotics (baytril 10 %) and analgesics (buprenorphrine, 0.3 mg).

Termination and organ harvest

For termination animals were sacrificed after anaesthesia was induced as described above (induction of myocardial infarction). A venous ear catheter was placed and the anaesthesia was deepened with propofol (3 mg / kg body weight). Afterwards animals were euthanized with 0.3 ml / kg body weight potassium chloride 15 %. For the explantation of the heart the body was placed in right lateral recumbency. In this position the heart was explanted by performing a left lateral thoracotomy.

Histological analysis

The coronary arteries were perfused with 100 ml 2 % paraformaldehyde. The fixed heart was sliced into 3 pieces according to the injection sites and photographed. Afterwards, heart pieces were incubated for 5 h in 2 % paraformaldehyde before they were washed in 15 % saccharose for 1 h. All tissue samples were stored at -20 °C in 70 % alcohol. The organs were embedded in paraffin and cut into 2 - 3 μm sections. One HE-staining was performed and for immunohistochemistry stainings, serially cut unstained sections on positive charged slides were rehydrated in 100 %, 95 %, and 70 % ethanol after deparaffinization with xylene. Afterwards the slides were rinsed in tap water and counterstained for 3 to 4 minutes in hemalum. Endogenous peroxidase was inactivated with 3 % H_2O_2 and a protein block (DAKO, Hamburg, Germany, Protein-Block Serum-Free Ready to Use, X0909) was applied for 10 min at room temperature (RT). An antigen retrieval with citrate puffer (DAKO REAL, Target Retrieval Solution, S2031, ph6) for 20 min in the microwave was used.

6

Following primary antibodies were used: Rabbit anti GFP (Green Fluorescence Protein, Abcam, Cambridge, UK, ab6556; this antibody also detects the Venus derivative of GFP), Mouse anti OCT4 (C-10, sc-5279, Santa Cruz Biotechnology, Heidelberg, Germany), and Rabbit anti von Willebrand Factor (Factor VIII-related antigen) (DAKO, N150587). The anti GFP antibody was applied over night at RT at a dilution of 1 : 150, the OCT4 antibody was incubated at a dilution of 1 : 10 for 1 h at 37 °C. The slides for Factor VIII immunostaining were pretreated with Proteinase K (DAKO REAL™ Proteinase K S2019 40x) for 5 min at RT prior to incubation with the prediluted anti human von Willebrand Factor antibody for 1 hour at RT.

As secondary antibody the EnVision anti rabbit (DAKO, K4003), the Detection System (DAKO, K5003) and the Ms OUM Kit (Roche) was applied. As chromogen, 3-amino-9-ethylcarbazole (AEC, Invitrogen, 00-2007) was used. In between all steps the slides were washed thoroughly.

Whole body SPECT imaging

Whole body scans requiring a large field of view for assessing extracardiac activity were acquired on a dual-head camera (Infina, GE, Healthcare). All data were transferred to a dedicated workstation (Xeleris 2.1, GE Healthcare) for analysis and interpretation. An additional workstation (Advantage Workstation 4.3, GE Healthcare) served for imaging fusion of nuclear imaging and CCTA using CardIQ Fusion software package (GE Healthcare) as previously described and extensively validated.[8]

Quantification of graft-associated ¹²³I signals

The measurement of tracer uptake in the transplanted area (septal and lateral wall) was performed by volume of interest (VOI) Competitive Analysis Tool (Xeleris 2.1, GE - Healthcare) analysis after placing a VOI on the injection areas. A reference VOI (same size) from a remote territory was used for background correction.

7

Radiotoxicity of Iodide

10^6 NIS[pos]-hiPSCs were seeded in 6 well plates and incubated in the presence of 3µCi ^{125}I. After 2h cells were washed and further cultivated in culture medium without ^{125}I. The proportion of trypan blue^{pos} dead cells was determined after 24, 48, 120 and 144 hours. Non-transgenic hiPSCs as well as hiPSCs without ^{125}I treatment were used as control.
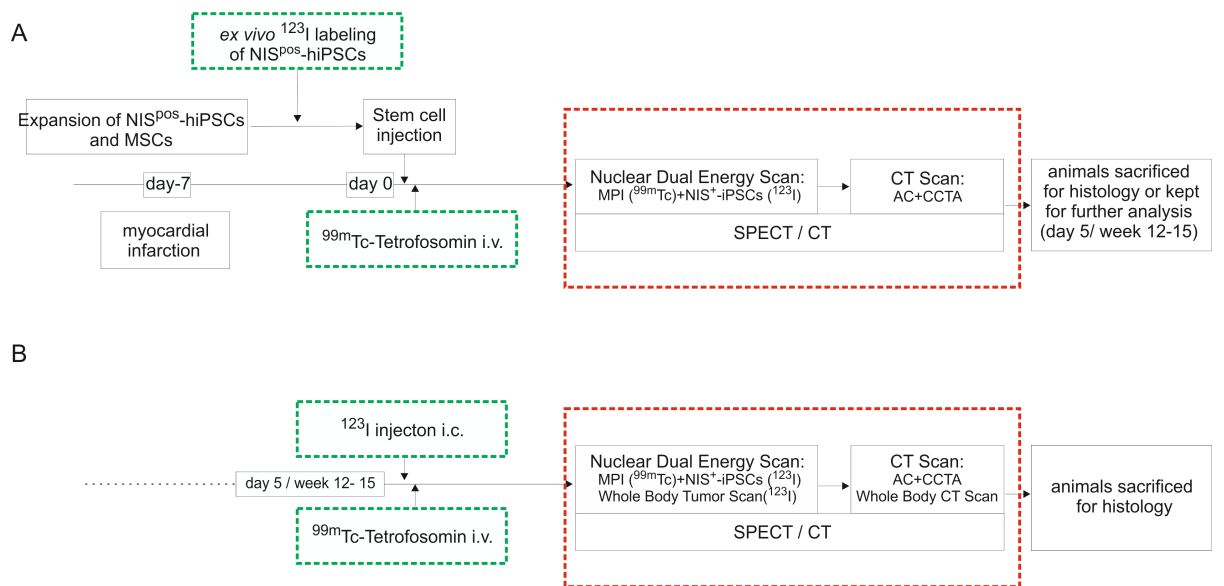
Supplemental Table

Supplemental Table 1: Comparative semiquantitative assessment of ^{123}I signal intensities and histologically detectable intramyocardial Venus[pos] NIS-hiPSC derivatives.

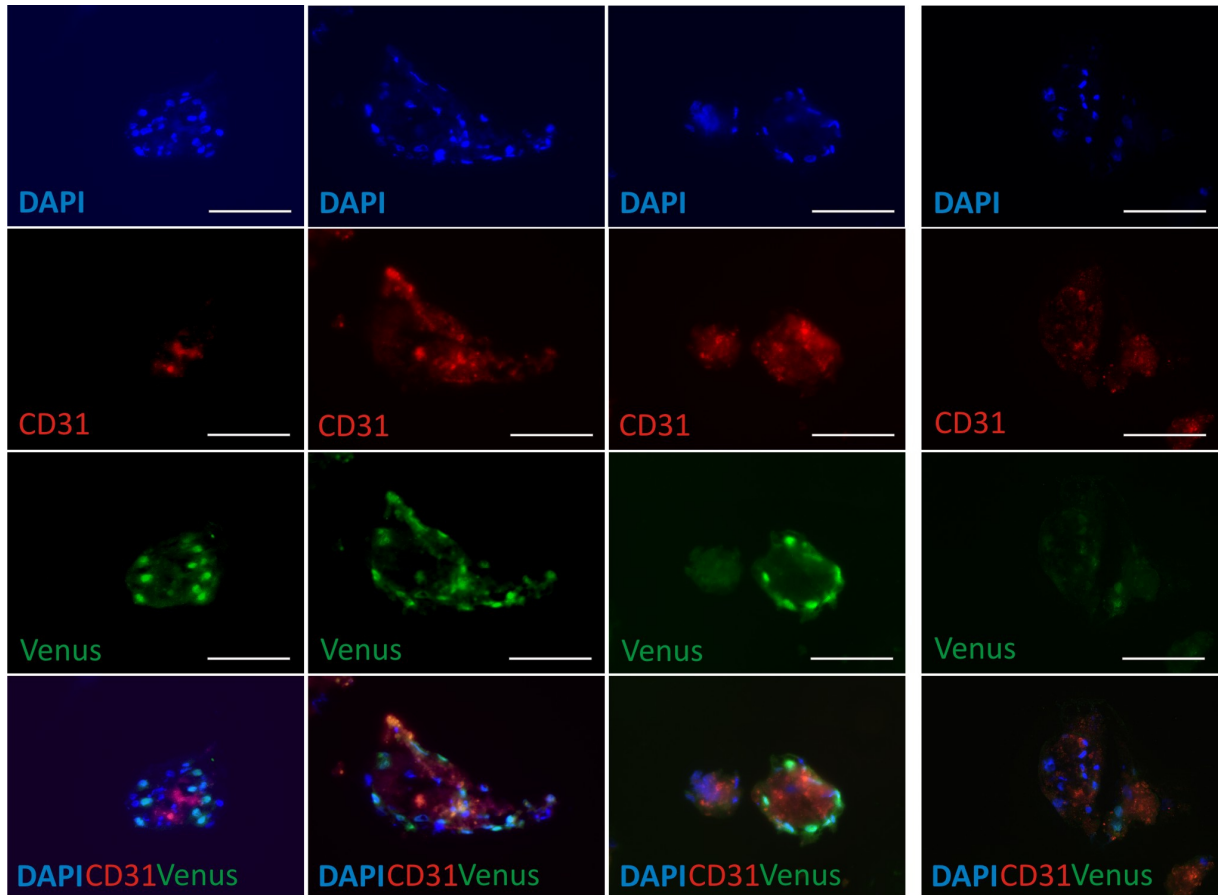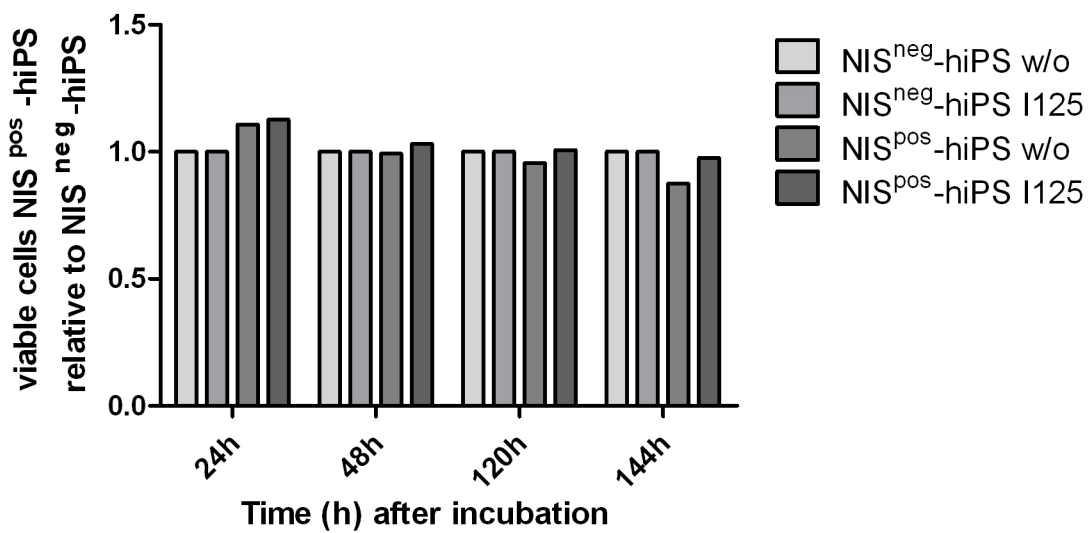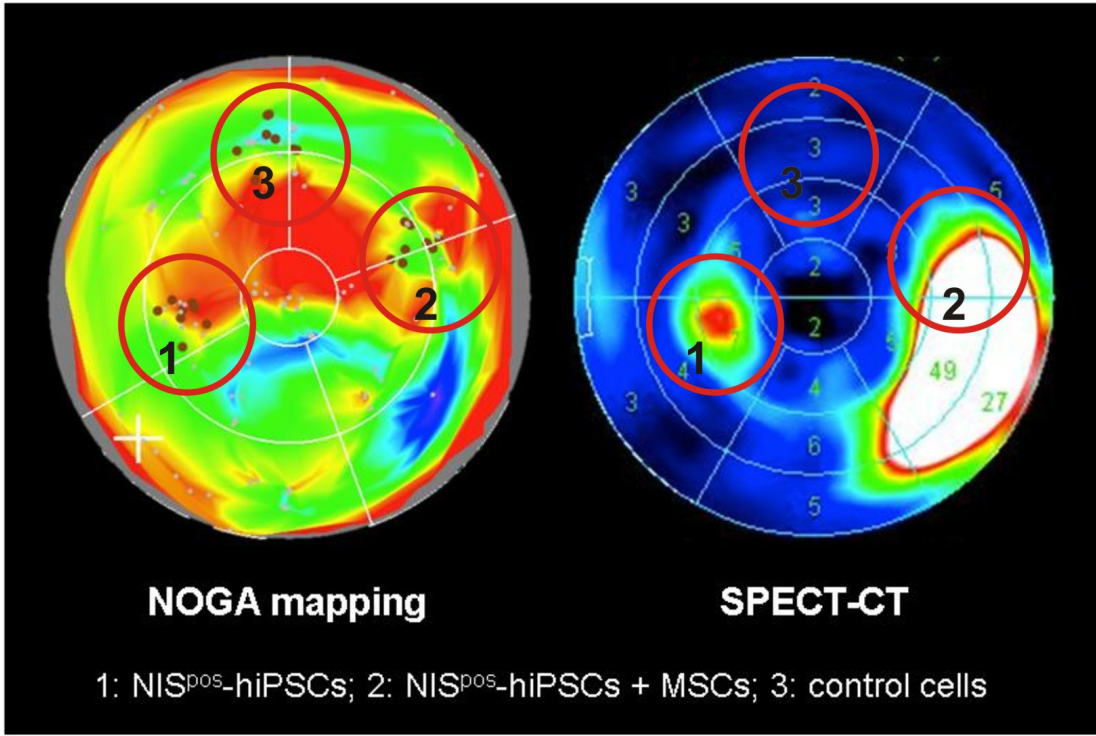|	Day 1		Day 5		Week 12-15	
	SPECT (^{123}I signal)	Histology (Venus^{pos} cells)	SPECT (^{123}I signal)	Histology (Venus^{pos} cells)	SPECT (^{123}I signal)	Histology (Venus^{pos} cells)
Control cells	-	-	-	-	-	-
iPSCs	++	++	-	-	-	-
iPSCs + MSCs	+++	++	+	+	+	+

Supplemental Figures

Supplemental Figure 1

A

ex vivo ^{123}I labeling
of NIS^{pos}-hiPSCs

Expansion of NIS^{pos}-hiPSCs
and MSCs

Stem cell
injection

day-7   day 0

myocardial
infarction

^{99m}Tc-Tetrofosomin i.v.

Nuclear Dual Energy Scan:
MPI (^{99m}Tc)+NIS$^+$-iPSCs (^{123}I)

CT Scan:
AC+CCTA

SPECT / CT

animals sacrificed
for histology or kept
for further analysis
(day 5/ week 12-15)

B

^{123}I injecton i.c.

day 5 / week 12- 15

^{99m}Tc-Tetrofosomin i.v.

Nuclear Dual Energy Scan:
MPI (^{99m}Tc)+NIS$^+$-iPSCs (^{123}I)
Whole Body Tumor Scan(^{123}I)

CT Scan:
AC+CCTA
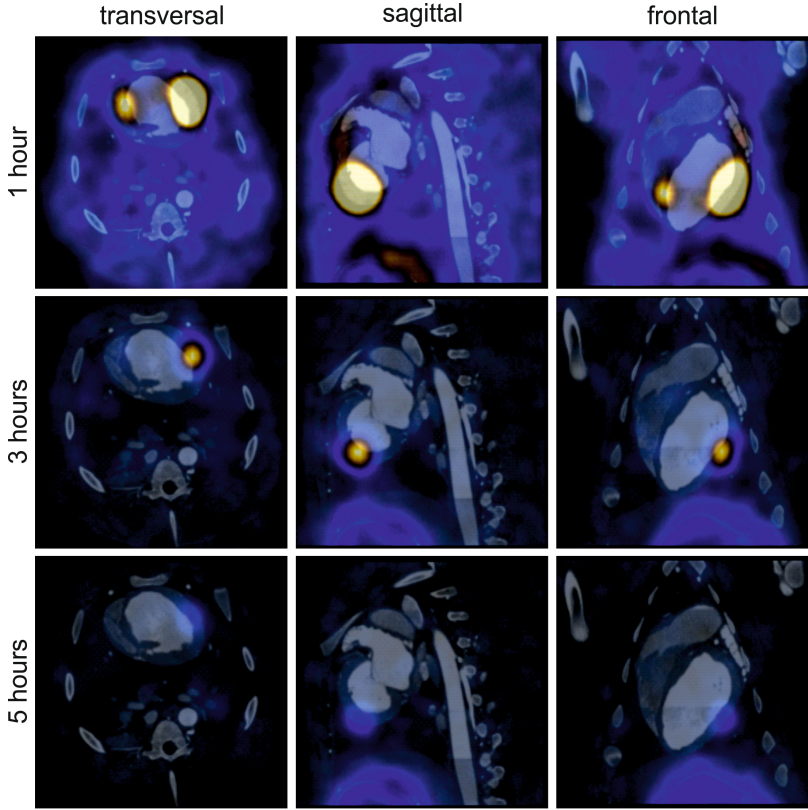Whole Body CT Scan

SPECT / CT

animals sacrificed
for histology

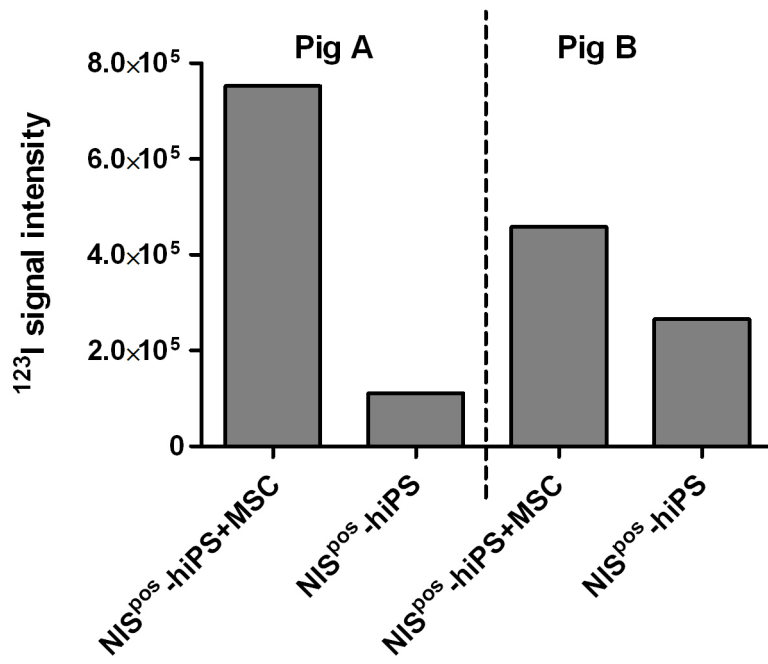Supplemental Figure 2

9

Supplemental Figure 3

Supplemental Figure 4

NOGA mapping   SPECT-CT

1: NIS^pos-hiPSCs; 2: NIS^pos-hiPSCs + MSCs; 3: control cells

Supplemental Figure 5

transversal   sagittal   frontal

1 hour

3 hours

5 hours

Supplementary Figure 6

Supplemental Figure 7

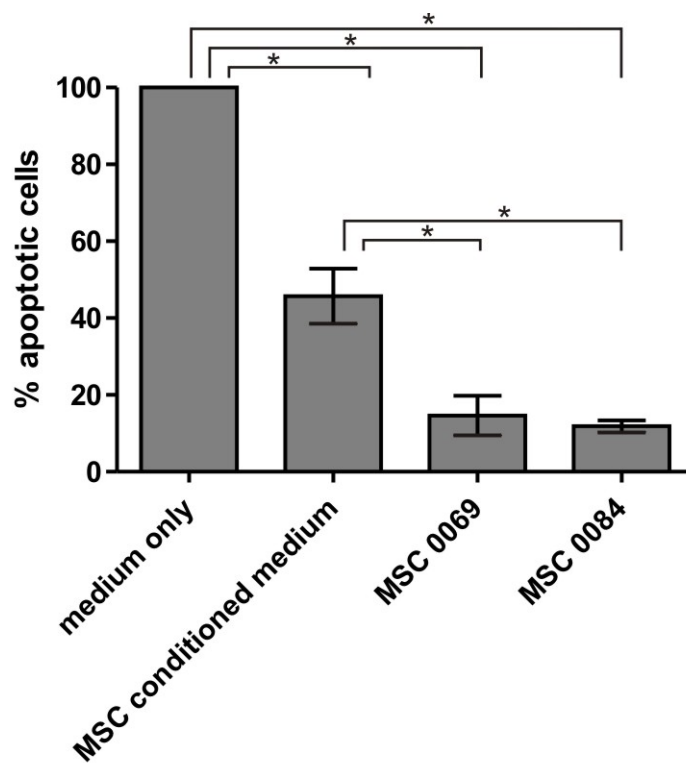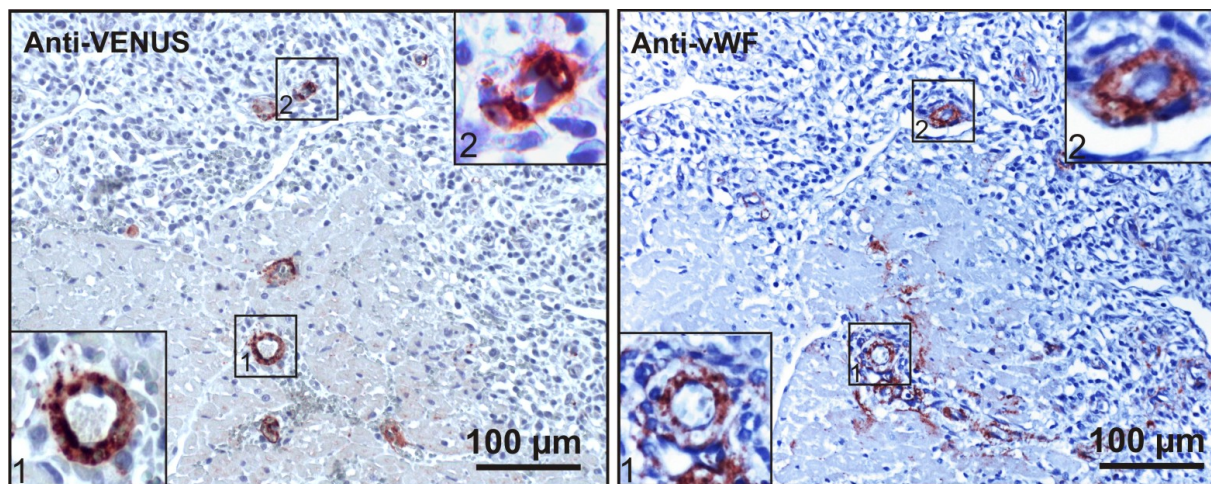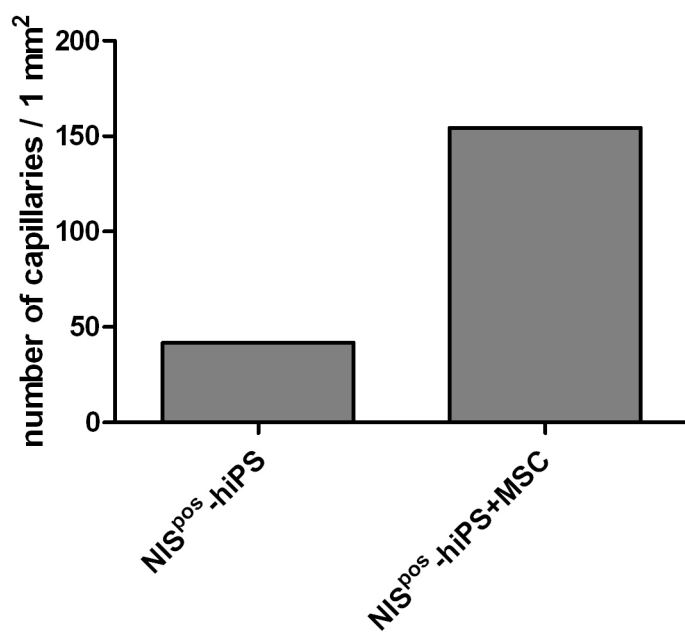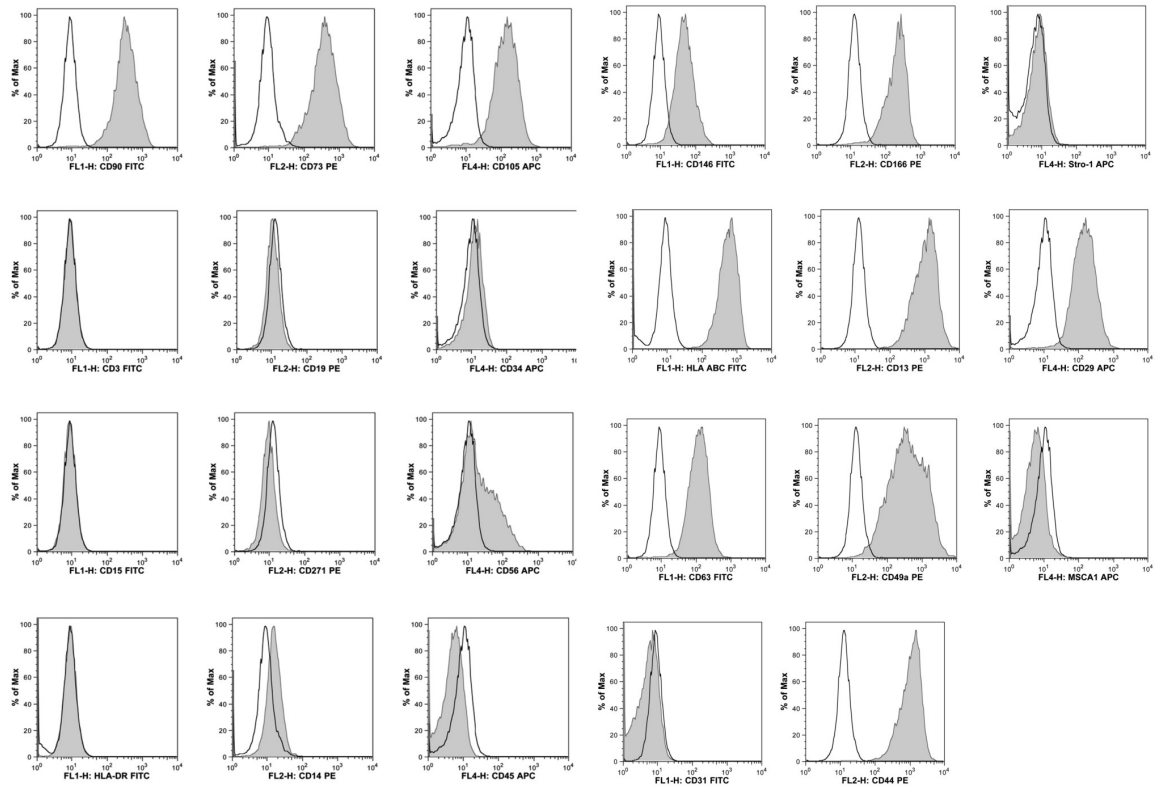Supplemental Figure 8

12

Supplemental Figure 9

Supplemental Figure 10

13

Supplemental Figure 11

Supplemental Figure Legends

Supplemental Figure 1: Fluorosphere-based intramyocardial fluorescence is macroscopically visible and enables the localisation of intramyocardial cell injection sites under UV light.

Injection sites are marked by white arrows.

Supplemental Figure 2: Schematic overview on the imaging protocol.

(A) Imaging of *ex vivo* labeled iPSCs combined with myocardial perfusion imaging followed by CT scan on day 1.

(B) Follow up imaging with identical protocol after intracoronary injection of ^{123}I for *in vivo* iPSC labeling. A complementary whole body nuclear and CT tumor scan were added.

AC = attenuation correction, CCTA = coronary computed tomography angiography, hiPSCs = human induced pluripotent stem cells, MPI = myocardial perfusion imaging, MSCs = mesenchymal stem cells.

Supplemental Figure 3: *In vitro* differentiation of NIS-hiPSCs into endothelial cells and maintainance of transgene expression.

Venus expression could be detected in CD31^{pos} endothelial NIS-hiPSC-derivatives after *in vitro* differentiation. Notably, as exemplarily depicted on the right hand, not all CD31^{pos} endothelial NIS-hiPSC-colonies showed continued transgene expression indicating partial silencing of the transgenes during differentiation.

Supplemental Figure 4: Tracer loading and NIS expression does not diminish the viability of NIS expressing iPS cells.

NIS^pos-hiPSCs as well as NIS^neg-hiPSCs were incubated in the presence of ^{125}I for 2h. The proportion of trypan blue^pos dead cells was determined after 24, 48, 120 and 144 hours. Mock-treated hiPSCs were used as control.

Supplemental Figure 5: Magnified images of the polar plots of NOGA map and ^{123}I SPECT-CT.

Representative polar plots of a heart of one animal that was sacrificed 6 h after cell injection is shown.

Left side: NOGA™ mapping of the left ventricle recorded during cell injection. NOGA™ colours represent unipolar voltage values, red = scar, green to blue = viable tissue. Cell injection sites in the septal (hiPSCs; 1), lateral (hiPSCs + MSCs; 2), and anterior (control cells; 3) walls are shown as brown dots.

Right side: SPECT-CT imaging of left ventricle 1 h after catheter-based intramyocardial cell injection demonstrating intense ^{123}I signals (white/red/yellow/green) in the lateral and septal wall that correspond exactly to the injection sites of iPSCs (1) and iPSCs+MSCs (2) as recorded by NOGA™ mapping; control cells (3) did not result in a detectable radiotracer signal.

Supplemental Figure 6: SPECT-CT imaging of transplanted ^{123}I-pre-labelled NIS^pos-hiPSCs demonstrates major loss of ^{123}I signals within 5 hours after myocardial injection

SPECT-CT images (transversal, sagittal and frontal views) of a pig heart *in vivo* 1, 3 and 5 hours after cell transplantation are shown. In the transversal and frontal views, two ^{123}I signals were detected; the brighter one represents ^{123}I pre-labelled hiPSCs co-transplanted with human MSCs, the dimmer signal ^{123}I pre-labelled hiPSCs injected without MSCs.

Supplemental Figure 7: ^{123}I signal intensities at the injection sites in two pigs sacrificed after day 1 follow up.

16

The measurement of tracer uptake at the injection sites (septal and lateral wall) was performed by volume of interest (VOI) analysis. A reference VOI from a remote territory was used for background correction.

Supplemental Figure 8: MSCs can reduce iPSC apoptosis *in vitro*.

Influence of MSCs on apoptosis of iPSCs was studied after 24 hours of culture under hypoxia (1% O2) mimicking in vivo conditions. MSCs (two umbilical cord donors: MSC 0069 and MSC 0084; corresponding passage two cells from the same donors were used in vivo) were compared to MSC-derived supernatants (MSC conditioned medium) and to conditions without MSCs (medium only) for their potential to reduce iPSC apoptosis as measured by percentage of Annexin V positive, 7-AAD negative cells (n=3). The apoptosis rate of iPSCs in medium only was set to 100%. Mean ± SD results from three measurements are shown (* P < 0.05).

Supplemental Figure 9: Endothelial differentiation and vascular integration of long term surviving derivatives of NIS[pos]-hiPSCs in pig hearts after 5 days and 15 weeks, respectively

Immunohistochemical staining of a tissue section of the left ventricular wall corresponding to the site of NIS[pos]-hiPSC / MSC co-injection demonstrates the presence of Venus[pos] (stained with crossreacting anti GFP antibody) NIS[pos]-hiPSC derivatives that formed intramyocardial blood vessel walls (left). Immunostaining of a corresponding adjacent tissue section for the endothelial marker von Willebrand Factor (vWF) further supports that the cells have adopted an endothelial phenotype (right).

Supplemental Figure 10: Comparative evaluation of capillary density

For capillary density analysis, tissue sections from areas injected with either NIS[pos]-hiPS or NIS[pos]-hiPS+MSC 15 weeks after cell transplantation were utilized. Sections were stained for the endothelial marker von Willebrand Factor (vWF). Capillary density was assessed by

17

counting positive events on representative tissue sections. Larger vessels with a distinct

lumen were omitted from the evaluation.

Supplemental Figure 11: Phenotype of the used mesenchymal stem cells

The isolated human MSCs were characterised by flow cytometry determining presence or

absence of common surface markers.

Supplemental References

1. Reinisch A, Strunk D. Isolation and animal serum free expansion of human umbilical cord derived mesenchymal stromal cells (mscs) and endothelial colony forming progenitor cells (ecfcs). *J Vis Exp*. 2009
2. Schallmoser K, Bartmann C, Rohde E, Bork S, Guelly C, Obenauf AC, Reinisch A, Horn P, Ho AD, Strunk D, Wagner W. Replicative senescence-associated gene expression changes in mesenchymal stromal cells are similar under different culture conditions. *Haematologica*. 2010;95:867-874
3. Strunk D, Rohde E, Lanzer G, Linkesch W. Phenotypic characterization and preclinical production of human lineage-negative cells for regenerative stem cell therapy. *Transfusion*. 2005;45:315-326
4. Okita C, Sato M, Schroeder T. Generation of optimized yellow and red fluorescent proteins with distinct subcellular localization. *Biotechniques*. 2004;36:418-422, 424
5. Dai W, Field LJ, Rubart M, Reuter S, Hale SL, Zweigerdt R, Graichen RE, Kay GL, Jyrala AJ, Colman A, Davidson BP, Pera M, Kloner RA. Survival and maturation of human embryonic stem cell-derived cardiomyocytes in rat hearts. *J Mol Cell Cardiol*. 2007;43:504-516
6. Haase A, Olmer R, Schwanke K, Wunderlich S, Merkert S, Hess C, Zweigerdt R, Gruh I, Meyer J, Wagner S, Maier LS, Han DW, Glage S, Miller K, Fischer P, Scholer HR, Martin U. Generation of induced pluripotent stem cells from human cord blood. *Cell Stem Cell*. 2009;5:434-441
7. Mauritz C, Martens A, Rojas SV, Schnick T, Rathert C, Schecker N, Menke S, Glage S, Zweigerdt R, Haverich A, Martin U, Kutschka I. Induced pluripotent stem cell (ipsc)-derived flk-1 progenitor cells engraft, differentiate, and improve heart function in a mouse model of acute myocardial infarction. *European heart journal*. 2011;32:2634-2641
8. Gaemperli O, Schepis T, Valenta I, Husmann L, Scheffel H, Duerst V, Eberli FR, Luscher TF, Alkadhi H, Kaufmann PA. Cardiac image fusion from stand-alone spect and ct: Clinical experience. *Journal of nuclear medicine : official publication, Society of Nuclear Medicine*. 2007;48:696-703

Supplemental Online Video Legend

Supplemental Online Video 1: Hybrid SPECT-CT imaging of transplanted ^{123}I-pre-labelled NIS^{pos}-hiPSCs

Hybrid SPECT-CT imaging of a pig heart 1 hour after cell transplantation demonstrating a tracer uptake in the septal wall (iPSCs) and an enhanced tracer uptake in the lateral wall (iPSCs and MSCs) of the left ventricle.

Publikation 3

Titel der Arbeit: „Cardiac Quadruple-Fusion Imaging: A Brief Report on a Novel Integrated Multimodality Approach for in vivo Visualization of Transplanted Stem Cells"

Autoren: Fiechter M, Ghadri JR, Sidler M, Martin U, Landmesser U, Kaufmann PA, Lüscher TF, **Templin C**.

Publikationsorgan: Int J Cardiol. 2012 Jul 18. [Epub ahead of print].

eigener Beitrag: - Studienidee und Studiendesign
                        - Kultur und Labeling der NIS$^+$-hiPSCs mit Radiotracern
                        - Induktion des experimentellen Myokardinfarktes durch intrakoronare Ballonokklusion
                        - NOGA-Mapping des linksventrikulären Myokards
                        - Intramyokardiale Stammzellapplikation mittels MyoStar-Injektions-katheter
                        - SPECT-CT-Untersuchungen
                        - Autopsie der Versuchstiere und Gewebepräparation
                        - histologische Aufarbeitung der Gewebe
                        - Analyse und Interpretation der Daten
                        - Schreiben des Manuskriptes

[15] Imazio M, Trinchero R, Brucato A, et al. COlchicine for the Prevention of the Post-pericardiotomy Syndrome (COPPS): a multicentre, randomized, double-blind, placebo-controlled trial. Eur Heart J 2010;31:2749–54.
[16] Imazio M, Bobbio M, Cecchi E, et al. Colchicine as first-choice therapy for recurrent pericarditis: results of the CORE (COlchicine for REcurrent pericarditis) trial. Arch Intern Med 2005;165:1987–91.
[17] Imazio M, Bobbio M, Cecchi E, et al. Colchicine in addition to conventional therapy for acute pericarditis: results of the COlchicine for acute PEricarditis (COPE) trial. Circulation 2005;112:2012–6.
[18] Imazio M, Brucato A, Cemin R, et al. Colchicine for recurrent pericarditis (CORP): a randomized trial. Ann Intern Med 2011;155:409–14.

Cardiac quadruple-fusion imaging: A brief report on a novel integrated multimodality approach for *in vivo* visualization of transplanted stem cells ☆

Michael Fiechter [a,1], Jelena R. Ghadri [a,b,1], Michèle Sidler [c,d], Ulrich Martin [e], Ulf Landmesser [b], Philipp A. Kaufmann [a,b], Thomas F. Lüscher [b], Christian Templin [b,e,*]

[a] Cardiovascular Center, Cardiac Imaging, University Hospital Zurich, Raemistrasse 100, 8091 Zurich, Switzerland
[b] Cardiovascular Center, Cardiology, University Hospital Zurich, Raemistrasse 100, 8091 Zurich, Switzerland
[c] Veterinary Anaesthesia Services—International, Winterthur, Switzerland
[d] Musculoskeletal Research Unit (MRSU), Vetsuisse Faculty, University of Zurich, Switzerland
[e] Leibniz Research Laboratories for Biotechnology and Artificial Organs, Cardiothoracic, Transplantation and Vascular Surgery, Hannover Medical School, Carl-Neuberg-Str. 1, 30625 Hannover, Germany

ARTICLE INFO

A prerequisite for successful monitoring of stem cell therapy after myocardial infarction is the *in vivo* visualisation of transplanted cells [1]. Therefore, imaging techniques with a high sensitivity and spatial resolution are desirable. Current imaging modalities that have been advocated and used for *in vivo* tracking of stem cells include magnetic resonance imaging, nuclear imaging and bioluminescence imaging. However, each of these imaging modalities has its unique advantages and limitations with respect to cell detection sensitivity, specificity, temporal and spatial resolution [2–4].

While single photon emission computed tomography (SPECT) permits exact localization of increased radiotracer uptake in any plane, one major disadvantage is the lack of precise anatomic landmarks. Coronary computed tomography angiography (CCTA), on the other hand, allows accurate localization of anatomic structures, while lacking the ability to detect transplanted cells. NOGA-technology which was introduced primarily for the use in electrophysiology can differentiate viable from non-viable myocardium, and thus permits exact visualization of the injection points of transplanted stem cells in the border zone of viable and non-viable myocardial tissue to warrant a successful application in the target territory. An integrated modality approach is desirable to monitor stem cells after their implantation into infarcted myocardial tissue using simultaneously all 3 techniques. Recently, the feasibility of detecting ^{123}I labeled human induced pluripotent stem cells (hiPSCs) transfected with sodium–iodine symporter (NIS) in border zones of infarcted territories by using cardiac hybrid imaging has been demonstrated by our group [5].

The aim of the current study was to establish a novel approach integrating all four imaging modalities, which would enable the detection of NIS-transfected hiPSCs in a porcine model of myocardial infarction revealing the exact anatomic location of the injected stem cells with the corresponding perfusion defect together with the related coronary vessels.

Myocardial infarction in pigs was induced by 180-min percutaneous occlusion of the mid-segment left anterior descending artery followed by three-dimensional (3D) NOGA-mapping and intramyocardial injection of ^{123}I labeled NIS-transfected hiPSCs into the border zones of the infarcted territory. Thereafter, ^{99m}Tc-tetrofosmin SPECT was performed to verify the perfusion defect of the infarcted area and ^{123}I SPECT to detect successful transplantation of NIS-transfected hiPSCs into the myocardium. Finally, each pig underwent contrast enhanced CCTA with prospective ECG-triggering to image coronary and cardiac anatomy.

Acquired image data from ^{99m}Tc-tetrofosmin and ^{123}I SPECT were aligned and integrated on PMOD (V3.2, PMOD Technologies Ltd., Zurich, Switzerland) and then transferred to a dedicated workstation (Advantage Workstation 4.6, GE Healthcare) to generate SPECT/CCTA hybrid images (CardIQ Fusion software package, GE Healthcare). This cardiac hybrid images offer a 3D view of cardiac anatomy and perfusion together with exact localization of NIS-transfected hiPSCs as shown in rendered hybrid SPECT/CCTA volumes of perfusion (Fig. 1A) and [123]I (Fig. 1B) resulting in a 3D cardiac triple fusion for simultaneous detection of previously injected and radiolabeled NIS-transfected hiPSCs together with myocardial perfusion and cardiac anatomy (Fig. 1C). Moreover, we present NOGA unipolar voltage mapping and linear local shortening (LLS, Fig. 1D) of the left ventricle together with the 3D rendered NOGA-LLS volume (Fig. 1E) depicting sites of stem cell injection as brown spheres. Cardiac Quadruple-Fusion consisting of an overlay of NOGA-injection sites with the obtained triple fusion hybrid image further allows to clearly identify injection sites of ^{123}I labeled NIS-transfected hiPSCs from unlabeled control cells as shown in Fig. 1F.

* Corresponding author at: Department of Cardiology, University Hospital Zurich, Ramistrasse 100, CH-8091 Zurich, Switzerland. Tel.: +41 44 255 9585; fax: +41 44 255 4401.
  E-mail address: christian.templin@usz.ch (C. Templin).
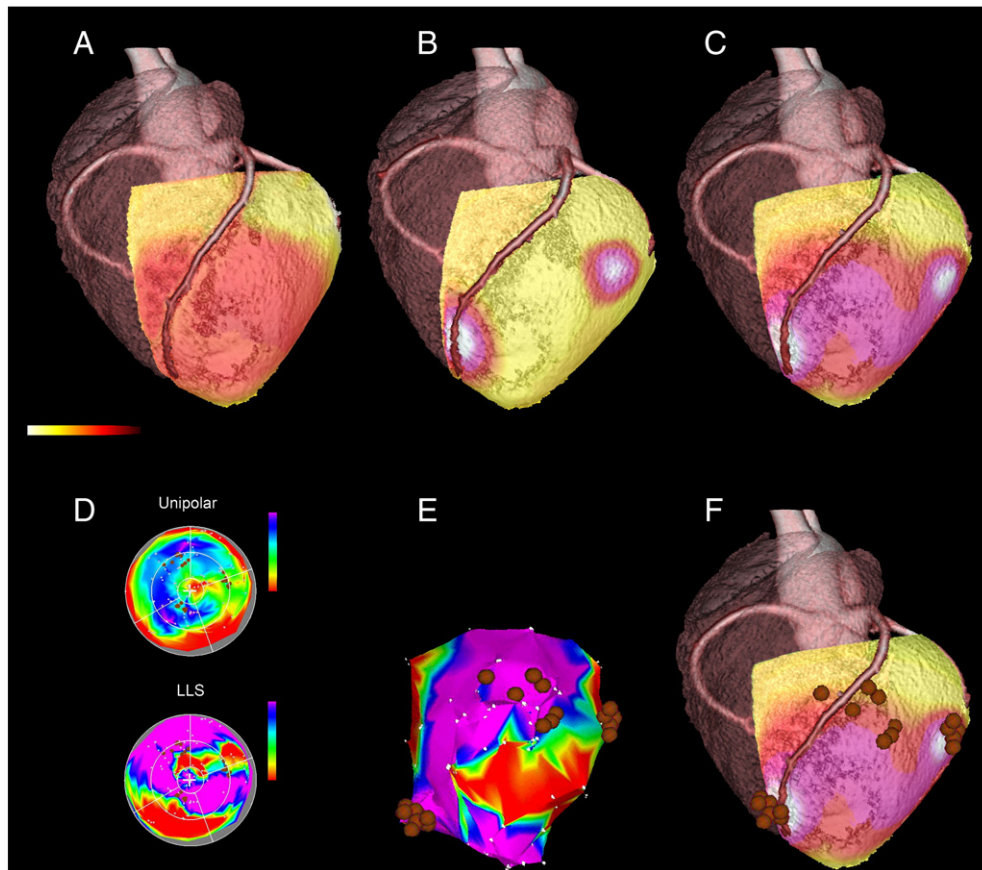[1] The first two authors contributed equally to this work.

Fig. 1. Multidimensional imaging in a porcine model of myocardial infarction injected with human induced pluripotent stem cells (hiPSCs) transfected with sodium–niodine symporter (NIS). (A) Cardiac 3D fusion of coronary computed tomography angiography (CCTA) with ^{99m}Tc-tetrofosmin single photon emission computed tomography (SPECT) revealing anterior myocardial perfusion defect at rest (red area, normal myocardium depicted in yellow) of the left ventricle. Aortic arch together with adjacent coronary tree clearly identifies cardiac anatomy. Right cardiac chambers are visualized transparently. (B) Cardiac 3D fusion of CCTA and SPECT locating ^{123}I labeled NIS-transfected hiPSCs (depicted as white hot spots with red border zones) in the anterior wall (myocardium shown in yellow) of the left ventricle. (C) Cardiac 3D triple fusion of CCTA, ^{99m}Tc-tetrofosmin SPECT and ^{123}I SPECT clearly visualizing myocardial perfusion defect (shown in red/pink) and myocardial regions containing NIS-transfected hiPSCs (white spots) demonstrating accurate localization of stem cells in the border zone of the infarcted myocardial tissue. (D) Polar plots of NOGA unipolar voltage mapping and linear local shortening (LLS) together with 3D rendered volume of LLS (E) with NOGA-guided intramyocardial injected stem cells (brown spheres). Red areas indicate a loss of electrical activity (perfusion defect), blue a normal voltage signal (normal myocardium), and yellow and green areas of decreased perfusion (border zone of the infarcted myocardial tissue). (F) Overlay of NOGA-guided intramyocardial injected NIS-transfected hiPSCs on cardiac triple fusion hybrid image resulting in 3D Quadruple-Fusion volume revealing accurate positioning of intramyocardial sites of injection to myocardial areas containing ^{123}I labeled NIS-transfected hiPSCs. Note sites of injection of control cells lacking ^{123}I which are not co-localized with ^{123}I hot spots.

Our study shows for the first time a novel cardiac Quadruple-Fusion multimodality imaging approach integrating 3D cardiac triple fusion (myocardial perfusion, stem cell detection and anatomy) combined with a fourth dimension of stem cell injection sites by NOGA. Cardiac Quadruple-Fusion imaging may offer to efficiently monitor *in vivo* the distribution and potential therapeutic success of cardiac stem cell therapy.

The author(s) of this manuscript have certified that they comply with the Principles of Ethical Publishing in the International Journal of Cardiology [6].

References

[1] Wu JC. Molecular imaging: antidote to cardiac stem cell controversy. J Am Coll Cardiol 2008;52:1661–4.

[2] Li Z, Suzuki Y, Huang M, et al. Comparison of reporter gene and iron particle labeling for tracking fate of human embryonic stem cells and differentiated endothelial cells in living subjects. Stem Cells 2008;26:864–73.

[3] Gyongyosi M, Blanco J, Marian T, et al. Serial noninvasive in vivo positron emission tomographic tracking of percutaneously intramyocardially injected autologous porcine mesenchymal stem cells modified for transgene reporter gene expression. Circ Cardiovasc Imaging 2008;1:94–103.

[4] Wu JC, Chen IY, Sundaresan G, et al. Molecular imaging of cardiac cell transplantation in living animals using optical bioluminescence and positron emission tomography. Circulation 2003;108:1302–5.

[5] Templin C, Zweigerdt R, Schwanke K, et al. Transplantation and Tracking of Human Induced Pluripotent Stem Cells in a Pig Model of Myocardial Infarction: Assessment of Cell Survival, Engraftment and Distribution by Hybrid SPECT-CT Imaging of Sodium Iodide Symporter Trangene Expression. Circulation 2012 Jul 5. [Electronic publication ahead of print].

[6] Coats AJ, Shewan LG. Statement on authorship and publishing ethics in the international journal of cardiology. Int J Cardiol 2011;153(3):239–40.

ERKLÄRUNG ZUR DISSERTATION

Hiermit erkläre ich, dass ich die Dissertation

Etablierung eines neuen integrativen multimodalen Imaging-Ansatzes für das Monitoring von kardial transplantierten induzierten pluripotenten Stammzellen im präklinischen Großtiermodell

selbstständig verfaßt habe und alle benutzten Hilfsmittel sowie evtl. zur Hilfeleistung herangezogene Institutionen vollständig angegeben wurden.

Die Dissertation wurde nicht schon als Diplom- oder ähnliche Prüfungsarbeit verwendet.

Hannover, im Oktober 2012

PD Dr. med. Christian Templin